

Response to Reviews of “CRI-HOM: A novel chemical mechanism for simulating Highly Oxygenated Organic Molecules (HOMs) in global chemistry-aerosol-climate models” by Weber et al.

We are very grateful to both reviewers for their comments and efforts which have helped us improve this manuscript. Following the structure recommended by ACP, we have responded to each reviewers' comments sequentially below with italicised text showing the reviewer's comments and plain text showing our response. Text which has been added to the manuscript is coloured red. Original manuscript text is in blue and any text which has been removed from the manuscript is blue and has been struck through. The locations of changes are stated. We hope these revisions address the concerns of the reviewers.

While responding to the reviewers' comments, three errors were discovered. These have been corrected and are detailed below. While the corrections are important, we do not believe any of the errors diminish the validity of the conclusions drawn.

Correction to yield calculation

While working on the response to the reviewers' comments, a minor error in the calculation of the yield was discovered. In brief, the correction reduces the HOM yield but it still remains within the range of experimentally-measured values. Importantly, the sensitivity to NO_x and temperature remain unchanged. This error has been corrected and resulted in changes to Figure 6 and the corresponding text. While the correction of this error is important, it does not change the conclusions of the paper. The results of the other simulations performed with the CRI-HOM mechanism were not affected and so the strong performances of the model against observations in Alabama and Hyytiälä remain valid. The response to the reviewer comments have been written factoring in the correction to the HOM yield. To address this correction in the manuscript, the following changes have been made.

Figure 6(a) has been updated.

The sentence beginning on line 24 has been amended to read:

The mechanism predicts a HOM yield of ~~4-6%~~ **2-4.5%** under conditions of low to moderate NO_x , in line with experimental observations, and reproduces qualitatively the decline in HOM yield and concentration at higher NO_x .

The paragraph starting line 516 has been amended as follows.

The model predicted total HOM yields at 290 K of ~~4.5±0.4~~ **1.9±0.2%** (0.01 ppb NO) to ~~5.7±0.4~~ **3.9±0.5%** (1 ppb NO) ~~with the quoted range resulting from the range of temperature dependencies considered. This is within the ranges previously suggested by Jokinen et al (2014) (1.7-6.8%) and close to the values from Ehn et al (2014) (3.5-10.5 %) at similar temperature and α -pinene concentrations as well as comparing favourably to yield measured by and Sarnela et al (2018) (3.5-6.5%), Jokinen et al (2014) (1.7-6.8 %) and while lower than Roldin et al (2019) (7%) indicating that the mechanism is doing a good job at simulating HOM yield.~~ In addition, the HOM yield at 270 K of ~~~0.7-3~~ **0.6-1.9%** compared favourably with the yield

of ~2% determined by Roldin et al (2019). This suggests that the mechanism is doing a good job at simulating HOM yield. The slight low bias may be in part due the values of k14 and k15 which were shown to influence the HOM yield relatively strongly. Sensitivity tests involving universal doubling and halving of the rate coefficients produced HOM yield changes of around +65% and -40% respectively (Fig. S4(a)) while preserving the general dependencies on NO_x and temperature (Table S6). This area of uncertainty will be the focus of future work.

Correction to Model Surface Concentrations

An error in the code used to calculate photolysis frequencies for May as used in the calculation of surface concentrations at Alabama and Hyytiala (Table 5) was discovered. This error did not affect the calculation of the code for June which was used for the calculation of vertical profiles and nucleation rates (Figs. 7, 8, S23). Correcting this error resulted in changes to the modelled surface concentrations in both locations.

In Alabama the modelled surface concentrations changed to 4.5 - 13.3 ppt (compared to 8.1-12.1 ppt before correction). While this is a large relative change, the only conclusion drawn in the text from the comparison to the observational data from Alabama (30 ppt) is that the model returned a “reasonable value” with more detailed comparison not possible due to the wider range of species included in the observational data. We believe this conclusion is still valid.

In Hyytiala, the modelled concentrations changed to 0.75-0.85 ppt for 10-carbon HOM (0.33-0.37 ppt previously) and 0.28-0.30 ppt for 20-carbon HOM (0.20 ppt previously). The 10-carbon HOM concentration remains within the mean observational range (0.2-0.8 ppt) and the 20-carbon HOM is now around double the mean observed maximum (0.16 ppt) but still lower than the maximum concentrations observed of 0.7 ppt. Therefore, we do not believe these new results invalidate our conclusions that the model “*mechanism compares favourably to some of the limited observations of [HOM] observed in the boreal forest in Finland and in the south east USA*”. Table 5 has been updated to include the new values and the the following amendments has been made to line 590:

“In the boreal forest in Hyytiala, the range of predicted 10-carbon [HOM] falls at the higher end of the mean observational range is close to the mean observational value and well below the maximum observed concentrations (1-1.5 ppt) (Roldin et al., 2019), and the predicted 20-carbon accretion product concentration is around double slightly above the mean observational range and well below the maximum observed values (0.6-0.7 ppt).”

Correction to mass conservation in the mechanism

Several reactions in the mechanism were discovered not to conserve mass, specifically the reactions forming the C15d species, several reactions of O3RO2 with the RO2_b pool and a few HOM photolysis reactions. These reactions have been corrected in the updated mechanism and the effect of these changes were thoroughly assessed. None of these corrections caused significant change to the results or altered our

conclusions. Full detail is given in the response to comment pertaining to line 321 from the second reviewer.

Review 1

The article demonstrates the implementation of a reduced HOM mechanism into a reduced mechanism, CRI, which was derived from MCM3.3.1. HOM were discovered a few years ago. They are supposedly formed by a fast process called autoxidation. Since from their structure HOM and accretion products have low to extreme low vapor pressure, they are important candidates for SOA formation and persistence. This links HOM to relevant issues related to aerosol effects, e.g. for climate warming. The purpose of the presented work was to provide a simple enough version of HOM formation mechanism within a CRI for implementation in larger models.

The authors describe quite clearly the steps of the implementation with respect to the changes in the CRI. Their attention turned to the implementation of autoxidation in competition to bimolecular termination reactions. In addition they put efforts also in the implementation of HOM accretion products, as those may play a role in atmospheric nucleation. HOM accretion products are supposedly formed by recombination reactions of (HOM) peroxy radicals. By splitting the sum of peroxy radicals in three classes and considering class interactions they enabled a treatment of the recently described interaction of HOM peroxy radicals with low molecular weight peroxy radicals, specifically the interaction of α -pinene and isoprene. They further implemented the temperature dependence of HOM formation as recently observed. Aspects of their improvement of the CRI – HOM mechanism were tested against flow tube experiments by Berndt et al., with satisfying results. These parts of the work are very interesting and important.

We are glad that the reviewer found the section describing the implementation of the mechanism into the existing CRI framework clear and appreciate the reviewer's comments that the work to incorporate accretion product formation and temperature dependence as well as the tests against flow tube experiments are interesting and important.

The new CRI-HOM was then used to calculate vertical profiles over two stations in Hyytiälä and Manaus. Here the descriptions of the results are not fully congruent with the graphical representations. Overall, the vertical profiles of HOM and HOM accretion products are however in a reasonable range. That means within general experience it could be possible. Any verification of the height profiles by observation is missing. Things become even more speculative when the authors try to predict PI and PD nucleation and the role of biogenics and HOM. I am not sure if that part is really helpful. They authors admit that any validation is currently impossible (in the first sentence of the according paragraph). Despite of the latter, overall the article is timely, well written and can be published in ACP after addressing the comments below.

We appreciate the reviewer's comments on the timeliness and quality of the writing. We respectfully disagree with the reviewer's suggestion that the description in the text is not in agreement with the vertical profile and believe that the text presents a fair representation of the figures. With regards to the

reviewer's comments on height profiles, the input data for several key chemical species in both Hyytiala and the Amazon were scaled by observational data to account for model biases and produce a more realistic picture for the present day profiles. In response to the reviewer's comments we also compared the modelled profiles of isoprene and α -pinene to observations from the ATTO tower and saw reasonable agreement (see comment pertaining to line 467 and response). Regarding nucleation rates, which were calculated using unaltered model data, we believe such work is useful as it provides an approximation of the nucleation rates that would be expected should CRI-HOM be incorporated in its current format into the UKCA global chemistry-aerosol-climate model. The large uncertainty surrounding the nucleation rates is acknowledged, but this reflects current scientific understanding of nucleation processes and the complexity in their simulation. However, despite these uncertainties nucleation is an essential process for composition-climate modelling and a major contributor to overall uncertainty in climate projections. Work is therefore urgently needed to improve its representation in models, and we believe our work is an important contribution to this topic. While Kirkby et al (2016), whose work provides the basis for the nucleation rate equations used here, observed new particle formation from 10-carbon HOMs, the recent study by Heinritzi et al (2020) suggests that 20-carbon accretion product may be the key species in nucleating new particles resulting in a possible reduction to total nucleation rate. This is already acknowledged in the supplement (line 154-156) and to this end, we have added the following to line 620:

“All HOMs were treated as being equally efficient at nucleating new particles, in agreement with approach and nucleation rates used by Kirkby et al (2016) and Gordon et al (2017). Recent work by Heinritzi et al (2020) suggests that 20-carbon accretion products may be better at nucleating new particles and therefore the results presented are likely to be an upper bound although nevertheless informative. Representing the different nucleation efficiencies of different HOM species will be investigated in future work .”

Specific Comments from Reviewer 1:

line 53: Bianchi et al., is a review; here you reference to the original papers in order to give the authors the credits

Additional references have been added to include relevant work cited in Bianchi's review on line 53:

“...formation of “highly oxygenated organic molecules” (HOMs) (Mentel et al., 2014, Ehn et al., 2014, Kurtén et al., 2016, Bianchi et al., 2019)”

line 199f: I think it must be RTN24O2, instead of RTN24BO2. Or it must be “RTN26BO2 - RTN23BO2”. Or something else in the nomenclature is not consistent in this paragraph.

This was a typographical error. RTN24O2 is correct and this change has been made to line 199.

line 204 and line 236: If you want to make the mechanism efficient, why do you start lumping O3-HOM from the 5th generation, while you starting for OH HOM with the 4th generation?

The lumping of the 5th gen and higher O3RO2 was done as there existed experimental data for 1st-4th gen O3RO2 while only existed experimental data for the 1st-3rd gen OHRO2. However, it is acknowledged that further mechanism reduction is possible and this will be an aim for updated versions of CRI-HOM.

line 219: “Alkoxy radicals are not represented explicitly due to their rapid reactions which, typically for larger peroxy radicals, are decomposition or isomerisation. “ The statement doesn’t make sense to me; alkoxy instead of peroxy?”

The intended message of this sentence was that for the alkoxy radicals formed from large peroxy radicals isomerisation and decomposition would be more important than reaction with O₂ and carbonyl formation. To clarify this, the sentence in question has been amended to the following:

“Alkoxy radicals are not represented explicitly due to their rapid reactions which, typically for alkoxy radicals formed from larger peroxy radicals, are decomposition or isomerisation.”

line 339: How much effort would it be to implement and to test a range lifetimes typical for sticky molecules applied to your HOM species. Isn’t deposition always a weak point in atmospheric models? If deposition is faster than upward transport, your vertical profiles would be obsolete.

The HOM species themselves are not advected vertically as stated on line 611 and advection and deposition of the sources gases (α -pinene, isoprene etc) is already factored in by the parent model. We are implicitly assuming that the HOMs are short lived enough that advection is a minor contribution. Thus any change to HOM deposition or loss to the CS at one altitude will not affect HOM at other altitudes. Rather the profiles show the concentration of [HOM] predicted by the box model when supplied with input data (temperature, pressure, concentration of various parent species) from the UKCA climate model data with loss to the CS implemented by scaling the measured surface CS by relative aerosol surface area density at the level of interest.

The sensitivity for loss to the CS, predicted to be the major loss process for HOM (Bianchi et al (2017), Dal Maso et al (2002), Petäjä et al (2009), Tan et al (2018), Wu et al (2018)), is explored in the paper by scaling the CS by factors of 10 and 0.1. The results are shown to be significant (Fig S.24) and identified as an area for future work (line 676 - 677).

line 403-409 and Table 4: If I understand the autoxidation process correctly, the autoxidation rate must slow down at the end as suited H atoms are already consumed in previous autoxidation steps. This is the case for OH, but not for ozone? The overprediction of the highest generations compared to Berndt et al. is not necessarily only due to missing loss processes, it can be also due to overestimated source strength, by your last step autoxidation rate coefficients.

The availability of H atoms will play a part in the autoxidation rate although, as there are more than 5 hydrogens which could be removed, exhausting the supply of hydrogens is unlikely to be a dominant issue given the number of autoxidation steps this mechanism considers. In addition, the extent of functionalisation of peroxy radical is also believed to be important; with enhanced functionalisation increasing autoxidation rate (e.g. Schervish et al (2019), Jenkin et al (2019a), Bianchi et al (2018), Otkjær et al (2018)). The shape of the molecule also plays a part, with restrictions from ring structures (of different sizes in the O₃ and OH pathways) also affecting the rate of H shift reactions (Rissanen et al.,

2015). All these factors result in an overall rate coefficient which is very challenging to predict and, as some of the factors enhance the rate coefficient and others reduce it, the fact that autoxidation coefficients for the O₃ and OH pathways do not follow quite the same pattern is not surprising. The complexity of this issue means fitting to experimental data such as that from Berndt et al (2018b) is the best method.

Regarding the issue of source strength, it is appreciated that the concentration of any RO₂ species is determined by its source and sink. The approach taken here involved constraining the sink (dominated by the autoxidation coefficient in the case of Berndt's experiment) for the 1st generation RO₂ and then, using this as source of the 2nd generation RO₂, constraining the sink of the 2nd generation RO₂ and so on. We believe this is the best approach as it allows for the maximum possible level of constraint but we do acknowledge that if there were additional loss processes for any RO₂, their inclusion would necessitate a reduction in the autoxidation coefficient of the corresponding RO₂ and thus source strength for the next generation RO₂. This remains a key challenge for future work and has been clarified for the reader with the following amendment to line 406 :

~~Addition of such process would likely change the autoxidation coefficients and is an area for further study.~~ Additional loss process would likely reduce the fitted autoxidation coefficients because they would provide an additional sink for the RO₂ species which does not lead to the production of the next generation RO₂. Therefore, the autoxidation coefficients determined in this work are likely to be upper limits but further insight into this is not possible with the data currently available. This is a key area for further study.

line 426-429: Overpredicting the first generation of OHRO2 has nothing to do with the HOM-mechanism, correct? From this point of view it may be a severe principal failure of your CRI scheme. What could be reasons for that? This should be discussed a little more extensively.

JMW thoughts: In terms of the remaining discrepancy, Finally, it is worth conceding that there may be an error in the CRI mechanism (although the overall rate of APINENE + OH is consistent between CRI and the MCM has been used by others, e.g. Pye et al (2018) but argue that it is not as large (i.e. not a "severe principal failure") as reviewer suggests the CRI scheme.

The modelled 1st generation OHRO₂ was dominated by RTN28AO₂ which had a concentration around 10 times greater than RTN28BO₂. RTN28AO₂ does not autoxidise to form later generation RO₂ and therefore cannot contribute to HOM. Thus, the overprediction of the 1st generation OHRO₂ is unlikely to have a significant impact on HOM concentrations. The concentration of the 1st generation OHRO₂ was believed to be underestimated in the experimental work (Berndt et al., 2018b) by a factor of 5. The most likely reason for this is the lower binding energy of the 1st generation OHRO₂ with the reagent ions used in the mass spectrometry which arises from the lower number of heteroatoms in the peroxy radical. Since the CRI-HOM model simulations are 10 times greater than the experimental data for 1st gen OHRO₂, the model is likely to be overpredicting the 1st generation OHRO₂ by only a factor of 2. The rate coefficient for the production of the 1st generation OHRO₂ has undergone extensive evaluation and the same coefficient is used in the CRI v2.2 parent mechanism which has been optimised against the Master Chemical Jenkin (Jenkin et al., 1997, Saunders et al., 2003, Jenkin et al., 2015, Jenkin et al., 2019).

Therefore we respectfully disagree that this is a “severe principal failure” of the CRI. A more likely explanation is the presence of additional, as yet unknown loss processes not currently included in the model, but in the absence of additional data, no further insights can be made at this time. To clarify this, the following adjustment has been made to line 428:

“The experimental measurements of 1st generation OHRO2 concentration from Berndt et al (2018b) were believed to be underestimated by about a factor of 5, ~~which explains some, but not all of the model-experimental discrepancy~~ (Fig. S3). This suggests the model overprediction of the concentration of OHRO2 may be about a factor of 2. The cause of the discrepancy between modelled and measured 1st generation OHRO2 remains unclear. The rate coefficient for the production of the 1st generation OHRO2 has undergone extensive evaluation and the same coefficient is used in the CRI v2.2 parent mechanism which has been optimised against the Master Chemical Jenkin (Jenkin et al., 1997, Sanders et al., 2003, Jenkin et al., 2015, Jenkin et al., 2019a). Sensitivity tests perturbing the branching ratio between RTN28AO2 and RTN28BO2 revealed that even doubling the fraction of RTN28BO2, a significant deviation from literature (Berndt et al., 2016, Pye et al., 2018), had negligible effect as did changing initial [OH] by +100 % / -90%. Another explanation is the presence of additional, as yet unknown loss processes not currently included in the model, but in the absence of additional data, no further insights can be made at this time. More importantly, the 1st generation OHRO2 does not form HOM itself and so it is unlikely to have a significant impact on HOM concentration. Furthermore, the modelled 1st generation OHRO2 was dominated by RTN28AO2, the species which does not autoxidise to form later generation RO₂. Nevertheless, this remains an important area for future work but one where more data is needed for additional constraints to be put in place.” [EDIT]

line 467: In section 4, I do not understand the selections of sites for comparison. Why compare Alabama with Southern Finland at the ground, but calculating vertical profiles over Southern Finland and Amazonia. You should compare with the Manus ground data, too. Moreover, there were big campaigns over Amazonia and Finland, also with airplanes. Can't you use data to validate at least parts of your vertical profiles, e.g. OH, O₃, NO_x, α -pinene, isoprene, selected OVOC?

The sites in Alabama and Finland were chosen because there exists data of HOM (or related species) concentrations at these sites along with the concentrations of several other important species (isoprene, O₃, OH etc) which were used as model inputs to facilitate more faithful modelling of the surface conditions. Surface conditions for the Amazon were not considered in detail as no studies exist of surface HOM measurements in the Amazon (Bianchi et al., 2019) and Zhu et al (2019) notes that nucleation at ground level is almost never observed in the Amazon, a finding in agreement with the results from simulations in this work.

The Amazon and Finland sites were chosen to explore the importance of the Isoprene/MT ratio since these locations are markedly different in this context. In the Amazon, the vertical profiles of isoprene and α -pinene concentration, which were used as input data for each box model run, were adjusted based on multiple vertical measurements (Kuhn et al., 2007) to account for biases in UKCA model data (l. 583-

584) and improve the validity of the simulated profiles. The same approach was taken for the runs over Hyttiala with concentrations for α -pinene scaled to agree with data from Roldin et al (2019) and there was good agreement between the modelled OH and O₃ used by Roldin et al (2019) and the OH and O₃ UKCA data used as CRI-HOM model input. In addition, we have now also compared the lower parts of the isoprene and α -pinene profiles to those measured at the ATTO tower (Yáñez-Serrano et al., 2015) measured over the lowest 80 m. We find that the modelled isoprene showed good agreement with the observed isoprene column, falling within the observed data's standard deviation, while the α -pinene fell just outside the upper limit of the observed data's standard deviation. To highlight this, a new figure (Fig S22) has been added to the SI and the following text has been added in line 584:

“The scaled values of isoprene and α -pinene showed reasonable agreement with observations taken up to 80 m in altitude at the ATTO tower (Yáñez-Serrano et al., 2015). Modelled isoprene fell within 0.5 ppb of observation taken at 2 pm in June while modelled monoterpene were within 0.1 ppb of observation, well within the observational standard deviation in both cases (Fig. S22).”

line 589: Do really mean “semi-qualitative”. That would implicate not even qualitative. . .? The profiles look quite reasonable, overall. And you highlight features of the profiles. . .

The confusion surrounding “semi-qualitative” is acknowledged and it has been replaced with “illustrative” on line 588 which better conveys the intended meaning that the shape of the profiles are useful but there is uncertainty in the absolute values:

“Therefore, we can suggest that our simulated vertical profiles be regarded as ~~illustrative~~~~semi-qualitative~~ as more work is required to identify if the condensation sink should be species dependent.”

line 592-594: What is the sense of the comparison then (see comment above)? Can't you split off from the observations the compounds which are in your model?

The comparison to the observations from Alabama was performed to assess whether the CRI-HOM mechanism was producing reasonable values in a second location rather than serve as an opportunity for deep scrutiny. Furthermore, separating out the C10 and C9 compounds is unlikely to provide much greater clarity as some of the observed C10 compounds will probably come from other species such as β -pinene, whose concentration is not stated, and therefore direct comparison is not possible. We believe that the conclusion we have drawn, that the CRI-HOM model produces a “reasonable value”, is fair and does not exceed the level of confidence we can have in the model given the observed data..

line 596-602 and Figure 7: In contrast to your statement, the OH data decrease with height and O3-HOM and OH-HOM do not have the same share there anymore. Why do the OH-HOM decrease in upper troposphere? It would be helpful to show vertical profiles for OH, O3 and possibly NO, too. Moreover, in legend of Figure 7 you describe features (arrows) which I cannot see. And the color code for O3-HOM is brown, while the line is orange.

Figure 7 has been adjusted to include plots of O₃, OH and NO as requested. The decline at high altitude in HOM from OH relative to HOM from O₃ arises from the greater sensitivity to temperature of HOM formed from OH-oxidation than ozonolysis. This comes from the fact that 2nd generation and higher O₃RO₂ can form HOMs via reaction with HO₂, meaning only 1 autoxidation step is required. However,

only 3rd generation and higher OHRO2 can form HOMs via the same mechanism (due to the lower number of oxygen atoms in the initial α -pinene oxidation product and discussed in Section 2 of the manuscript), necessitating two autoxidation steps. As the autoxidation coefficients are highly temperature dependent, the need for two steps confers a greater temperature sensitivity to HOM from OH. This is less noticeable at high temperatures where autoxidation can compete effectively with bimolecular reactions but this ceases to be the case at ~ 250 K (based on typical NO and HO₂ concentrations) and it is around this temperature that significant divergence starts to occur between HOM from OH and HOM from O₃. This occurs at ~ 5 -6 km in Hyytiälä but at 8-9 km in the Amazon due to its elevated temperature profile. This is also illustrated by the significant difference in HOM from OH profiles resulting from autoxidation activation energies of 12077 K and 6000 K. The divergence occurs at a much higher temperature (lower altitude) in the 12077 K case because autoxidation is outcompeted by bimolecular reactions more easily. To clarify this point in the manuscript, the following addition has been made to line 599:

“HOM from OH showed a significantly greater sensitivity to temperature, diverging from the HOM from O₃ at around 5 km in Hyytiälä and 8 km in the Amazon due to the elevated temperature profile. This was attributed to the requirement for 1st generation OHRO2 to undergo two autoxidation steps before HOMs can be formed (Section 2.2) while 1st generation O3RO2 only need to undergo one autoxidation step and thus have a weaker temperature dependence. This effect only becomes noticeable at temperatures below ~ 250 K when autoxidation ceases to compete effectively with bimolecular reactions.”

The arrows in Figure 7 were previously removed and analysis transferred to Table 5. The caption has been corrected by the following removal.

~~In (a) the reasonable performance of the model is shown by the overlap of the upper inward-facing arrows (total modelled surface concentrations for 10-carbon HOMs (red) and 20-carbon accretion products (black)) and the lower outward-facing arrows (mean observed surface concentrations).~~[DONE]

The colours used for O₃-HOM have been checked and the author confirms that the same colour, red, is used in the legend and for lines.

line 672: There were no vertical profiles over Alabama, right?

Yes, there were no vertical profiles over Alabama.

Captions, Figure 1 and 2: I suggest to introduce the meaning of RO_{2s}, m, b also in the captions.

The following text has been added to the captions of Figures 1 and 2.

The RO₂ pool is split into subsections covering big (RO_{2b}), medium (RO_{2m}) and small (RO_{2s}) peroxy radicals to facilitate addition of accretion product formation.

Typos, errors:

line 70: reference Sindelarova et al., 2014, is missing in the reference list

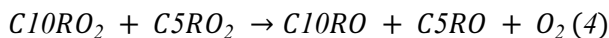
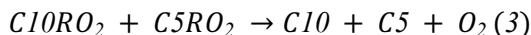
Sindelrova et al (2014) has been added to the reference list.[DONE]

line 141: reference Kiendler-Scharr, instead of Kiendler-Scherr

This has been corrected. **[DONE]**

line 150-160: in the reaction equation 3 and 4: it should be C5RO2 instead of C10RO2

This has been corrected. Equations (3) and (4) are now:



line 245: in equ. (9) 10x instead of 10z

This has been corrected, equation (9) now reads:



line 274: Jenkin et al. 2019, a or b missing

This has been corrected. **[DONE]**

line 287: m instead of me

This has been corrected. **[DONE]**

line 306: than instead of that

This has been corrected. **[DONE]**

line 625: you call the underestimation of H2SO4 slightly, I see 1-2 orders of magnitude

This point is acknowledged and both uses of the word “slightly” have been removed from this paragraph to yield the following from line 623:

“Modelled concentrations in the Amazon ($3 \times 10^4 \text{ cm}^{-3}$) were ~~slightly~~ lower than observation (10^5 - 10^6 cm^{-3} (Wimmer et al., 2018)) although the observations were taken in a pasture site downwind of Manaus surrounded by the rainforest not in the rainforest itself and are therefore likely to be higher than in-situ rainforest values. Thus, the nucleation rates we have calculated for SA_{act} are likely to be a reasonable estimate in Hyytiala and ~~slightly~~ low biased in the Amazon.”

Given that the Amazon measurements are from a region which is likely to have higher SO_2 than the more remote jungle (as it is influenced by the Manaus plume), we believe that the nucleation profiles are still informative.

There are frequently passages in the text using a different font size. e.g. lines 57/58, line 378/379, line 421, line 422, line 458/459, line 464/465, line 561

These amendments have been made.

Table 1: “gen.”

This has been corrected.

Table 3: needs reformatting of the text fields. . .

This has been corrected.

In general, some page formatting issues with Figures and Tables. Figures S17, S18: The subscripts are too small.

Figures S17 and S18 (now Figures S19 and S20) have been enlarged to remedy the issue relating to the subscripts.

Review 2

General comments:

*The manuscript represents a valuable addition to the recent surge in literature reports regarding HOM formation from monoterpenes, as it synthesizes inputs from various sources into a modular chemical mechanism that can be applied to further research into the role of HOMs in the atmosphere. However, with an eye toward those future projects to which this mechanism will surely make an important contribution, it is **imperative that the authors make clear the remaining uncertainties, sensitivities, and assumptions inherent to the key parameters and output of this CRI-HOM mechanism**. The mechanism is an important first step, but in order for future fine-tuning to be conducted, it will be necessary to not just acknowledge but to actively advertise the aspects of the mechanism that remain most uncertain. This will give the critical dialog between models, observations, and laboratory studies room to improve this mechanism as new constraints become available. To that end, I think a number of efforts could be made in this manuscript to clarify the sources and magnitudes of uncertainty, the origins of certain specific assumptions, the sensitivity of mechanism parameters (e.g. branching ratios, rate coefficients) to assumptions made, and the ranges of parameter values that would be consistent with the limited and/or highly uncertain HOM and RO₂ observations.*

As has already been alluded to, the mechanism relies on a number of assumptions and extrapolations between species for many branching ratios and reactions rates. That in itself isn't bad and doesn't invalidate any of this, but requires careful attention to the sensitivity to those assumptions and the resulting uncertainty in the mechanism's parameterizations and output. I would hate to suggest running more models; instead I think

(a) some of this sensitivity analysis already exists in the SI (e.g. L 364-366) and should be given a more prominent billing;

(b) some parameters and model output could benefit from bootstrap back-of-envelope calculations (or comparisons to previous literature, as I suspect exists for e.g. the first-

generation pinene ozonolysis yields) as to their sensitivities to certain inputs or ranges that would be consistent with observations, and

(c) descriptions of the mechanism would benefit from more careful attention to what can be stated with certainty and what results of the simulations are so sensitive to highly uncertain numbers that they can't be considered conclusive.

Along these lines, see especially the comments to L222-224, 304-314, 341-347, 507-508 below.

We thank the reviewer for their comments and are pleased that they assess the work as a valuable contribution to the field. We acknowledge the suggestions made by the reviewer and briefly summarise our response to points (a) - (c) below with more detailed responses provided to the reviewer's specific comments.

In response to comment (a) more detail of the sensitivity analysis has been transferred from the SI to the main text and this is detailed in response to the reviewer's comment on lines 416-418.

In response to (b), more detailed comparison to literature has been added to the manuscript regarding multiple mechanistic parameters and the associated uncertainty (see response to comment beginning "*Finally, it's somewhat unclear without reading...*"). We have also performed multiple sensitivity studies to assess the impact of the uncertainty in the branching ratio of alkoxy radicals (see response to the comment pertaining to line 222), magnitude of rate coefficients k_{14} and k_{15} (see response to the comment pertaining to line 304) and their branching ratio, accretion product formation rate coefficient (see response to the comment pertaining to Figure 5) and HOM loss to OH (see response to the comment pertaining to lines 341-347.)

In response to (c), in addition to details of the sensitivity studies added in the main text, additional information has been added to the manuscript regarding multiple mechanistic parameters and our confidence in them. Furthermore, Table S6 has been repurposed to summarise the impact of uncertainty in different mechanistic parameters discussed in the main text.

The large uncertainty bounds on measurements to which the mechanism was compared (as noted in L 428-429) suggests a need for reporting a range of mechanistic parameterizations consistent with the measurements, rather than single values. The kind of analysis you do on L 364-366 of the SI is hugely useful for these purposes, and should be incorporated into the main text (and, as mentioned below, the ranges and sources reported in Table S6 would also be useful in the main text).

The sensitivity studies have been added into the main text and more detail is provided in the response to the comment pertaining to lines 416-418. The contents on original Table S6 has been added to Table 4 in the revised version.

However, these sensitivity studies could benefit from more detailed descriptions. It sounds as though the uncertainties were only estimated by changing one rate at a time and comparing the

resulting changes in the concentration of the peroxy radical in question with the upper and lower bounds of the experimental uncertainty. This would neglect any compounding effects from simultaneous changes in multiple autoxidation coefficients, or in both autoxidation coefficients and alkoxy decomposition: isomerization branching ratios, correct? This should be acknowledged (or, if possible without too much additional work, the cumulative uncertainties could be estimated and reported).

Uncertainties were estimated as the reviewer describes. The limitations of this method are acknowledged but with this addition, as recommended by the reviewer, we feel the method used is now sufficiently clear. We also note that an alternative approach would be a Monte Carlo simulation but feel this is beyond the scope of this paper. To clarify this in the manuscript the following amendments were made on line 401:

~~“Estimation of the uncertainty in the autoxidation coefficient values is given in the Table S6. An~~ estimation of the uncertainty in the autoxidation is also provided in Table 4. These values were calculated by adjusting the autoxidation rate coefficients one at a time to determine the maximum and minimum values of an autoxidation rate coefficient for which the corresponding peroxy radical would fall within the experimental uncertainty region. This approach neglects any cross-sensitivities through the joint uncertainty in several rate coefficients. A full Monte Carlo uncertainty analysis addressing this issue is beyond the scope of this manuscript but would make a valuable follow up for future work in this field. Therefore, the autoxidation rate coefficient uncertainties are large as the experimental error uncertainties are large.”

Also, if similar sensitivities exist to show the range of HOM yields from RO2-RO2 chemistry that is consistent with the large uncertainty bounds shown in Figure 5, those would be useful to see as well.

The accretion products were observed to make a negligible contribution to HOM yield given their much lower concentration compared to the HOM monomers (C10x and C10z). Accordingly, the uncertainty in total HOM yield arising from the experimental uncertainty in accretion product formation is negligible. However, we do address the issue of uncertainty in the rate coefficients for C20d and C15d formation arising from the experimental uncertainty and this is described in detail in response to the comment pertaining to Figure 5.

Finally, it's somewhat unclear without reading the whole paper and SI very carefully what branching ratios / rates are fit, which are plugged in from measured values or extrapolated from similar species, and which are educated guesses. Someone wanting to use this mechanism or adapt it for their own uses might want to know which coefficients are flexible and which are most tightly constrained (or measured). Can a quick representation of that be provided? Either as an expanded Table 4 / Table S6 (with, say, a superscript character on each rate or branching ratio to denote which come from what sources) or additional annotations to figures 1 and 2 that make

it clear (e.g. colour-coded arrows corresponding to which rates and branching ratios come from which sources).

We agree that a key aim of this work is for this mechanism to be used by others and, following the reviewer's suggestion, we have repurposed Table S6 to provide more information about the source and confidence in model parameters. In addition to Table S6, we have made further additions to the text which address this issue in response to specific comments below.

To make it easier for others to use the mechanism, we have also made available the KPP documentation files used for the mechanism and deposited them in the University of Cambridge repository. We have added the following to line 701:

“Data Availability. All modelled data is available upon request from James Weber and all experimental data from Torsten Berndt. The KPP files for the CRI-HOM mechanism have been deposited in the University of Cambridge data repository and can be viewed at doi.org/10.17863/CAM.54546.”

Specific Comments from Reviewer 2:

L 154-155: For mass conservation and to fit with the explanation in L 145-147, I assume reactions 3-4 are supposed to have C10RO2 + C5RO2 as the reactants?

Yes, this error has been corrected as discussed in the response to 1st reviewer's comments pertaining to lines 150-160.

L 194-195: Figure 1 implies that these TNCARB26 and RCOOH25 co-products, along with the major products of RN26BO2 and RTN24O2, are formed in fixed yields from pinene ozonolysis. However, this sentence (and my understanding of Criegee intermediates) would imply that the branching ratios to these products depends on the relative abundance of the Criegee intermediates' reaction partners, such as water. Could you clarify here and/or in the caption to Figure 1 whether/how this Criegee chemistry is represented, and whether it matters?

Criegee intermediates are not considered explicitly in this mechanism. The 17.5% and 2.5% static branching ratios for TNCARB26 and RCOOH25 respectively, used to parameterize some of the effects of Criegee intermediate chemistry, remain unchanged from the Common Representatives Intermediates v2.2 mechanism and are supported by numerous studies (IUPAC Task Group on Atmospheric Chemical Kinetic Data Evaluation (<http://iupac.pole-ether.fr>, last accessed 17th May 2020), Atkinson and Arey (2003), Johnson and Marston (2008)). While the relative abundance of the Criegee reaction partners is likely to affect the product distribution to some extent, these branching ratios are believed to be acceptable in most ambient conditions. To clarify the matter, the following addition has been made to lines 194-195:

“In addition, TNCARB26 (closed shell carbonyl species) and RCOOH25 (pinonic acid) arise from the reaction of Criegee intermediates with water. The yields of these species, 17.5% and 2.5% respectively, remain unchanged from the CRI v2.2 mechanism and are well supported in the literature (IUPAC Task

Group on Atmospheric Chemical Kinetic Data Evaluation (<http://iupac.pole-ether.fr> , last accessed 17th May 2020), Atkinson, Arey et al (2003), Johnson, Marston et al (2008)).”

L 199: This sentence refers to "RTN24BO2", but the co-product in Figure 1 is "RTN24O2".

This typographical error has been resolved with RTN24BO2 corrected to RTN24O2 as discussed in response to the 1st reviewer’s comments. **[DONE]**

*L 222-224: Are there any constraints or uncertainty bounds on this 50:50 ratio of decomposition and isomerization pathways used here? It seems that in environments where reaction with NO is competitive with the other reaction pathways (and even in very low-NO conditions, since the alkoxy radicals are formed in RO₂-RO₂ reactions as well), the resulting HOM yield could be highly sensitive to this branching ratio. In the absence of concrete evidence for these specific alkoxy intermediates’ branching ratios, can you provide some estimate of the sensitivity of your mechanism’s output to the chosen ratio? **This would be useful either here or later, when you describe the important of this NO-derived HOM in the context of the model output (~L 505–511)***

To investigate the sensitivity of the mechanism to this branching ratio, we ran two sensitivity tests with decomposition : isomerisation ratios of 75:25 and 25:75 respectively. These changes did not affect the ability of the model to reproduce data from Berndt et al (2018b) (Simulations A and B) which is unsurprising given the conditions of Berndt’s experiment which promoted autoxidation as the dominant loss mechanism for RO₂. Therefore, the uncertainty in this branching ratio does not affect the values of the rate coefficients determined for autoxidation and accretion product formation.

We also performed these sensitivity tests with Simulation C to look at the effect on HOM yield. In this case, the difference in HOM yield for low NO_x (up to 200 ppt) was negligible. At 2ppb of NO_x a greater discrepancy of around ±0.7 percentage points (at 290 K) (~ 20%) was observed with the test with lower isomerisation producing a lower HOM yield as expected. Above 2 ppb NO_x, the difference between perturbation increased but this coincided with a significant drop in HOM yield as autoxidation was outcompeted by reaction of RO₂ with NO. To illustrate this further, we have included a new figure in SI (Fig. S4(b)) and refer to it in the added text. Importantly, the range of HOM yields arising from the uncertainty in autoxidation temperature dependence was larger than the range of HOM yields spanned by the isomerisation-decomposition ratio perturbation (for NO_x ≤ 2 ppb), and this was even more the case at 270 K, suggesting that, while important, the isomerisation-decomposition ratio is less important than the refining our understanding of the autoxidation temperature dependence.

To clarify this in the manuscript, the following additions have been made:

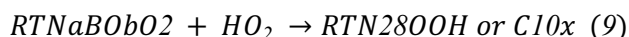
Line 224: “Sensitivity tests perturbing the branching ratio between 75:25 and 25:75 were performed to probe the consequences of this uncertainty. These tests suggested the precise values of this branching ratio within this range did not affect the fitting of rate coefficients for autoxidation and accretion product formation (Section 3.1). These branching ratio perturbations did lead to changes in HOM yield (Fig. S4(b)) and are discussed in more detail in Section 3.2.”

Line 520: “The HOM yield showed negligible sensitivity to the alkoxy radical decomposition-isomerisation branching ratio below 200 ppt of NO_x and around ±0.7 percentage points (~20%) at 2 ppb NO_x. However, this range was easily encompassed by the range arising from autoxidation temperature dependence uncertainty. Above 2 ppb NO_x, this ratio had greater influence as NO reactions with RO₂ started to compete more efficiently with autoxidation but this coincided with the sharp drop in HOM yield (Fig. S4(b)). Therefore, while further work is needed to develop the isomerisation-decomposition branching ratio description, it is unlikely to have a significant influence in the low-NO_x conditions where HOM are predicted to be most prevalent and in these conditions the uncertainty in temperature dependence of autoxidation is predicted to have a larger effect.”

Table S6 has also been adjusted to include an entry summarising these conclusions.

244-246: Should equation 9 (and the line preceding it) read C10x or C10z? I realize the difference is described in Table 1, but it would be helpful to spell it out in the text as well so the reader doesn't get confused on this point.

The correct HOM species is C10x. The equation is has been corrected to read:



The complexity is acknowledged and to this end the sentence beginning on line 243 has been amended to as follows:

~~All later generations OHRO2 produce the HOM species C10x~~ The HOM produced by all later generation OHRO2 is termed C10x (Eq. 9).

L 283-294: Either this semicolon is meant to be a colon, or something's missing in the description of the UCARB10/UCARB12 products that would turn it into a standalone clause.

This should be a colon and the sentence has been corrected.

L 287: Does this "me" mean medium? If so, doesn't this contradict the statement (previous page, L272-3) that medium peroxy radicals react individually with each peroxy radical pool too?

“me” should read medium - this error has been corrected. Yes there is a contradiction. When considering the reaction of a particular medium peroxy radical, we model it to react only with the entire pool. However, when considering a large peroxy radical, this reacts not with the whole pool but with the big, medium and small pools individually. The phrase “Each big and medium peroxy radical reacts separately with each peroxy radical pool while, to minimise the total number of reactions, all small peroxy radicals react with the total pool as accretion product formation is much less favourable (Jenkin et al., 2019)” was not updated when the decision to make medium peroxy radicals react with whole peroxy radical pool (lines 288-289) was taken. The above phrase (lines 272-3) has been amended to:

~~Each big and medium peroxy radical reacts separately with each peroxy radical pool while, to minimise the total number of reactions, all small peroxy radicals react with the total pool as accretion product formation is much less favourable (Jenkin et al., 2019).~~ Medium peroxy radicals are discussed below.

L 304-314: The citation of MCM implies that k14 and k15 were derived from Jenkin et al. 2019a, but the citation two lines later implies they are from Molteni et al. 2018. Which were they?

k14 and k15 were based on Molteni et al (2019) for O3RO2 and Roldin et al (2019) for OHRO2 and the text has been amended to reflect this as shown below.

“...resulted in R13 being more important than R14 and R15 which had rate coefficients based on literature (MCM, Jenkin et al., 2019a) (Molteni et al., 2019, Roldin et al., 2019) up to an order of magnitude lower.”

Also, this presents another fixed input in the mechanism to which the model output and parameter fitting might be highly sensitive. Are there uncertainty bounds on the rate coefficients from Molteni et al. or Roldin et al. 2019 that can be used to estimate this sensitivity?

Roldin et al (2019) does not provide an estimate of uncertainty in the rate coefficient. Molteni et al (2019) provides a range of experimentally-determined rate coefficients from different combinations of reacting O3RO2 species. The individual rate coefficients disclosed by Molteni spanned 2 orders of magnitude, illustrating the influence that the reacting RO₂ has on the rate coefficient. The mean of all available rate coefficients was taken. The uncertainty in rate coefficients k14 and k15 is acknowledged and the challenge of deriving a lumped value for a parameter which varies between RO₂ is evident. To this end, we first ran several sensitivity tests scaling all RO₂-RO₂ rate coefficients of the large peroxy radicals (except for the accretion product formation rate coefficients) were scaled values by factors of 10 and 0.1 to explore the likely outer bounds of parameter space. Applying these scalings did not affect the model output when simulating runs from Berndt et al (2018b) (Simulations A and B). Therefore we can conclude that the uncertainty in k14 and k15 did not affect the fitting of the rate coefficients for autoxidation or accretion product formation which is unsurprising as Berndt's experiments were designed so that losses via RO₂-RO₂ reactions were small.

To explore the impact of the uncertainty further, the simulation run to examine HOM yield (Simulation C) was rerun with the aforementioned scalings. In this case, HOM yield proved more sensitive to this perturbation. More modest scalings were also considered with scalings of +100% and -50% produced changes in HOM yield of +65% and -40% respectively, suggesting significant sensitivity to these rate coefficients. To illustrate this further we have included a new figure in the SI (Fig. S4(a)) showing this dependence and refer to it in the text. We acknowledge that this approach will not capture the fact that HOM yield may be more sensitive to changes in the values for k14 and k15 for some RO₂ than others. To fully investigate this would require a Monte Carlo simulation which is beyond the scope of this work. To clarify the matter and emphasise the sensitivity of HOM yield to this parameter, the following additions have been made:

Line 311 “Sensitivity tests where all values of k14 and k15 were scaled by the same factor revealed that the uncertainty in the value of these rate coefficients did not affect the fitting of rate coefficients for autoxidation and accretion product formation (Section 3.1). These branching ratio perturbations did lead to changes in HOM yield (Fig. S4(a)) and are discussed in more detail in Section 3.2.”[DONE]

Line 520 (already introduced a very start of response) “The slight low bias may be in part due the values of k14 and k15 which were shown to influence the HOM yield relatively strongly. Sensitivity tests involving universal doubling and halving of the rate coefficients produced HOM yield changes of around +65% and -40% (Fig. S4(a)) respectively while preserving the general dependencies on NO_x and temperature (Table S6). This area of uncertainty will be the focus of future work.”.

Are there constraints on the 50:50 branching between R14 and R15, or any particular reason to have chosen that branching? Can any estimates be made of the mechanism’s sensitivity to this branching?

Jenkin et al (2019a) suggests a branching ratio of 60% alkoxy radical (k14) to 40% closed shell species (k15) for primary and secondary RO₂ species, extending this to 80:20 for tertiary RO₂ species. Thus the 50:50 value used by CRI-HOM encompasses the range of similar literature values. To investigate this further, we ran two sensitivity tests with alkoxy : closed shell branching ratios of 60:40 and 80:20 respectively. These changes did not affect the ability of the model to reproduce data from Berndt et al (2018b) and thus uncertainty in this branching does not affect the values of the rate coefficients determined for autoxidation and accretion product formation. The effect on HOM yield (Simulation C) was also negligible and much smaller than the range arising from the uncertainty in the temperature dependence of the autoxidation rate coefficient.

To clarify this in the manuscript, the following sentence has been added to line 311:

“This value is close to the value of closed shell : alkoxy radical of 40:60 ratio suggested for primary and secondary peroxy radicals by Jenkin et al (2019a) but further from the 20:80 suggested for tertiary peroxy radicals. However, sensitivity tests where the mechanism was run with branching ratios of 40:60 and 20:80 revealed that the precise values of this branching ratio within this range did not affect the fitting of rate coefficients for autoxidation and accretion product formation (Section 3.1). These branching ratio perturbations led to changes in negligible HOM yield (Section 3.2, Simulation C) which were much smaller than the range in the HOM yield simulated to arise from the uncertainty in the autoxidation temperature dependence and are therefore considered to be of minor importance.”

An entry has also been made to Table S6 summarising these points.

L 325 & L309: You report a range of chosen fitted values for k13 and k16. Is this range of different values for the different peroxy radicals within each group, or does it represent some sort of uncertainty?

For both the 20 carbon and 15 carbon accretion products, different rate coefficients were used for different reacting RO₂ species to reflect the enhanced propensity to form accretion products when more functionalised. Full detail of this is provided in the SI, specifically reactions 21, 23, 25, 27, 29, 46, 63, 64, 65 and 66 for the 20 carbon accretion product and reactions 36, 37, 38, 39, 40, 47, 71, 72, 73 and 74. To provide additional clarity for the reader, the relevant reactions in the SI list have been provided in full (see additions made below in response to the next comment). [Add ref to KPP files]

Referring forward to section 3.1.3 as suggested here does not clarify the fitting procedure. The repeated use of "chosen" and "assigned" sounds more like the values were user-selected out of a

pre-defined range rather than fit to data, and the model output then compared favourably to the highly uncertain aggregate HOM measurements (which, as far as I can tell, don't distinguish between the generation in which the HOM was formed). How was the initial range over which to "fit" chosen?

It is agreed that “assigned” and “chosen” could be misinterpreted and the rate coefficients were indeed derived from fitting against data via numerous rounds of optimisation. The initial range of values were chosen from literature (Berndt et al., 2018b) but this data only covered a small subset of the possible reactions, hence the need for optimisation. To clarify the issue the following additions have been made.

Line 302 “The rate coefficient for C20d formation, k_{13} , increased with the extent of oxidation of the reacting peroxy radical. This was done to simulate the observed behaviour that accretion product formation becomes faster as the reacting peroxy radicals become more functionalised (Berndt et al., 2018a, Berndt et al., 2018b). ~~The fitting of k_{13} rate coefficients to experimental data is discussed in Section 3.1.3.~~ Thus the reaction forming C20d from the 1st generation peroxy radicals had a lower rate coefficient than the analogous reactions involving higher generation RO₂ species (see reactions 21, 23, 25, 27, 29, 46, 63, 64, 65 and 66 in the SI reaction list for full breakdown). The rate coefficients values used, $0.4\text{--}3.6 \times 10^{-11} \text{ cm}^3 \text{ molecule}^{-1}$, were derived from fitting against experimental data (Berndt et al., 2018b), as discussed in Section 3.1.3, and were in line with the range measured by Berndt et al (2018b) ($0.97\text{--}7.9 \times 10^{-11} \text{ cm}^3 \text{ molecule}^{-1} \text{ s}^{-1}$). ~~and This resulted in R13 being more important than R14 and R15 which had rate coefficients based on literature (Molteni et al., 2019, Roldin et al., 2019 MCM, Jenkin et al., 2019a) up to an order of magnitude lower.”~~”

Line 327 “In a manner similar to C20d formation, the rate coefficient for C15d formation, k_{16} , ~~is simulated in the mechanism to~~ increases with the extent of oxidation of the reacting large peroxy radical; ~~the reaction forming C15d from the 1st gen peroxy radicals had a lower rate coefficient than the analogous reactions involving higher generation RO₂ species (see reactions 36, 37, 38, 39, 40, 47, 71, 72, 73 and 74 in the SI reaction list for full breakdown). The fitting of k_{16} rate coefficients to experimental data is discussed in Section 3.1.3. The fitted values of $1.28\text{--}7.55 \times 10^{-12} \text{ cm}^3 \text{ molecule}^{-1} \text{ s}^{-1}$ were lower than the range measured by Berndt et al (2018b) ($1.2\text{--}3.6 \times 10^{-11} \text{ cm}^3 \text{ molecule}^{-1} \text{ s}^{-1}$).”]~~”

Line 439 “The 20-carbon accretion products were measured in both the isoprene-free, varying α -pinene experiment (as in Fig. 3) and, separately, under conditions of constant α -pinene and varying isoprene (as in Fig. 4). ~~As discussed in Section 2.3,~~ ~~t~~ The fitted rate coefficients for 20-carbon accretion product formation were fitted against experimental data (Berndt et al., 2018b) and incorporated the increase in propensity to form accretion products with RO₂ oxidation ~~varied based on the extent of oxidation of the reacting peroxy radical with the value of k_{13} ranging over $0.4\text{--}3.6 \times 10^{-11} \text{ cm}^3 \text{ molecule}^{-1} \text{ s}^{-1}$.~~ This reproduced, within experimental error, the total observed C20d concentrations for both experiments (Fig. 5 and Fig. S1) ~~and compared favourably to the values calculated by Berndt of $0.97\text{--}7.9 \times 10^{-11} \text{ cm}^3 \text{ molecule}^{-1} \text{ s}^{-1}$.~~”

Line 446 “The species with the lowest functionality, the 1st generation OHRO2 (RTN28AO2 and RTN28BO2), which contain only oxygens, ~~were assigned~~ had the lowest value of k_{13} ($0.4 \times 10^{-11} \text{ cm}^3 \text{ molecule}^{-1} \text{ s}^{-1}$) while the 1st generation O3RO2 (RN26BO2) - with 4 oxygens ~~were assigned~~ had $k_{13} = 0.97 \times 10^{-11} \text{ cm}^3 \text{ molecule}^{-1} \text{ s}^{-1}$, its self-reaction rate coefficient determined by Berndt et al (2018b).

The most functionalised species for O3RO2 (RNxBOyO2) and OHRO2 (RTNxBOyO2) were assigned had values of k_{13} of $3.6 \times 10^{-11} \text{ cm}^3 \text{ molecule}^{-1} \text{ s}^{-1}$ and $3.5 \times 10^{-11} \text{ cm}^3 \text{ molecule}^{-1} \text{ s}^{-1}$ respectively. The fitted rate coefficients used were in line with the range $0.97\text{-}7.9 \times 10^{-11} \text{ cm}^3 \text{ molecule}^{-1} \text{ s}^{-1}$ measured (with an uncertainty no greater than a factor of 3) by Berndt et al (2018b) and the full list of values is given in the reaction list in the SI. This reproduced, within experimental error, the total observed C20d concentrations for both experiments (Fig. 5 and Fig. S1) as well as the RO₂ in Simulations A and B. Sensitivity studies which scaled all k_{13} values by the same factor before rerunning Simulation B and comparing the output to experimental data suggested that variations in the C20d formation rate coefficients of +100 % / -35 % spanned the experimental uncertainty (Table S6).

Line 458 “The fitted rate coefficients for 15-carbon accretion product formation, fitted against experimental data, were also varied increased with based on the extent of oxidation of the reacting peroxy radical. Values of k_{16} ranging over from $1.2 \times 10^{-12} \text{ cm}^3 \text{ molecule}^{-1} \text{ s}^{-1}$ for the least oxidised RO₂ to $5 \times 10^{-12} \text{ cm}^3 \text{ molecule}^{-1} \text{ s}^{-1}$ for the most oxidised species reproduced observed levels of the C15d accretion product (Fig. 5 and Fig. S2) from the constant α -pinene and variable isoprene experiments (as in Fig. 4) and were lower than the values measured by Berndt ($1.3\text{-}2.3 \times 10^{-11} \text{ cm}^3 \text{ molecule}^{-1} \text{ s}^{-1}$ with an uncertainty no greater than a factor of 3). Sensitivity studies which scaled all k_{13} values by the same factor before rerunning Simulation B and comparing the output to experimental data suggested that variations in the C15d formation rate coefficients of ± 50 % spanned the experimental uncertainty (Table S6).

L 321: Why doesn't R16 conserve mass the same way R13 does?

The reviewer is correct that there is an error in the original reaction R16 which caused a loss of mass, artificially, for these peroxy radicals. This has been amended to the following reaction which does conserve mass:



To investigate the consequence of this correction, the updated mechanism was run in Simulation B and the rate coefficients for R16 were adjusted so that the model could reproduce observed C15d concentrations. Scaling the rate coefficient in nearly all cases by a factor of 1.5 allowed the model to reproduce the experimental data. This simple adjustment was suitable because the formation of C15d was a minor sink for O3RO2 and OHRO2 and so increasing the rate coefficient had a negligible effect on O3RO2 and OHRO2 while maintaining the original production flux of C15d.



$$\text{RN23BO6O2} = 0.667\text{C15d} : 6.5\text{E-12 RO2}_m ;$$

$$\text{RNxBOyO2} = \text{C15d} : 5\text{E-12 RO2}_m ;$$

$$\text{RNxBOyO2} = 0.667\text{C15d} : 7.5\text{E-12 RO2}_m ;$$

$$\text{RTN28AO2} = 0.667\text{C15d} : 1.2\text{E-12*RO2}_m ;$$

$$\text{RTN28AO2} = 0.667\text{C15d} : 1.8\text{E-12*RO2}_m ;$$

$$\text{RTN28BO2} = 0.667\text{C15d} : 1.2\text{E-12 RO2}_m ;$$

$$\text{RTN28BO2} = 0.667\text{C15d} : 1.8\text{E-12 RO2}_m ;$$

$$\text{RTN27BO2O2} = 0.667\text{C15d} : 2.5\text{E-12 RO2}_m ;$$

$$\text{RTN27BO2O2} = 0.667\text{C15d} : 3.75\text{E-12 RO2}_m ;$$

$$\text{RTN26BO4O2} = 0.667\text{C15d} : 2.5\text{E-12 RO2}_m ;$$

$$\text{RTN26BO4O2} = 0.667\text{C15d} : 3.75\text{E-12 RO2}_m ;$$

$$\text{RTNxBOyO2} = 0.667\text{C15d} : 2.5\text{E-12 RO2}_m ;$$

$$\text{RTNxBOyO2} = 0.667\text{C15d} : 3.75\text{E-12 RO2}_m ;$$

In addition, after further inspection it was realised that several other reactions in the mechanism were not conserving mass and these were also corrected in the updated mechanism. The updated reactions involved the photolysis of HOM, a minor sink for HOM as discussed in the main text, and some of the reactions of O3RO2 with the RO2_b pool. The original (blue) and updated (red) reactions are shown below and have also been amended in the reaction list in the SI. Note that separately some photolysis reactions had been labelled erroneously as having frequency J15 instead of J22, the frequency used. This correction has also been made.

$$\text{C10z} = \text{RN25BO2O2} : \text{J15};$$

$$\text{C10z} = \text{RN25BO2O2} : \text{J22} ;$$

$$\text{C10x} = \text{RTN27BO2O2} : \text{J15};$$

$$\text{C10x} = \text{RTN27BO2O2} : \text{J22};$$

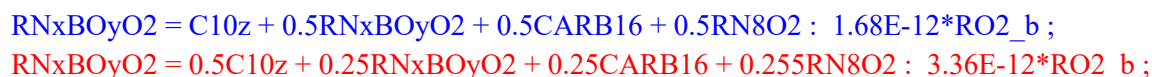
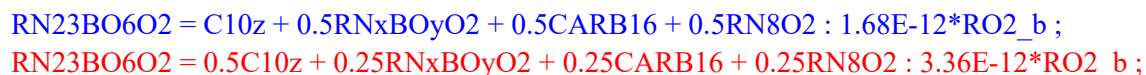
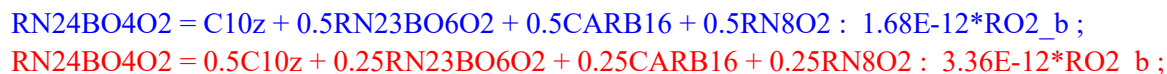
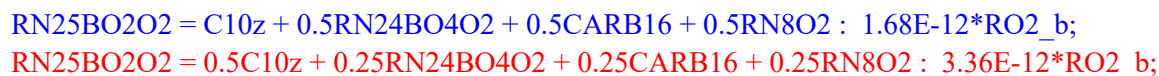
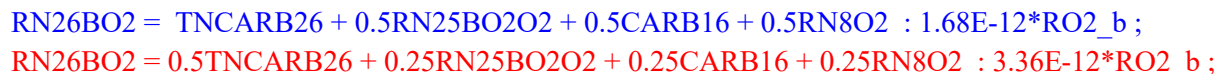
$$\text{C20d} = 0.5\text{RN25BO2O2} + 0.5\text{RTN27BO2O2} : \text{J15};$$

$$\text{C20d} = \text{RN25BO2O2} + \text{RTN27BO2O2} : \text{J22};$$

$$\text{C15d} = 0.5\text{RN25BO2O2} + 0.5\text{RTN27BO2O2} : \text{J15};$$

$$\text{C15d} = \text{UCARB12} + 0.5\text{RN25BO2O2} + 0.5\text{RTN27BO2O2} : \text{J22};$$

For the following reactions of O₃RO₂ with the RO_{2b} pool, it was realised that two reactions had been lumped into one but the rate coefficient had not been adjusted properly (by a doubling of the rate coefficient and halving of each product's fractional coefficient). This has been corrected in the updated version:



The effect of these corrections was thoroughly investigated by re-running simulations A-D and recalculating the altitude and nucleation profiles. In all the cases the effect was very small. In Simulations A and B, the change to the k₁₆ values had no effect on the other fitted rate coefficients for accretion product formation (k₁₃) or the autoxidation coefficients. This is unsurprising as the photolysis of HOM was turned off in these simulations and the losses of O₃RO₂ and OHRO₂ to C₁₅d formation and of O₃RO₂ to the reactions with the RO_{2b} pool were small relative to autoxidation. In the yield calculation in Simulation C, the change was much smaller than the change arising from the correction to the yield calculation. In Simulation D the effect on all 4 HOM species was very small (<3% change) and the changes to other species such as O₃ and OH indistinguishable. Fig 6(b) has been updated with the new HOM concentration values. In the altitude profiles, concentrations of HOM changed by < 2% in Hyytiälä and the Amazon, leading to negligible changes in the profiles and nucleation rates. Figures 7 and 8 have been updated. Modelled surface concentrations in Hyytiälä changed by 0.01 ppt and by 0.05 ppt in Alabama. Neither change affects the conclusion drawn in each location. Table 5 has been updated to reflect these changes.

L 341-347: What is the rate coefficient for the reaction of RTN28OOH + OH (and was it measured?), and why is this the one to stand in for the HOMs?

This rate coefficient is 2.38×10^{-11} molecules⁻¹ cm³ s⁻¹ and is used by CRI v2.2 for the reaction of large 10-carbon species such as RTN28OOH, which is the closest existing species to a HOM, with OH. The rate coefficient between OH + HOM is not known. Bianchi et al (2019) speculated that it could be close to the collision limit of 1×10^{-10} molecules⁻¹ cm³ s⁻¹ noting that functionalisation of species typically increases the

rate coefficient for its reaction with OH (Atkinson (2000)). Sensitivity tests were done with OH + HOM at 1×10^{-10} molecules⁻¹ cm³ s⁻¹ but this had negligible effect on simulated [HOM] or HOM yield which agrees with the suggestion in Bianchi et al (2019) that HOM loss is dominated by physical removal. This also makes sense when considering that at an OH concentration of 10^{-6} cm³, even a rate coefficient at the collision limit would result in an first order rate coefficient of 10^{-4} s⁻¹, smaller than the condensation sinks from observation used in this paper by at least an order of magnitude. Faced with a lack of further evidence, the rate coefficient was kept at 2.38×10^{-11} molecules⁻¹ cm³ s⁻¹. However, we have added the following text to line 343 to clarify the rate coefficient used and the sensitivity of the model to this parameter.

“This rate coefficient was 2.38×10^{-11} molecules⁻¹ cm³ s⁻¹ and, in light of suggestion that the rate coefficient of OH with HOM could be higher (Bianchi et al., 2019), sensitivity tests increasing the rate coefficient to 1×10^{-10} molecules⁻¹ cm³ s⁻¹ were performed but no material effect was observed.”

Where did the MCM photolysis frequencies come from – were they measured or also extrapolated from other species?

The MCM photolysis frequencies are documented in several papers (Saunders et al (2003), Jenkin et al (1997)) and more detailed regarding the sources are provided on the MCM website. Photolysis frequencies for larger molecules are extrapolated from those for smaller molecules where more extensive measurements have been made. For example, the photolysis of the peroxide linkage in RTN28OOH is based on the photolysis of the same functional group in C₂H₅OOH.

Again, are there any estimates of the uncertainty in these photolysis/reactions rate coefficients or the sensitivity of the mechanism to them?

The uncertainty in the photolysis frequency is not readily available and will be a topic for future work. Furthermore, HOM loss via photolysis in the CRI-HOM scheme was a minor loss mechanism; at least an order of magnitude smaller than loss to the condensation sink even at the lower end of CS values. This is supported by the conclusion of Bianchi et al (2019), compiling data from Dal Maso et al (2002), Petäjä et al (2009), Tan et al (2018) and Wu et al (2018), that the major loss mechanism for HOM is physical removal and the following has been added to line 348 to to emphasise this point:

“Physical loss is believed to be the major sink for HOM (Dal Maso et al., 2002, Petäjä et al., 2009, Tan et al., 2018, Wu et al., 2018, Bianchi et al., 2019).”

While your reasoning that their gas phases losses are unlikely to affect OH or O3 seems reasonable, the loss rates should be very important to new particle formation in some circumstances.

For each level in the vertical profiles, new particle formation (NPF) rates were calculated using established methodology (Kirkby et al (2016), Gordon et al (2017)) combined with the HOM concentration output by the box model. As discussed (line 584) and shown (Fig. S23), loss of HOM to the CS has a large impact on HOM concentration and thus on NPF rates, especially as new particle formation via the pure biogenic nucleation mechanism shows a non-linear dependence on [HOM]. We agree with

the reviewer that the loss rates are therefore important and feel we have made the sensitivity to this parameter clear to the reader and identified this as an important area for future work.

L 392-397: As mentioned in the comment above to L 194-195, couldn't these yields be variable instead of static, and dependent on the environmental conditions that affect the branching pathways of the Criegee intermediates? Numerous past experimental efforts have quantified product yields from α -pinene ozonolysis; are these branching ratios consistent with those past efforts? With what certainty is the 0.206 s⁻¹ autoxidation rate coefficient known, and how sensitive are all the subsequent steps in this mechanism to it?

As discussed in the response to the comment pertaining to lines 194-95, the branching of α -pinene products from ozonolysis into closed shell species (pinonic acid and pinonaldehyde) and peroxy radical is well understood and fixed values are used as standard (IUPAC Task Group on Atmospheric Chemical Kinetic Data Evaluation) for representative ambient conditions (i.e., mid latitude boundary layer) in the parent CRI v2.2 mechanism and this mechanism. Well established yields of TNCARB26 (16-17%) and RCOOH25 (2%) are combined with the remaining 80% which proceeds via peroxy radical intermediates and produces a range of different products (Atkinson and Arey (2003), Johnson and Marston (2008)). An addition is made to the text (discussed earlier) to highlight to the reader the confidence we can have in this approach. The mechanism in this paper conforms to the 80% yield and the breakdown of the peroxy radical pathway of 30% RTN24O2 and 50% RN26BO2 is similar to the 20:60 split in the MCM of single 9 carbon species C96O2 and C10 species.

The value of 0.206 s⁻¹ is based on the theoretical calculations of the relative energies of possible 1st generation O3RO2 and their autoxidation coefficients (Kurten et al., 2015). Kurten et al. (2015) do not provide any error estimates and so in order to understand the impacts of uncertainty in this rate coefficient we have followed the same process as outlined in the main text on line 401 (previously in Table S6, now moved to Table 4 as requested) as for other rate coefficients. This process, which constrains the uncertainty in the rate constants by the measured concentrations of radicals, yields an uncertainty for this reaction of +0.025/ -0.04 s⁻¹. Subsequent simulations probing the bounds of this uncertainty result in impacts on the down-stream chemistry and highlight that this is an important parameter for which further constraints in future work would be valuable.

L 404-406: This sentence seems grammatically incomplete. Perhaps the "and" isn't needed?

This has been corrected with the addition of the following amendment.

“The autoxidation coefficients in Table 4 are higher than those considered in the theoretical study of Scherivish et al (2019) but closer to the values measured by Zhao et al (2018) and the values suggested by Roldin et al (2019).”

L 406-408: This is a crucial point for the present study, and one that I don't think should be so quickly discarded. How (i.e. to what extent) would this change the autoxidation coefficients?

We acknowledge the importance of this issue and extensive efforts were made to determine the cause. It should be noted that the fitted autoxidation coefficients in this work are not too dissimilar to those used by Roldin et al (2019) or Zhao et al (2018) and so we do not believe the effect to be overwhelming but we do not believe further progress can be made with the currently available data. The presence of additional loss processes would reduce the fitted autoxidation coefficients because they would provide additional sinks for each RO₂ without producing the next generation RO₂. Therefore, the autoxidation rate coefficients derived here are most probably upper limits. To clarify this, the following adjustment (already discussed in the response to the comments of the 1st reviewer) has been made to line 408:

~~“Addition of such process would likely change the autoxidation coefficients and is an area for further study. Additional loss process would likely reduce the fitted autoxidation coefficients because they would provide an additional sink for the RO₂ species which does not lead to the production of the next generation RO₂. Therefore, the autoxidation coefficients determined in this work are likely to be upper limits but further insight into this is not possible with the data currently available. This is a key area for further study but no further conclusions can be made with the data currently available.”~~

Line 416-418: This type of sensitivity study is very helpful for understanding the strength of the constraints on your mechanism parameters, but I am confused by the wording of "realistic deviations". Are these the maximum deviations consistent with the autoxidation coefficients, or the maximum deviations consistent with the experiments? If the former, do we have reason to believe that the experiments fell within this range? And if the latter, how were they deemed "realistic"?

We believe these deviations are representative in the context of the experimental setup. NO and NO₂ concentrations were believed to be 4 ppt (10⁸ cm⁻³) given the purity of the gas used (personal communication with T. Berndt) and so increases of 250 % and decreases of 75% were considered to span the likely range of concentrations. In the absence of measurements, an OH concentration of 10⁶ cm⁻³ was deemed reasonable while the common ratio approximation of 100:1 applied to yield HO₂ of 4 ppt (10⁸ cm⁻³). OH was further investigated with an 100 % increase and 90% decrease and HO₂ with a 250 % and decrease of 75%. To clarify this, the following adjustment has been made to line 410-418.

~~“Unfortunately, the flow tube studies of Berndt et al (2018b) lack observations to constrain the full chemical space simulated by the box model. In particular there were no measurements of NO, HO₂ and OH. Therefore, a rigorous series of sensitivity tests (described in the SI) were carried out to quantify the importance of uncertainty in the initial concentrations of OH, NO and HO₂ on the results of the model. Initial OH was shown to have no effect on the measured parameters (O₃RO₂, OHO₂ and accretion products) while NO and HO₂ had some effect on OHRO₂ (mainly through the change to OH) and C₂₀d (via the change to radical termination rate). Initial conditions of 10⁶ cm⁻³ for OH and 4ppt for HO₂, NO and NO₂ were used. Based on the sensitivity simulations it was concluded that realistic deviations in concentration of +10 ppt / - 3 ppt for HO₂, NO and NO₂ and + 10⁶ cm⁻³ / - 5×10⁵ cm⁻³ for OH from the initial values would not lead to deviations in the concentrations of RO₂ or accretion products sufficient to warrant a change in the autoxidation coefficients. Likewise increasing and decreasing in OH of (100 %~~

~~increase, 90 % decrease) did not affect model output.~~ The effect of the uncertainty in the initial experimental concentrations of NO, HO₂ and OH on the modelled concentrations of O₃RO₂, OHRO₂ and accretion products and thus fitted the autoxidation coefficients and accretion production formation rates coefficients was investigated with a series of sensitivity tests. Initial conditions of 10⁶ cm⁻³ for OH and 4 ppt for HO₂ were used. NO and NO₂ were initialised at 4 ppt, based on the purity of the flow gas (personal communication with T. Berndt). For HO₂, NO and NO₂ sensitivity simulations indicated that increases of 10 ppt (250% increase) and decreases of 3 ppt (75% decrease) did not lead to deviations in the concentrations of RO₂ or accretion products sufficient to warrant a change in the rate coefficients for autoxidation or accretion product formation. Initial OH concentration had negligible effect (<5% change) on O₃RO₂, OHRO₂ and C_{20d} when varied over 1×10⁵ – 2×10⁶ cm⁻³ (90 % decrease, 100 % increase).”

L 426: Should this refer to Fig. 3b instead of a?

Yes, this correction has been made.

L 428-429: Why are these measurement believed to be so drastically underestimated? Whether or not they are, the results suggest that some element of the first-generation OH-derived peroxy radical chemistry is substantially biased in the mechanism; do you have any indication of what this might be?

This question has been answered in the response to the first reviewer’s comments (line 426).

L 490: This sentence mentions 4 mechanism versions, but the rest of the paragraph only seems to describe 3.

The following amendment has been made.

“Given the lack of additional literature in this area, 43 new versions of the new mechanism were created to probe the effects of temperature and activation energy on HOM yield and subsequent evolution.”

L 507-508: See comment above on lines 222-224: this NO_x-dependent behaviour derives from a highly uncertain 50:50 alkoxy radical decomposition : isomerization branching ratio, but is described here as an important consequence of the mechanism. Would this behaviour hold true for a range of reasonable estimates of the branching ratio? How sensitive is it to the chosen branching?

This response to this comment is included in the response to the comment pertaining to line 222.

L 516: Are the model uncertainty ranges reported here for the different temperature dependences? It’s very important to distinguish this from some sort of total uncertainty estimate.

The model uncertainty ranges reported in this section arise from the different temperature dependences. To acknowledge this, the following amendment has been made to the sentence beginning on line 516.

The model predicted total HOM yields at 290 K of 4.5±0.41.9±0.2% (0.01 ppb NO) to 5.7±0.43.9±0.5% (1 ppb NO) with the quoted range resulting from the range of temperature dependencies considered.

L 518: Missing a word in "comparing favourably to yield measured by" ?

The error has been corrected in the amendment to the previous comment.

L 527: What explains the drastic decrease in the simulated acetone production?

In CRI v2.2, acetone is produced at a fixed 80% yield from α -pinene ozonolysis in a step which is a simplification of the multiple chemical steps which occur in reality. This approach is suited to the CRI's original purpose, simulating air quality in Western Europe with relatively high NO_x, but is less accurate at lower NO_x. It is in these lower NO_x conditions where CRI-HOM produces less acetone than CRI v2.2 and this is because the autoxidation pathways become more important and funnel material away from pathways which produce acetone.

L 571: "We also at the effect" ... something's wrong here.

This error has been corrected with the following amendment to line 571.

“We also look at the effect of the simulated HOMs on nucleation rates in the lower troposphere.”

L 588: What does it mean for a result to be semi-qualitative? That even some non- quantitative qualities of the simulated vertical profiles are expected to be erroneous? What ones?

The term “semi-qualitative” has been amended to “illustrative” as discussed in response to the first reviewer's comment pertaining to line 589.

Table 4: The uncertainties and sources of these rates are important enough that I think Table S6 should be combined into Table 4.

This has been done and a further explanation as to how the errors were calculated has been added.

Figure 3: Why are there no error bars on the 3rd and 4th generation O3RO2 observations? Where do the error bars come from (e.g. are they instrument uncertainty on the measurements or something else)?

The error bars were omitted for the 3rd and 4th generation as they would be almost exactly the same size as those of the 2nd generation species and make the graph harder to read. The error bars are from experimental uncertainty. To clarify this uncertainty, the caption of Figure 3 was adjusted to read.

“Figure 3 - Comparison of the HOM-precursors (a) O3RO2 and (b) OHRO2 produced by the model and from Berndt et al (2018b) for experiments performed with different initial concentrations of α -pinene (Simulation A). The model reproduces the increase in O3RO2 and 2nd and 3rd generation OHRO2 with initial α -pinene well. The model struggled to reproduce concentrations of the 1st generation OHRO2 (not shown). Note that the error shown is the experimental error from Berndt et al (2018b) and the error bars for the 3rd and 4th generation O3RO2 species are of very similar size to the error bars of the 2nd generation species but have been omitted for clarity.”

To clarify this, the following text has been added to the Figure 4 as well:

“The error shown is the experimental error from Berndt et al (2018b).”

L 979-980: While the note that first-generation OHRO2 are poorly reproduced is appreciated, it seems misleading not to put them on the graph, and deprives the reader of a visual representation of this important element of the mechanism. Are the concentrations too high to fit on this graph?

We acknowledge the issue with the 1st generation OHRO2 but feel that the additional detail which has been added in response to comments from both reviewers means that this issue, and the plausible suggestions for its occurrence, has been made sufficiently clear to readers. In addition, the large estimated underprediction in the 1st generation OHRO2 in the work of Berndt et al (2018b) would complicate plotting of the 1st generation OHRO2 alongside the plots of the 2nd and 3rd generation OHRO2 where the experimental error in the observed concentration was much lower. To this end, an additional plot has been added to the SI (Fig. S3) showing the 1st generation OHRO2 experimental and modelled concentrations for Simulation A. Attention is drawn to this in the main text with the following adjustment on line:

“The experimental measurements of 1st generation OHRO2 concentration from Berndt et al (2018b) were believed to be underestimated by about a factor of 5 ~~which explains some, but not all of the model-experimental discrepancy.~~ (Fig. S3).”

Figure 5: Can the y-axes be adjusted to show the reader the extent of the measurement uncertainty? The large uncertainties suggest that a wide range of HOM yields would be consistent with the observations, including some yield parameterizations that wouldn't display the much-heralded decrease in C20 (and total) accretion products and increase in C15 products. Were any sensitivity estimates made regarding HOM yields in the mechanism that could be shown here?

The y-axes of Figure 5 have been adjusted as requested. We acknowledge the issue presented by the large experimental uncertainty and note that HOM yield is not parameterised directly but is influenced by mechanistic parameters like autoxidation coefficients and dimerisation rate coefficients and as such, we feel these are the parameters which should be probed further. In addition, the accretion products contributed negligibly to the HOM yield, given their much lower concentration, and therefore the uncertainty in their concentration will not affect HOM yield appreciably. To investigate the impact of experimental uncertainty on the confidence we can have in the rate coefficient for accretion product formation, we performed some additional sensitivity tests in response to the reviewer's comments where all rate coefficients for reactions forming C20d were scaled by the same factor. Scalings of 0.66 and 2 spanned the region of experimental uncertainty. The same approach was applied separately for the rate coefficients for the formation of the C15d species and scalings of 0.5 and 1.5 spanned the range of experimental uncertainty. To provide the reader with a better idea of the certainty in these mechanistic parameters, as requested by the reviewer, these uncertainty limits have been included in Table S6 and discussed in the main text (see the response to comments pertaining to lines 325 & L309). We acknowledge that this approach will not capture the fact that C20d or C15d concentrations may be more sensitive to changes in the formation rate coefficients for some RO₂ than others. To fully investigate this would require a Monte Carlo simulation which is beyond the scope of this work and we feel that the

additional information given in the manuscript and Table S6 from this sensitivity study provides the reader with a fair idea of the impact of the uncertainty in the rate coefficients for accretion product formation.

CRI-HOM: A novel chemical mechanism for simulating Highly Oxygenated Organic Molecules (HOMs) in global chemistry-aerosol-climate models.

James Weber¹, ~~Scott Archer-Nicholls¹, Alexander T. Archibald^{1,2}~~, Paul Griffiths^{1,2}, ~~Scott Archer-Nicholls¹~~, Torsten Berndt³, Michael Jenkin⁴, Hamish Gordon⁵, Christoph Knote⁶, ~~Alexander T. Archibald^{1,2}~~

¹Centre for Atmospheric Science, Department of Chemistry, University of Cambridge, Cambridge, CB2 1EW, UK

²National Centre for Atmospheric Science, Department of Chemistry, University of Cambridge, CB2 1EW, UK

³Atmospheric Chemistry Department (ACD), Leibniz Institute for Tropospheric Research (TROPOS), Leipzig, 04318, Germany

⁴Atmospheric Chemistry Services, Okehampton, Devon, UK

~~⁵College of Engineering, Carnegie Mellon University, Pittsburgh, PA 15213, USA~~
Engineering Research Accelerator and Center for Atmospheric Particle Studies, Carnegie Mellon University, Pittsburgh, PA 15213, USA

⁶Meteorologisches Institut, Ludwig-Maximilians-Universität München, Munich, 80333, Germany

Correspondence to: James Weber (jmw240@cam.ac.uk)

Abstract.

We present here results from a new mechanism, CRI-HOM, which we have developed to simulate the formation of highly oxygenated organic molecules (HOMs) from the gas phase oxidation of α -pinene, one of the most widely emitted BVOCs by mass. This concise scheme adds 12 species and 66 reactions to the Common Representative Intermediates (CRI) mechanism v2.2 Reduction 5 and enables the representation of semi-explicit HOM treatment suitable for long term global chemistry-aerosol-climate modelling, within a comprehensive tropospheric chemical mechanism. The key features of the new mechanism are (i) representation of the autoxidation of peroxy radicals from the hydroxyl radical and ozone initiated reactions of α -pinene, (ii) formation of multiple generations of peroxy radicals, (iii) formation of accretion products (dimers) and (iv) isoprene-driven suppression of accretion product formation, as observed in experiments. The mechanism has been constructed through optimisation against a series of flow tube laboratory experiments. The mechanism predicts a HOM yield of ~~2-4.5%~~ 4-6% under conditions of low to moderate NO_x , in line with experimental observations, and reproduces qualitatively the decline in HOM yield and concentration at higher NO_x . The mechanism gives a HOM yield that also increases with temperature, in line with observations, and our mechanism compares favourably to some of the limited observations of [HOM] observed in the boreal forest in Finland and in the south east USA.

The reproduction of isoprene-driven suppression of HOMs is a key step forward as it enables global climate models to capture the interaction between the major BVOC species, along with the potential climatic feedbacks. This suppression is demonstrated when the mechanism is used to simulate atmospheric profiles over the boreal forest and rainforest; different isoprene concentrations result in different [HOM] distributions, illustrating the importance of BVOC interactions in atmospheric composition and climate. Finally particle nucleation rates calculated from [HOM] in present day and pre-industrial atmospheres suggest that “sulphuric acid free” nucleation can compete effectively with other nucleation pathways in the boreal forest, particularly in the pre-industrial, with important implications for the aerosol budget and radiative forcing.

40 **1 Introduction**

Aerosols play an important role in the Earth system by affecting the Earth's radiative balance as well as local air quality and thus human health (Carslaw et al., 2010). Aerosols can interact directly with solar radiation through scattering or absorption and indirectly by influencing cloud properties by seeding cloud droplets as well as increasing cloud albedo (Forster et al., 2007, Twomey., 1974). Thus, aerosols change the balance between the energy received from the Sun and the energy emitted
45 from the planet at the top of the atmosphere. However, a major uncertainty in climate change predictions arises from aerosols and aerosol-cloud interactions (Stocker et al., 2014). This arises in part from a lack of understanding of pre-industrial (PI) aerosol and it is the change in aerosol burden from the PI to the present day (PD) which determines the effective radiative forcing (ERF) of aerosols. As PI aerosols sources are almost exclusively natural, an understanding of natural sources and the associated aerosol formation processes is essential if better predictions for climate change are to be made.

50

An important formation route for aerosols is oxidation of volatile organic compounds which form less volatile species that can partition into the aerosol phase or nucleate new particles (Kirkby et al., 2016, Shrivastava et al., 2017). Recently it has been established that the oxidation of organic compounds can lead to the formation of “highly oxygenated organic molecules” (HOMs) ([Mentel et al., 2014](#), [Ehn et al., 2014](#), [Kurtén et al., 2016](#), Bianchi et al., 2019) (also referred to as “highly
55 oxidised multifunctional organic compounds (Ehn et al., 2012)) which are formed by multiple intramolecular oxidation steps, termed autoxidation (Crouse et al., 2013, Bianchi et al., 2019). Autoxidation typically involves the abstraction by a peroxy radical of a hydrogen atom bonded to a carbon elsewhere on the molecule resulting in an alkyl radical and hydroperoxide group. The alkyl radical reacts rapidly with atmospheric oxygen to form a new peroxy radical, ultimately **reducing the species' volatility and enabling particle formation/condensation**. HOMs are defined as
60 closed-shell species with at least 6 oxygens formed by initial atmospheric oxidation and subsequent autoxidation steps (Bianchi et al., 2019). HOM formation has been observed from anthropogenic species (Berndt et al., 2018a) and biogenic species such as α -pinene (Molteni et al., 2019, Berndt et al., 2018b). The semi-explicit mechanism described for the first time in this paper describes the formation of HOMs from α -pinene in a form suitable for
65 biogenic nucleation into a global model and, ultimately, allowing for a more rigorous description of aerosol formation and the climatic consequences. α -pinene is considered as it is the most widely studied and widely emitted monoterpene (~ 32 Tg yr⁻¹, Sindelarova et al., 2014) and, with measured HOM yields around 3-10 % (Ehn et al., 2014, Jokinen et al. 2015), has the potential to produce 2-7 Tg HOM yr⁻¹ with the range arising from uncertainties in emissions, HOM yield and difference in mass between the precursor BVOC and the HOMs which will have at least 6 additional oxygen
70 atoms but in some cases, considerably more. HOM yields from β -pinene (the second most widely emitted monoterpene, Sindelarova et al., 2014) and isoprene (the most widely emitted BVOC, Sindelarova et al., 2014) are negligible (Ehn et al., 2014). Limonene has emissions around 25% of α -pinene (Sindelarova et al., 2014) and is likely to have a higher HOM yield (Ehn et al., 2014, Jokinen et al., 2015) although a much wider range of values have been reported than for α -pinene. Limonene thus may have the potential to produce a similar mass of HOM as α -pinene and its consideration may be an area of future
75 work. Emissions of anthropogenic VOCs account for $\sim 10\%$ of total VOC emissions (Guenther et al., 1995), roughly the same quantity as monoterpene emissions, and, as no species have HOM yields above 2.5% ([Ehn et al., 2014](#), [Jokinen et al., 2015](#), [Kirkby et al., 2016](#), Bianchi et al., 2019), the contribution of anthropogenic VOCs to HOM is likely to be significantly smaller. Nevertheless, the speciation of anthropogenic VOCs in the mechanism means that addition of HOMs from these sources will be possible and, from an urban air quality perspective very important.

80

Nucleation of new particles from sulphuric acid is an important means of new particle formation (NPF) in the atmosphere (Kulmala et al., 1998). Sulphuric acid can also form new particles with oxidised organic species (Riccobono et al., 2015). However, extremely involatile HOMs can participate in NPF, without necessarily needing a sulphuric acid seed in a process termed pure biogenic nucleation (PBN) (Kirkby et al., 2016, Gordon et al., 2016). Despite playing important roles in aerosol formation and growth, the relatively recent discovery of HOMs and the complexity of their formation means that their role in particle formation and contribution to aerosol has been assessed in only very few global model studies (Gordon et al., 2016, Zhu et al., 2019). The ability of PBN to change atmospheric aerosol loading by providing a route to particle formation without sulphuric acid has been illustrated (Gordon et al., 2016) with this effect particularly important in the pre-industrial (PI) atmosphere, where lower SO₂ emissions resulted in greater sensitivity of aerosol loading to alternative formation routes (i.e. including PBN) and a higher simulated aerosol burden than previous studies. As a result, Gordon et al (2016) calculated that the radiative forcing change from the PI to PD caused by cloud cover change was 27% lower than previous estimates. Meanwhile, Zhu et al (2019), highlighting the fact that many chemistry schemes fail to reproduce nucleation rates in low sulphuric acid concentrations, showed the complex effect PBN has in the PI and PD with a more complicated mechanism but one which also omitted autoxidation and accretion product formation. Including PBN in a global chemistry-aerosol scheme resulted in a much larger increase in the magnitude of the (negative) aerosol indirect effect (AIE) in the PI than the PD. This has potentially important consequences as it means that the effective radiative forcing (ERF) of aerosols from the PI to PD may be smaller than previously expected. This in turn would mean that climate sensitivity is lower than previously thought as aerosols are offsetting a smaller amount of warming arising from the enhanced concentrations of greenhouse gases than previously thought, with implications for predictions of future climate change as well.

100

The peroxy radicals produced from α -pinene oxidation by OH or O₃ have been observed to undergo autoxidation under typical atmospheric conditions (Ehn et al., 2014, Jokinen et al., 2014, Berndt et al., 2016, Berndt et al., 2018b). The autoxidation competes with the bimolecular reaction of peroxy radicals with NO, NO₃, HO₂ and other peroxy radicals and its yield is thus dependent on background atmospheric composition. Therefore, an accurate description of HOMs requires consideration of NO_x and oxidant concentrations as well as autoxidation; indeed, elevated NO_x has been observed to suppress HOM formation (Lehtipalo et al., 2018). The first order rate constants for autoxidation can vary over several orders of magnitude ($\sim 10^{-6} - 10^2$ s⁻¹) depending on nearby functional groups (Otkjær et al., 2018, Bianchi et al., 2019, Crouse et al., 2013, Xu et al., 2018, Kurten et al., 2015). Autoxidation rates also exhibit a significant positive temperature dependence (Jenkin et al., 2019a, Bianchi et al., 2019) and HOM yield has been observed to be highly temperature dependent (Quéléver et al., 2019). Thus, the overall competitiveness of autoxidation is dependent on the background atmospheric composition and ambient temperature as well as the molecule undergoing oxidation.

110

In addition to autoxidation, the formation of HOM accretion products (also called dimers (Kurten-Kurtén et al., 2016, Bianchi et al., 2019)) by reactions between two peroxy radicals has been observed to be significant with large peroxy radicals (Kirkby et al., 2016, Berndt et al., 2018a, Berndt et al., 2018b, Jenkin et al., 2019a, Molteni et al., 2019). These species are predicted to be more involatile than 10-carbon HOMs (also termed monomers (Kurten-Kurtén et al., 2016)) with important implications for new particle formation and contribution to SOA. In established schemes such as the Master Chemical Mechanism (MCM) (Jenkin et al., 1997, Saunders et al., 2003), the Common Representative Intermediates (CRI) (Utembe et al., 2010, Watson et al., 2010, Jenkin et al., 2010, Jenkin et al., 2019) and the Chemistry of the Stratosphere and Troposphere (Strat-Trop) used in the climate model UKCA (United Kingdom Chemistry and Aerosol) (Archibald et al., 2019), formation of accretion products is not included as it was previously considered negligible or too complex to include. However, experimental work suggests that accretion product formation is a competitive pathway for larger peroxy radicals, such as those formed from α -pinene

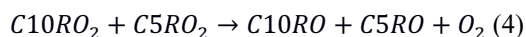
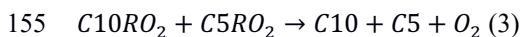
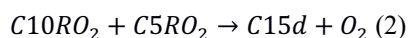
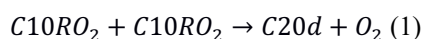
120

(Berndt et al., 2018b, Molteni et al., 2019, [Simon et al., 2020](#)) and indeed becomes more favourable with increasing functionality and size; the rate coefficient for the accretion reaction between two α -pinene derived peroxy radicals was observed to be 16-80 times greater (depending on the extent of oxidation) than for the analogous reaction between two isoprene derived peroxy radicals (Berndt et al., 2018a, Berndt et al., 2018b).

The mechanistic treatment of HOMs in numerical models has varied considerably from simple steady state approximations (Gordon et al., 2016) through basic mechanisms linked to a volatility basis set (Schervish et al., 2019) to more explicit descriptions based on the MCM featuring either a limited subset of HOMs without accretion product formation or autoxidation (Zhu et al., 2019) or a near explicit description involving over 1700 reactions (Roldin et al., 2019). Whilst the addition of PBN represents an important process level improvement in models, the approaches discussed above all have some degree of limitation. As well as omitting accretion product formation, simpler models (Gordon et al., 2016, Schervish et al., 2019) do not fully capture the influence of oxidant levels, NO_x or temperature while the more explicit schemes (Zhu et al., 2019, Roldin et al., 2019) are too computationally expensive for long term climate studies. Further, none of the schemes include the relatively novel observation of suppression via reactive RO_2 cross reactions (McFiggans et al., 2019), although this has been identified as an important area for future research (Zhu et al., 2019, Roldin et al., 2019) and is addressed in this work.

New experimental evidence suggests that isoprene may suppress the formation of the most involatile accretion products and thus the smallest aerosol particles (Berndt et al. 2018b, McFiggans et al., 2019, [Heinritzi et al., 2020](#)) and reproducing the effect of isoprene has been identified as an important requirement for future mechanisms (Roldin et al., 2019). This inhibition is driven firstly by isoprene scavenging OH radicals (Lee et al., 2016, Kiendler-Schaerr et al., 2009, Berndt et al., 2018b) thus reducing the formation of large peroxy radicals by reaction of α -pinene with OH. The second driver is the scavenging of the 10-carbon α -pinene peroxy radicals (“C10RO₂”) by isoprene peroxy radicals (“C5RO₂”) and the other smaller peroxy radicals from species such as CO and CH₄ (McFiggans et al., 2019). These C10RO₂ could otherwise form 20-carbon accretion products (Eq. 1) which are predicted to be highly involatile ([Kurtén Kurten et al., 2016](#)). The reaction of isoprene peroxy radicals with the α -pinene radicals produces the 15-carbon accretion product (“C15d”) (Eq. 2) as well as closed shell species (“C10” and “C5”) (Eq. 3) and alkoxy radicals (“C10RO” and “C5RO”) (Eq. 4) which isomerise or fragment (Jenkin et al., 2019a).

150



This inhibition affects the aerosol size distribution (an important parameter for the radiative forcing of aerosol (Zhu et al., 2019)) by favouring the growth of larger existing aerosol particles by promoting the production of smaller, more volatile species which can partition to pre-existing aerosol rather than the nucleation of new particles from larger, less volatile species. This has the potential to have important consequences for future predictions of SOA and the negative feedback proposed to exist between biogenic VOC emissions and atmospheric temperature (Kulmala et al., 2004, Carslaw et al., 2010, Sporre et al., 2018). Such predictions, based on the modelled increases in isoprene and monoterpene emissions in a warmer climate (Kulmala

165 et al., 2013, Sporre et al., 2018) have not considered the potential perturbation to NPF and atmospheric aerosol loading by isoprene and the changes in radiative forcing which may result. Reassessing the sign and size of this feedback by coupling the chemistry scheme described in this work to an aerosol scheme within a global climate models is a key long-term aim of this work.

170 In this study we describe our work developing a new mechanism sufficiently concise for global chemistry climate models that can simulate the process of autoxidation, the formation of HOMs from α -pinene and the influence of isoprene. In Section 2 the development of the mechanism from the principles of gas phase chemistry is described and in Section 3 we discuss mechanism optimisation and validation against experimental data and the parent mechanism, CRI v2.2. In Section 4, the mechanism is used to simulate atmospheric HOM profiles and explore implications for new particle formation. Finally, in Section 5,
 175 conclusions for further work are drawn.

2 Mechanism Development

Our new mechanism we have developed builds on the Common Representative Intermediates (CRI) scheme version 2.2 Reduction 5 (Jenkin et al., 2019b) (hereafter the “base mechanism”), developed from the fully explicit Master Chemical Mechanism (MCM) version 3.3.1 (Jenkin et al., 2015) which describes the degradation of organic compounds in the
 180 troposphere. In the CRI framework, species are lumped together into surrogate molecules whose behaviour is optimised against the fully explicit MCM. The CRI v2.2 R5 mechanism describes the degradation of α -pinene, β -pinene, isoprene and 19 other emitted VOC species.

The updates we have made to the base mechanism to produce the new HOM-forming functionality include the addition of
 185 autoxidation of α -pinene oxidation products and a more detailed peroxy radical pool scheme. These changes enable the formation of 10-carbon, 15-carbon and 20-carbon HOMs and add 12 species and 66 reactions to the base mechanism. The new chemical mechanisms for ozonolysis and OH oxidation are shown in Figure 1 and Figure 2 respectively. We now describe the changes made to the base mechanism to incorporate HOM chemistry in more detail.

190 2.1 Ozonolysis

To simulate the autoxidation reactions formed from ozonolysis 5 new peroxy radical species were added to the base mechanism. The peroxy radicals formed from ozonolysis of α -pinene and subsequent autoxidation steps are collectively termed “O3RO2”. In the base mechanism, α -pinene reacts with ozone to produce the single lumped peroxy radical RN18AO2 and
 195 acetone. This single mechanistic step represents multiple chemical steps, with RN18AO2 representing a 6 or 7 carbon species. In addition, TNCARB26 (closed shell carbonyl species) and RCOOH25 (pinonic acid) arise from the reaction of Criegee intermediates with water. The yields of these species, 17.5% and 2.5% respectively, remain unchanged from the CRI v2.2 mechanism and are well supported in the literature (IUPAC Task Group on Atmospheric Chemical Kinetic Data Evaluation, Atkinson and Arey (2003), Johnson, Marston et al (2008)). RN18AO2 goes on to react with standard peroxy radical reaction
 200 partners; HO₂ forming hydroperoxides; NO and NO₃ forming alkoxy radicals; and the peroxy radical pool forming alkoxy radicals, carbonyls and alcohols, as described in (Jenkin et al., 2019a).

In our new mechanism, RN18AO2 is replaced with the tracers RN26BO2 and RTN24BO2. RN26BO2 represents the 10-carbon peroxy radicals formed directly from the cleavage of the ozonide and subsequent addition of atmospheric oxygen,
 205 which can then undergo autoxidation. RTN24O2, a species already in the CRI mechanism, represents the 9 carbon peroxy

radical species (MCM species C96O2) which is also formed from ozonolysis but does not undergo autoxidation in this mechanism. RN26BO2 is termed “1st generation” as it has undergone one oxidation step and it can undergo autoxidation to form the 2nd, 3rd, 4th and lumped higher generation species, termed RN25BO2O2, RN24BO4O2, RN23BO4O2 and RNxBOyO2 species respectively (RNxBOyO2 does not undergo further autoxidation but does undergo all the other reactions).

210 In the base mechanism, the first number featured in a species’ name is an index which refers to the number of NO-to-NO₂ conversions possible, which depends on the number of C-C and C-H bonds. During the H-shift step of autoxidation, a C-H bond is usually broken to produce the alkyl radical which then forms the peroxy radical from atmospheric oxygen and so each autoxidation step reduces the index by one while the number of oxygens is increased by 2. For example, the autoxidation of the 2nd generation O3RO2 to 3rd generation is expressed by Eq.5.

215 ***RN25BO2O2 → RN24BO4O2*** (5)

Each generation of peroxy radical also undergoes bimolecular reactions. Reaction with HO₂ produces a hydroperoxide species; for the 2nd and later generations, the product is classified as a HOM (C10z) as they fulfil the criteria discussed by Bianchi et al (2019), while for the 1st generation species the resulting hydroperoxide is RTN26OOH, a species already present in the CRI (Eq. 6).

220 ***RNaBObO2 + HO₂ → RTN26OOH or C10z*** (6)

Reaction with NO and NO₃ yields nitrates or alkoxy radicals and accurately representing the behaviour of these products is crucial to reproducing the effect of NO_x on HOM formation. Alkoxy radicals are not represented explicitly due to their rapid reactions which, typically for [alkoxy radicals formed from](#) larger peroxy radicals, are decomposition or isomerisation.

225 Decomposition produces two smaller species, one closed shell and one a peroxy radical while isomerisation produces a more functionalised peroxy radical via an alkyl radical intermediate with one fewer oxygen than would have been added via autoxidation. Faced with very limited data and the fact that the precise fate of an alkoxy radical will depend considerably on molecular structure and neighbouring groups, a branching ratio 50:50 for decomposition and isomerisation was adopted. [“Sensitivity tests perturbing the branching ratio between 75:25 and 25:75 were performed to probe the consequences of this uncertainty. These tests suggested the precise value of this branching ratio within this range did not affect the fitting of rate coefficients for autoxidation and accretion product formation \(Section 3.1\). These branching ratio perturbations did lead to changes in HOM yield \(Fig. S4\(b\)\) and are discussed in more detail in Section 3.2.”](#)

230

The decomposition products are existing CRI species CARB16 and RN10O2 or RN9O2 and the isomerisation product the next generation peroxy radical as shown in the example reaction (Eq. 7).

235

RN25BO2O2 + NO → 0.5RN24BO4O2 + 0.5CARB16 + 0.5RN9O2 (7)

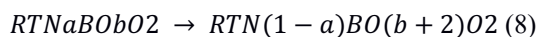
240 A schematic of the additions made to the CRI for the ozonolysis scheme is shown in Figure 1.

2.2 OH oxidation

Autoxidation through the OH initiated oxidation pathway resulted in the addition of 6 new species, including 5 new peroxy radicals. The peroxy radicals formed from OH oxidation of α -pinene and subsequent autoxidation steps are termed “OHRO2”.

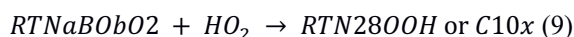
The single peroxy radical RTN28O2 in the base mechanism is replaced by RTN28AO2, representing the two species which do not undergo autoxidation (APINAO2 and APINBO2 in the MCM), and RTN28BO2 (MCM APINCO2) which can undergo autoxidation to form higher generation peroxy radicals (Xu et al., 2018). The 2nd and 3rd generation OHRO2 are represented explicitly (RTN27BO2O2 and RTN26BO4O2) and all 4th generation and higher species are lumped together as RTNxBOyO2 for mechanistic simplicity. The chemical treatment of RTN28AO2 is the same as the original CRI species RTN28O2 while all other OHRO2 (except RTNxBOyO2) can undergo autoxidation (Eq. 8).

250



Reaction of the 1st and 2nd generation OHRO2 (RTN28BO2 and RTN27BO2O2) with HO₂ yields the hydroperoxide RTN28OOH which is not classified as a HOM due to insufficient oxygens. ~~All later generations OHRO2 produce the HOM species C10x (Eq. 9).~~ The HOM produced by all later generation OHRO2 is termed C10x (Eq. 9).

255



Reaction with NO and NO₃ is treated in the same manner as O3RO2 except for RTN28BO2 which follows the reaction of the analogous species APINCO2 in the MCM. A schematic of the additions made to the base mechanism for the OH oxidation scheme is shown in Fig. 2.

260

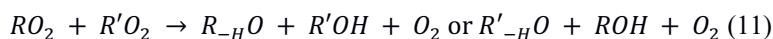
The pathway initiated by reaction of α -pinene with NO₃ was not considered in this work but is identified as an area for future work. A summary of the peroxy radical species in the two pathways is given in Table 1 and full mechanistic description provided in the SI.

265

2.3 Peroxy Radical + Peroxy Radical Interactions

Reactions between peroxy radicals can result in the formation of two alkoxy radicals (Eq. 10), a carbonyl and an alcohol (Eq. 11) or accretion product (Eq. 12) (Jenkin et al., 2019a).

270



Rather than represent every possible RO₂-RO₂ reaction combination, the base mechanism uses a peroxy radical pool. Each peroxy radical undergoes a unimolecular reaction with a first order rate coefficient determined by the total peroxy radical concentration and the geometric mean of the self-reaction rates of the methyl peroxy radical and radical of interest (Jenkin et al., 2019a).

While computationally efficient, such a mechanism fails to represent the effect of peroxy radical size on the distribution of products. While negligible for small peroxy radicals, accretion product formation is more favourable when larger, more functionalised peroxy radicals react (Berndt et al., 2018b, Schervish et al., 2019). To describe the reactions between the differently sized peroxy radicals, we have split the single peroxy radical pool into three pools for small (<4 carbons), medium

280

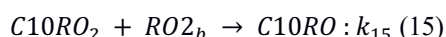
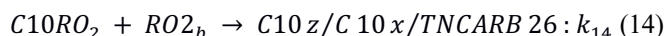
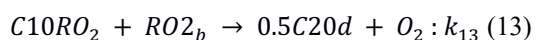
(4-7 carbons) and big (>7 carbons) peroxy radicals. Each big ~~and medium peroxy~~ radical reacts separately with each peroxy radical pool while, to minimise the total number of reactions, all small peroxy radicals react with the total pool as accretion product formation is much less favourable (Jenkin et al., 2019a). Medium peroxy radicals are discussed below. The use of large and medium peroxy radical pools allows for improved representation of the competition between peroxy radicals with different reactivity in our new mechanism and is a substantial improvement over the base mechanism.

Table 2 summarises the products for a specific peroxy radical reacting with the different peroxy radical pools. As discussed previously, alkoxy radicals were not simulated explicitly, rather they decomposed into closed shell products and peroxy radicals. A full list of the contents of each peroxy radical pool is given in the SI.

In practice, the alkoxy radicals formed from the reaction of isoprene-derived peroxy radicals (which are likely to dominate the medium size pool) with other peroxy radicals decompose rapidly into the major products: closed shell carbonyls methyl vinyl ketone and methacrolein (UCARB10) and the minor product hydroxy vinyl carbonyl (UCARB12) (Jenkin et al., 2015). The accretion of isoprene-derived peroxy radicals has been measured to be over an order of magnitude slower than the accretion of peroxy radicals derived from α -pinene (Berndt et al., 2018b), supporting the theory that accretion product formation becomes more favourable with increasing peroxy radical size. Therefore, to limit complexity, all ~~medium~~ peroxy radicals in the mechanism simply react with the overall peroxy radical pool and their accretion product formation was ignored.

2.3.1 Large Peroxy Radical Pool

The reaction of a large peroxy radical with the large peroxy radical pool (RO_{2b}) can produce an accretion product (Eq. 13), closed species (Eq. 14) or an alkoxy radical (Eq. 15) (Jenkin et al., 2019a) which then reacts as discussed in sections 2.1 and 2.2. Note that a single C₁₀RO₂ species will produce half a C_{20d} accretion product for the purposes of mass conservation.



The rate coefficient for C_{20d} formation, k_{13} , increased with the extent of oxidation of the reacting peroxy radical. This was done to simulate the observed behaviour that accretion product formation becomes faster as the reacting peroxy radicals become more functionalised (Berndt et al., 2018a, Berndt et al., 2018b). Thus, the reaction forming C_{20d} from the 1st generation peroxy radicals had a lower rate coefficient than the analogous reactions involving higher generation RO₂ species (see reactions 21, 23, 25, 27, 29, 46, 63, 64, 65 and 66 in the SI reaction list for full breakdown). The fitting of k_{13} rate coefficients to experimental data is discussed in Section 3.1.3. The chosen fitted values of k_{13} were derived from fitting against experimental data (Berndt et al., 2018b) and, as discussed in Section 3.1.3, and were in line with the range measured by Berndt et al (2018b) (0.97-7.9×10⁻¹¹ cm³ molecule⁻¹ s⁻¹). The rate coefficients used, 0.4-3.6×10⁻¹¹ cm³ molecule⁻¹ s⁻¹ were derived from fitting against experimental data (Berndt et al., 2018b) and, as discussed in Section 3.1.3, and were in line with the range measured by Berndt et al (2018b) (0.97-7.9×10⁻¹¹ cm³ molecule⁻¹ s⁻¹). This resulted in R13 being more important than R14 and R15 which had rate coefficients based on literature (Molteni et al., 2019, Roldin et al., 2019, MCM, Jenkin et al., 2019a) up to an order of magnitude lower.

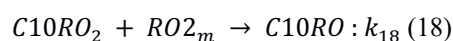
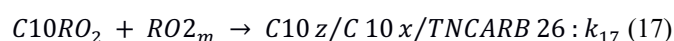
The rate coefficient for the formation of the closed shell species from O₃RO₂, k_{14} , was taken as the mean of the rate coefficients measured by Molteni et al (2018) (1.68×10⁻¹² cm³ molecule⁻¹ s⁻¹). The rate coefficient for alkoxy radical formation, k_{15} , was assumed to have the same value as k_{14} (i.e. a 50:50 branching ratio between these pathways). This value is close to the value of

closed shell : alkoxy radical of 40:60 ratio suggested for primary and secondary peroxy radicals by Jenkin et al (2019a) but further from the 20:80 suggested for tertiary peroxy radicals. However, sensitivity tests where the mechanism was run with branching ratios of 40:60 and 20:80 revealed that the precise values of this branching ratio within this range did not affect the fitting of rate coefficients for autoxidation and accretion product formation (Section 3.1). These branching ratio perturbations led to negligible changes in HOM yield (Section 3.2, Simulation C) which were much smaller than the range in the HOM yield simulated to arise from the uncertainty in the autoxidation temperature dependence and are therefore considered to be of minor importance (Table S6).

The rate coefficients for formation of closed shell species and alkoxy radicals from OHRO₂ with RO_{2b} were taken from Roldin et al (2019).

2.3.2 Medium and Small Peroxy Radical Pools

Reaction of a large peroxy radical with the medium peroxy radical pool (RO_{2m}) can produce a 15-carbon accretion product (Eq. 16), closed shell species (Eq. 17) or an alkoxy radical (Eq. 18) which is not modelled explicitly but rather decomposes rapidly into another closed shell product and peroxy radical.



In a manner similar to C20d formation, the rate coefficient for C15d formation, k_{16} , is simulated in the mechanism to increase with the extent of oxidation of the reacting large peroxy radical; the reaction forming C15d from the 1st gen peroxy radicals had a lower rate coefficient than the analogous reactions involving higher generation RO₂ species (see reactions 36, 37, 38, 39, 40, 47, 71, 72, 73 and 74 in the SI reaction list for full breakdown). The fitting of k_{16} rate coefficients to experimental data is discussed in Section 3.1.3. The chosen fitted values of $1.82\text{--}7.55 \times 10^{-12} \text{ cm}^3 \text{ molecule}^{-1} \text{ s}^{-1}$ were lower than the range measured by Berndt et al (2018b) ($1.2\text{--}3.6 \times 10^{-11} \text{ cm}^3 \text{ molecule}^{-1} \text{ s}^{-1}$).

Reaction of a large peroxy radical with the small peroxy radical pool (RO_{2s}) produces a closed shell species or an alkoxy radical, in a manner analogous to Eq. 17 and Eq. 18.

2.4 HOM Loss Mechanisms

The number of different molecules falling under the C10x, C10z, C15d and C20d umbrellas is huge, making the treatment of loss processes complex. Losses will occur via chemical or photolytic degradation as well as to condensation to aerosol, to the nucleation sink and dry and wet deposition. Physical loss is believed to be the major sink for HOM (Maso et al., 2002, Petäjä et al., 2009, Tan et al., 2018, Wu et al., 2018, Bianchi et al., 2019). For simplicity, in the simulations below, we ignore wet and dry deposition but do include loss to the condensation sink for modelling simulations C and D (Table 3).

Chemical losses of HOMs are highly uncertain. It is suggested that HOMs will react with OH (Bianchi et al., 2019). In this model, OH reacts with C10x, C10z, C15d and C20d with the rate coefficient of the large hydroperoxide, RTN28OOH to

produce the smaller closed shell CRI species CARB10 and CARB15 as well as UCARB10 (lumped methacrolein and methyl vinyl ketone) for 15-carbon dimers. This rate coefficient was 2.38×10^{-11} molecules⁻¹ cm³ s⁻¹ and, in light of suggestion that the rate coefficient of OH with HOM could be higher (Bianchi et al., 2019), sensitivity tests increasing the rate coefficient to 1×10^{10} molecules⁻¹ cm³ s⁻¹ were performed but no material effect was observed. Photolysis of peroxide and carbonyl linkages produce alkoxy radicals which behave as previously described. Photolysis frequencies are taken from the MCM (Jenkin et al., 1997, Saunders et al., 2003). Given the small concentrations of HOMs we predict that uncertainty in these gas phase loss processes are likely to have small impacts on the general features of tropospheric chemistry (i.e. OH reactivity or ozone production).

Physical loss is believed to be the major sink for HOM (Dal Maso et al., 2002, Petäjä et al., 2009, Tan et al., 2018, Wu et al., 2018, Bianchi et al., 2019). Loss to the condensation sink presents a complex challenge. The saturation vapour pressure will vary considerably (~~Kurten~~Kurtén et al., 2016) for HOMs, even within the C10 umbrella, affecting the fraction which partition to the aerosol phase. Furthermore, some HOMs are likely to have aldehyde and alcohol moieties which will enhance their removal via reactive uptake into the aerosol phase, particularly if it is aqueous. When using our new mechanism in different simulations (Table 3), condensation sinks have been set to fixed values or values taken from literature.

Having described the additions and changes made to the base mechanism to develop our new mechanism, we now discuss the optimisation and validation of the mechanism.

3 Mechanism Optimisation and Validation

Here we discuss the optimisation of the new mechanism and its validation. In total 4 simulations were performed with the mechanism as detailed in Table 3.

3.1 Comparison to Experimental Data

There exists a limited amount of experimental data which provides an insight into the behaviour of the multiple generations of peroxy radicals produced from ozonolysis and OH-oxidation of α -pinene (Berndt et al., 2018b). Using a flow cell, Berndt measured the concentration of α -pinene-derived peroxy radicals produced by ozonolysis (O3RO2) and OH oxidation (OHRO2) and 20-carbon (C20d) and 15-carbon (C15d) accretion products at the end of the flow tube using a chemical ionisation-atmospheric pressure interface-time of flight (CI-APi-TOF) mass spectrometer and a chemical ionisation-time of flight (CI3-TOF) mass spectrometer. The observed peroxy radicals spanned several generations of autoxidation, namely the 1st-4th generation for O3RO2 species and 1st-3rd generation for OHRO2. Berndt et al (2018b) also calculated rate coefficients for accretion product formation using the observation that accretion product concentration increased linearly with time with an assumed uncertainty no greater than a factor of 3. Reagent ions used in the CI-APi-TOF were C₃H₇NH₃⁺, CH₃COO⁻ and NO₃⁻ and in the CI3-TOF NH₄⁺. The flow tube experiments lasted for 7.9 s, at which point the flow was sampled by the mass spectrometers. Reactions proceeded under dark conditions at 1 atm and 297 K under low [NO_x] (<10⁸ cm⁻³). The low concentrations of bimolecular reaction partners HO₂ and NO meant that multiple autoxidation steps could occur in the reaction time.

Flow tubes operating under laminar flow are easily modelled using box models as there are very few complications to consider in terms of mixing and wall loss and no new particle formation was observed. A box model version of the mechanism was compiled in the BOXMOX framework (Knote et al., 2015). The experimental data allowed the autoxidation coefficients of the

peroxy radical species and the rate coefficients of accretion product formation to be constrained. The concentrations of peroxy
 410 radicals and accretion products in the box model were evaluated at the end of the 7.9 s reaction period and compared with
 experiments. A process of iterative adjustment to autoxidation and accretion product formation rate coefficients in the
 mechanism was performed to produce the best reproduction of the experimental data by the mechanism.

Two experiments from Berndt et al (2018b) were considered. In the first experiment, flow tube runs were performed with
 415 varying initial concentrations of α -pinene (3-50 ppb) with initial O₃ at 28 ppb (Simulation A). In the second experiment, runs
 were performed with fixed initial α -pinene (15.6 ppb) and O₃ (80 ppb) but with initial isoprene concentrations varying from
 0-60 ppb (Simulation B). Comparison to this experimental data facilitated examination of the model's ability to reproduce the
 concentration of HOM-precursors and accretion products with and without isoprene as well as at moderate and high O₃ mixing
 ratios.

420

An important parameter in the mechanism was the yield of RN26BO2 from ~~α -pinene~~ α -pinene ozonolysis. This yield is
 uncertain and it was found to affect the autoxidation coefficients required to reproduce the experimental data for the O3RO2
 species. To constrain it, a first-order autoxidation rate coefficient of 0.206 s⁻¹ for RN26BO2 was imposed, based on theoretical
 analysis of the ~~α -pinene~~ α -pinene ozonolysis system (Kurtén-Kurtén et al., 2015), and the yield adjusted until the mechanism
 425 was able to achieve the best possible fit to the data. This resulted in a yield of 50% for RN26BO2 and 30% for RTN24O2.
 However, this remains a source of uncertainty and warrants further investigation. The low NO_x conditions meant that the
 autoxidation coefficients dominated the concentration of later generation O3RO2 and OHRO2 and, from this starting point,
 the autoxidation rate coefficients for later generations were fitted against experimental data over multiple rounds of
 optimisation (Table 4). The autoxidation coefficient for the 1st generation OHRO2, RTN28BO2, was taken as 2.1 s⁻¹ based on
 430 Xu et al (2018). ~~Estimation of the uncertainty in the autoxidation coefficient values is given in the Table S6. An estimation of
 the uncertainty in the autoxidation is also provided in Table 4. These values were calculated by adjusting the autoxidation rate
 coefficients one at a time to determine the maximum and minimum values of an autoxidation rate coefficient for which the
 corresponding peroxy radical would fall within the experimental uncertainty region. This approach neglects any cross-
 sensitivities through the joint uncertainty in several rate coefficients. A full Monte Carlo uncertainty analysis addressing this
 435 issue is beyond the scope of this manuscript but would make a valuable follow up for future work in this field. Therefore, the
 autoxidation rate coefficient uncertainties are large as the experimental error uncertainties are large.~~

The autoxidation coefficients in Table 4 are higher than those considered in the theoretical study of Scherivish et al (2019) but
 closer to the values measured by Zhao et al (2018) and ~~the values~~ suggested by Roldin et al (2019). The mechanism using the
 440 autoxidation coefficients from Table 4 and predicted the lumped higher generation species (5th generation for O3RO2, 4th
 generation for OHRO2) at concentrations higher than observed in the work by Berndt et al (2018b). This suggests there may
 be additional, as yet unknown loss processes for the more highly oxidised peroxy radical species which are not incorporated
 in this work. ~~Addition of such process would likely change the autoxidation coefficients and is an area for further study.
 Additional loss process would likely reduce the fitted autoxidation coefficients because they would provide an additional sink
 445 for the RO₂ species which does not lead to the production of the next generation RO₂. Therefore, the autoxidation coefficients
 determined in this work are likely to be upper limits but further insight into this is not possible with the data currently available.
 This is a key area for further study.~~

Unfortunately, the flow tube studies of Berndt et al (2018b) lack observations to constrain the full chemical space simulated
 450 by the box model. In particular there were no measurements of OH, HO₂ or NO. ~~Therefore, a rigorous series of sensitivity tests
 (described in the SI) were carried out to quantify the importance of uncertainty in the initial concentrations of OH, NO and~~

HO₂ on the results of the model. Initial OH was shown to have no effect on the measured parameters (O₃RO₂, OHRO₂ and accretion products) while NO and HO₂ had some effect on OHRO₂ (mainly through the change to OH) and C₂₀d (via the change to radical termination rate). Initial conditions of 10⁶ cm⁻³ for OH and 4 ppt for HO₂, NO and NO₂ were used. Based on the sensitivity simulations it was concluded that realistic deviations in concentration of +10 ppt / - 3 ppt for HO₂, NO and NO₂ and ± 10⁶ cm⁻³ / - 5×10⁵ cm⁻³ for OH from the initial values would not lead to deviations in the concentrations of RO₂ or accretion products sufficient to warrant a change in the autoxidation coefficients. The effect of the uncertainty in the initial experimental concentrations of NO, HO₂ and OH on the modelled concentrations of O₃RO₂, OHRO₂ and accretion products and thus fitted the autoxidation coefficients and accretion production formation rates coefficients was investigated with a series of sensitivity tests. Initial conditions of 10⁶ cm⁻³ for OH and 4 ppt for HO₂ were used. NO and NO₂ were initialised at 4 ppt, based on the purity of the flow gas (personal communication with T. Berndt). For HO₂, NO and NO₂ sensitivity simulations indicated that increases of 10 ppt (250% increase) and decreases of 3 ppt (75% decrease) did not lead to deviations in the concentrations of RO₂ or accretion products sufficient to warrant a change in the rate coefficients for autoxidation or accretion product formation. Initial OH concentration had negligible effect (<5% change) on O₃RO₂, OHRO₂ and C₂₀d when varied over 10⁵ – 2×10⁶ cm⁻³ (90 % decrease, 100 % increase).

3.1.1 Varying α -pinene Experiment

In Simulation A, the mechanism was used to simulate various experiments with increasing initial mixing ratios of α -pinene with a fixed mixing ratio of 26 ppb of O₃. The modelled 1st-4th generation O₃RO₂ species (Fig. 3(b~~a~~)) agreed well with the observed concentrations, with all of the model results falling within experimental uncertainty bounds (although we note these are large).

The model was also able to reproduce the 2nd and 3rd gen OHRO₂ species well (Fig. 3(a)) but struggled with the 1st generation OHRO₂ species, overestimating it by a factor of 10, despite reproducing the general trend of variation with α -pinene. The experimental measurements of 1st generation OHRO₂ concentration from Berndt et al (2018b) were believed to be underestimated by about a factor of 5 ~~which explains some, but not all of the model experimental discrepancy.~~ (Fig. S3). This suggests the model overprediction of the concentration of OHRO₂ may be about a factor of 2. The cause of the discrepancy between modelled and measured 1st generation OHRO₂ remains unclear. The rate coefficient for the production of the 1st generation OHRO₂ has undergone extensive evaluation and the same coefficient is used in the CRI v2.2 parent mechanism which has been optimised against the Master Chemical Jenkin (Jenkin et al., 1997, Saunders et al., 2003, Jenkin et al., 2015, Jenkin et al., 2019a). Sensitivity tests perturbing the branching ratio between RTN28AO₂ and RTN28BO₂ revealed that even doubling the fraction of RTN28BO₂, a significant deviation from literature (Berndt et al., 2016, Pye et al., 2018), had negligible effect as did changing initial [OH] by +100 % / -90%. Another explanation is the presence of additional, as yet unknown loss processes not currently included in the model, but in the absence of additional data, no further insights can be made at this time. More importantly, the 1st generation OHRO₂ does not form HOM itself and so it is unlikely to have a significant impact on HOM concentration. Furthermore, the modelled 1st generation OHRO₂ was dominated by RTN28AO₂, the species which does not autoxidise to form later generation RO₂. Nevertheless, this remains an important area for future work but one where more data is needed for additional constraints to be put in place.

3.1.2 Varying Isoprene Experiment

In Simulation B, varying initial concentrations of isoprene were employed under conditions of fixed initial mixing ratios of α -pinene (15.6 ppb) and O₃ (80 ppb). The model was able to reproduce the observed decline in the 2nd and 3rd generation OHRO₂ species (Fig. 4(a)) with increasing isoprene while also reproducing the minor decrease in the O₃RO₂ species (Fig. 4(b)). The decline in OHRO₂ mirrored the modelled decrease in OH, providing a strong indication that OH scavenging by isoprene is playing a major role in decrease in OHRO₂, as suggested by McFiggans et al (2019), also highlighting the need for better understanding of HO_x-recycling during isoprene oxidation.

3.1.3 Simulation of Accretion Products

The 20-carbon accretion products were measured in both the isoprene-free, varying α -pinene experiment (as in Fig. 3) and, separately, under conditions of constant α -pinene and varying isoprene (as in Fig. 4). As discussed in Section 2.3, the fitted rate coefficients for 20-carbon accretion product formation were fitted against experimental data (Berndt et al., 2018b) and incorporated the increase in propensity to form accretion products with RO₂ oxidation, varied based on the extent of oxidation of the reacting peroxy radical with the value of k_{13} ranging over 0.4 – $3.6 \times 10^{-11} \text{ cm}^3 \text{ molecule}^{-1} \text{ s}^{-1}$. This reproduced, within experimental error, the total observed C₂₀d concentrations for both experiments (Fig. 5 and Fig. S1) and compared favourably to the values calculated by Berndt of 0.97 – $7.9 \times 10^{-11} \text{ cm}^3 \text{ molecule}^{-1} \text{ s}^{-1}$.

The species with the lowest functionality, the 1st generation OHRO₂ (RTN28AO₂ and RTN28BO₂), which contain only 3 oxygens, were assigned had the lowest value of k_{13} ($0.4 \times 10^{-11} \text{ cm}^3 \text{ molecule}^{-1} \text{ s}^{-1}$) while the 1st generation O₃RO₂ (RN26BO₂) with 4 oxygens were assigned had $k_{13} = 0.97 \times 10^{-11} \text{ cm}^3 \text{ molecule}^{-1} \text{ s}^{-1}$, its self-reaction rate coefficient determined by Berndt et al (2018b). The most functionalised species for O₃RO₂ (RN_xBO_yO₂) and OHRO₂ (RTN_xBO_yO₂) were assigned values of k_{13} of $3.6 \times 10^{-11} \text{ cm}^3 \text{ molecule}^{-1} \text{ s}^{-1}$ and $3.5 \times 10^{-11} \text{ cm}^3 \text{ molecule}^{-1} \text{ s}^{-1}$ respectively. The fitted rate coefficients used were in line with the range 0.97 – $7.9 \times 10^{-11} \text{ cm}^3 \text{ molecule}^{-1} \text{ s}^{-1}$ (with an uncertainty no greater than a factor of 3) measured by Berndt et al (2018b) and the full list of values is given in the reaction list in the SI. This reproduced, within experimental error, the total observed C₂₀d concentrations for both experiments (Fig. 5 and Fig. S1) as well as the RO₂ in Simulations A and B. Sensitivity studies which scaled all k_{13} values by the same factor before rerunning Simulation B and comparing the output to experimental data suggested that variations in the C₂₀d formation rate coefficients of +100 % / -35 % spanned the experimental uncertainty (Table S6).

Using values of $k_{13} = 0.1$ – $3 \times 10^{-12} \text{ cm}^3 \text{ molecule}^{-1} \text{ s}^{-1}$, as suggested by Roldin et al (2019) for C₂₀d formation, produced C₂₀d concentrations lower than those observed (Fig S1) while values of 1 – $8 \times 10^{-10} \text{ cm}^3 \text{ molecule}^{-1} \text{ s}^{-1}$ from Molteni et al (2019) produced values which were higher than observation.

The fitted rate coefficients for 15-carbon accretion product formation, fitted against experimental data, were also varied increased with based on the extent of oxidation of the reacting peroxy radical. Values of k_{16} ranging over from $1.2 \times 10^{-12} \text{ cm}^3 \text{ molecule}^{-1} \text{ s}^{-1}$ for the least oxidised RO₂ to $-5 \times 10^{-12} \text{ cm}^3 \text{ molecule}^{-1} \text{ s}^{-1}$ for the most oxidised species (Fig. 5 and Fig. S2) reproduced observed levels of the C₁₅d accretion product (Fig. 5 and Fig. S2) from the constant α -pinene and variable isoprene experiments (as in Fig. 4) and were lower than the values measured by Berndt (1.3 – $2.3 \times 10^{-11} \text{ cm}^3 \text{ molecule}^{-1} \text{ s}^{-1}$ with an uncertainty no greater than a factor of 3). Sensitivity studies which scaled all k_{13} values by the same factor before rerunning Simulation B and comparing the output to experimental data suggested that variations in the C₁₅d formation rate coefficients of ± 50 % spanned the experimental uncertainty (Table S6).

Figure 5 shows that the decrease in 20-carbon accretion products with increasing isoprene far outweighs the increase in 15-

535 carbon accretion products. The mechanism reproduces the general trend of suppression of **total accretion product concentration with increasing initial isoprene concentration**. This finding is in good agreement with McFiggans et al (2019) and highlights a key component of the new mechanism which simple mechanisms (e.g. Gordon et al., 2016) will miss. In the model this net decrease in accretion products concentrations is driven in part by OH scavenging (and the subsequent reduction in OHRO2 (Fig. 4)). In this work this was the major driver of C20d decrease. However, suppression was also observed due to scavenging
 540 of C10RO2 by isoprene-derived RO2 as observed by McFiggans et al (2019). The influence of smaller peroxy radicals such as that from methane on accretion product formation (McFiggans et al., 2019) will be an area of future investigation.

3.2 HOM yield variation with temperature **and NO_x**

Autoxidation reactions have significant positive temperature dependencies (Praske et al., 2018, Bianchi et al., 2019, Jenkin et al., 2019a). Accordingly, HOM yields are expected to be highly temperature sensitive. Quéléver et al (2019) recorded a 50-fold increase in HOM yield at 293 K relative to 273 K. This temperature variation cannot be attributed to the temperature dependence of the initial oxidation of α -pinene as the rate coefficient of ozonolysis increases only 17% between 273 K and 293 K while the reactions with OH and NO₃ exhibit negative temperature dependencies. Frege et al (2018) measured a decrease in O:C ratio values in HOMs with reducing temperatures, attributing this to a reduction in autoxidation.
 545

Variation in peroxy radical structure and functionality will result in different generation peroxy radicals having different barriers to autoxidation (Bianchi et al., 2019). A few modelling studies have considered the temperature dependencies of the autoxidation rate coefficient in peroxy radical from α -pinene derivatives. Schervish et al (2019) considered a simple approach where all generations of peroxy radicals from α -pinene ozonolysis had a fixed activation energy of 62.4 or 66.5 KJ mol⁻¹ ($\theta =$
 555 7500-8000 K when rate coefficient is expressed as $k=Ae^{-\theta/T}$), while noting that a reduction in barriers to autoxidation with increasing functionality is plausible but so far unproven. By contrast, Roldin et al (2019) considered a higher activation energy of 100.4 KJ mol⁻¹ ($\theta = 12077$ K) based on the theoretical work of Kurtén et al (2015) which identified activation energies of 90-120 KJ mol⁻¹ for α -pinene.

560 Given the lack of additional literature in this area, 43 versions of the new mechanism were created to probe the effects of temperature and activation energy on HOM yield and subsequent evolution. In each mechanism all autoxidation reactions (for O3RO2 and OHRO2) had the same activation energy while all other rate coefficients were the same across mechanisms (Table S2). Activation barriers of $\theta = 6000$ K, $\theta = 9000$ K and $\theta = 12077$ K were chosen as they included the range suggested by Roldin et al (2019) and Schervish et al (2019) and the mechanism versions termed HOM₆₀₀₀, HOM₉₀₀₀ and HOM₁₂₀₇₇
 565 respectively. For the temperature dependent versions, the pre-exponential factor of the autoxidation coefficient (Table S5) was adjusted so that the autoxidation coefficients were the same at 297 K as those derived from the comparison to experimental data from Berndt et al (2018b). It is recognised that the autoxidation steps are likely to have different activation energies, but this analysis provides a first approximation of the influence of activation energy on HOM formation.

570 In a simulation modelling an instantaneous injection of α -pinene (Simulation C), the HOM yield for the 10-carbon species, individually and in total (defined in the SI), was calculated with the three different temperature dependencies (HOM₆₀₀₀, HOM₉₀₀₀ and HOM₁₂₀₇₇) at temperatures of 270 K, 290 K and 310 K for initials conditions of α -pinene 15 ppb, O₃ 40 ppb and OH at 10⁶ cm⁻³ and a temperature independent condensation sink of 2×10⁻³ s⁻¹.

575 Figure 6(a) shows the results from the simulations performed with initial concentrations of NO and NO₂ of 0.01-10 ppb. These simulations showed that the 10-carbon HOM yield tends to increase slightly from very low (0.02~~1~~ ppb) to moderate (2~~1~~ ppb) NO_x and ~~before starting to decrease then decline rapidly~~ with increasing NO_x thereafter. This behaviour is likely to be due to the inclusion in the mechanism of the isomerisation pathway via reaction with NO which yields the next generation peroxy radical. This pathway has been suggested as an important route for forming more highly oxidised derivatives of ~~α -pinene~~ α -pinene due to the potential rapid ring-opening mechanism involving alkoxy radicals and the cyclobutyl ring found in ~~α -pinene~~ α -pinene ozonolysis products (Rissanen et al., 2015). Figure 6(a) indicates that the absolute yield is also sensitive to temperature, with the highest yields simulated at the highest temperatures. At low temperatures (blue data), the uncertainty in autoxidation temperature dependence has the greatest effect while at high temperature this feature is muted. The increase in yield with temperature is in qualitative agreement with observation (Quéléver et al., 2019, Simon et al., ~~2020~~2019).

585

The model predicted total HOM yields at 290 K of ~~4.51.9~~ ± 0.24 % (0.01 ppb NO) to ~~5.73.9~~ ± 0.54 % (1 ppb NO), ~~with the quoted range resulting from the range of temperature dependencies considered.~~ This is ~~well~~ within the ranges previously suggested by ~~Jokinen et al (2015) (1.7-6.8 %) and close to the values from Ehn et al (2014) (3.5-10.5 %) at similar temperature and α -pinene concentrations as well as comparing favourably to yield measured by and Sarnela et al (2018) (3.5-6.5%), Jokinen et al (2014) (1.7-6.8 %) and while lower than Roldin et al (2019) (~7%).~~ indicating that the mechanism is doing a good job at ~~simulating HOM yield~~. In addition, the HOM yield at 270 K of ~~~0.67-1.93~~ % compared favourably with the yield of ~2% determined by Roldin et al (2019). ~~This suggests that the mechanism is doing a good job at simulating HOM yield. The slight low bias may be in part due the values of k14 and k15 which were shown to influence the HOM yield relatively strongly. Sensitivity tests involving doubling and halving of the rate coefficients produced HOM yield changes of around +65% and -40% respectively while preserving the general dependencies on NO_x and temperature (Fig. S4(a)) (Table S6). This area of uncertainty will be the focus of future work.~~

600

~~The HOM yield showed negligible sensitivity to the alkoxy radical decomposition-isomerisation branching ratio below 200 ppt of NO_x and around ± 0.7 percentage points (~20 %) at 2 ppb NO_x. However, this range was encompassed by the range arising from autoxidation temperature dependence uncertainty. Above 2 ppb NO_x, this ratio had greater influence as NO reactions with RO₂ started to compete more efficiently with autoxidation but this coincided with the sharp drop in HOM yield (Fig. S4(b)). Therefore, while further work is needed to develop the isomerisation-decomposition branching ratio description, it is unlikely to have a significant influence in the low-NO_x conditions where HOM are predicted to be most prevalent and in these conditions the uncertainty in temperature dependence of autoxidation is predicted to have a larger effect~~

605

3.3 Comparison to CRI v2.2

The ability of the new mechanism to reproduce the concentrations of key atmospheric species from the CRI v2.2 under different emissions of NO_x and α -pinene was assessed using an 8 day box modelling run (Simulation D). Over the majority of emissions space, O₃ differed by less than 0.05 ppb (0.1%), OH by less than 0.4% and NO by less than 2.5 ppt (0.4%) (Fig. ~~S64-S86~~ S64-S86) with ~~similar (or better) agreement for other important species (Fig. S97-S175).~~ Acetone was routinely underpredicted (Fig. ~~S186~~ S186) by between a factor of ~14 at 50 ppt NO_x and by ~20 % at 2-10 ppb of NO_x but this did not result in significant deviation between the base mechanism and new mechanism for O₃ or OH. This indicates that the basic features of atmospheric chemistry, such as HO_x recycling processes added in the CRI v2.2, which have been shown to have important consequences for atmospheric composition (Jenkin et al., 2019b), are preserved in the new mechanism.

610

3.3.1 Peroxy Radicals and HOMs

As our model simulations indicate, and as has previously been observed (Lehtipalo et al., 2018), at higher concentrations of NO_x there is inhibition of HOM formation with the principle driver being the reaction of NO with peroxy radicals occurring at a rate outcompeting autoxidation. While reaction with NO can in part aid HOM formation by increasing the isomerisation pathway, the fragmentation pathway (forming smaller species) and formation of non-HOM nitrates leads to a reduction in total HOM. Accordingly, all these mechanisms predict a decrease in HOM concentration with increasing NO_x (Fig. 6(b)). Furthermore, very little difference is observed between the different HOM mechanisms, suggesting that uncertainty in the activation energy may not be too great an impediment to understanding general HOM behaviour, at least at the temperatures considered.

However, it should be remembered that, at present, the HOM tracers in the mechanism represent a range of species with varying levels of oxidation. For example, C10z corresponds to HOMs formed from 2nd to 5th O3RO2 generations of O3RO2 and C10x to HOMs from all generations of OHRO2. The predicted concentrations of different generations of O3RO2 (Fig. S197) and OHRO2 (Fig. S2048) were also observed to decrease with NO_x with little difference between different HOM mechanisms. Furthermore, the most abundant peroxy radicals for both pathways were the lumped highest generation species, highlighting the potential issue of lack of loss processes for the most highly oxidised RO₂ species as was encountered when fitting parameters to flow cell data.

635

3.3.2 Closed Shell and non-HOM Species

In the base mechanism, α -pinene oxidation predominantly leads to the formation of the closed shell species CARB16 and TNCARB26 (carbonyls) and RN18NO₃ and RTN28NO₃ (nitrates). Whilst the base mechanism has been optimised against the MCM, these pathways have not themselves been tuned extensively to reproduce concentrations observed in experimental systems. These species are still present in the new mechanism but the concentrations of RTN28NO₃ and TNCARB26 are predicted to be slightly lower than in the base mechanism (Fig. S2149) while CARB16 is simulated as being much lower in concentration than in the base mechanism at low NO_x with the difference attributed to the added competition from the autoxidation pathways.

645

The nitrate species formed from RN18AO₂ in the base mechanism, RN18NO₃, is significantly lower in the HOM mechanism. Nitrate yield is a complicated topic, not least because the MCM predicts that the peroxy radicals C107O₂ and C109O₂, which are used to represent the 1st generation O3RO₂ in part (RN26BO₂), do not form nitrate upon reaction with NO or NO₃. Importantly this does not affect the O₃ and OH concentrations, but this should be an area that future work addresses.

650 4 Simulation of HOM Vertical Profiles

Given the success of the mechanism in simulating the laboratory flow tube experiments and its ability to capture the sensitivity of HOMs to changes in the reactivity of the peroxy radical pool, we focus now on using the scheme to simulate tropospheric conditions to investigate, to first order, how the scheme would predict ambient HOM concentrations. Here we focus on using our new mechanism to simulate the surface [HOMs] and the vertical profile of [HOMs]. We also [look](#) at the effect of the simulated HOMs on nucleation rates in the lower troposphere.

655

The vertical profiles of HOMs over the boreal forest near Hyttiala in Finland (61° 9' N, 23° 4' E) and near Manaus in the Amazon rainforest (-2° 35' N, 60° 12' W) were investigated along with surface concentrations representative of Brent, Alabama (32.903°N, 87.250°W). For each altitude level, the sensitivity simulations were performed with three different activation energies for the autoxidation steps (HOM₆₀₀₀, HOM₉₀₀₀ and HOM₁₂₀₇₇). Vertical transport was neglected - a different box model was run at each vertical level with the inputs being the output of a simulation with the UKCA model (Archibald et al., 2019) sampled at 14:00 LT (photolysis frequencies were adjusted to account for the solar zenith angle but not for altitude variation). Hourly concentration data from UKCA were provided for O₃, OH, isoprene, α -pinene, HO₂, NO, NO₂, NO₃, N₂O₅, temperature and pressure for 16th June averaged over 2010-2014, from the grid boxes in UKCA corresponding to the respective locations discussed above, and supplemented with monthly mean concentrations of a further 23 species (Table S3) with the concentration of certain species adjusted to observations (Kuhn et al., 2007 and Table 4.1) and scaled vertically to account for biases in the UKCA output. The scaled values of isoprene and α -pinene showed reasonable agreement with observations taken up to 80 m in altitude at the ATTO tower (Yáñez-Serrano et al., 2015). Modelled isoprene fell within 0.5 ppb of observation taken at 2 pm in June while modelled monoterpene were within 0.1 ppb of observation, well within the observational standard deviation in both cases (Fig. S22). HOM condensations sinks (CS) (equal for all HOM species) discussed in Lee et al (2016) (Table S4) were used at the surface and scaled using the modelled vertical profile of aerosol surface area density. Sensitivity studies revealed that the output of the 1D box modelling shows significant sensitivity of [HOMs] to the magnitude and profile of the CS (Fig. S22~~9~~). Therefore, we can suggest that our simulated vertical profiles be regarded as ~~illustrative semi-qualitative~~ as more work is required to identify if the condensation sink should be species dependent.

Table 5 summarises the comparison of our model simulations of near surface [HOMs] compared to observations. In the boreal forest in Hyttiala, the range of predicted 10-carbon [HOM] ~~falls at the higher end of the mean observational range is close to the mean observational value and well below the maximum observed concentrations (1-1.5 ppt)~~ (Roldin et al., 2019). ~~and T~~ the predicted 20-carbon accretion product concentration is around double the slightly above the mean observational range and well below the maximum observed values (0.6-0.7 ppt). In Alabama, the model produces a reasonable value given that the observation dataset includes 9-carbon species not considered in the model at present. The model results in Table 5 provide strong support that when implemented in a global chemistry climate model, our new scheme should perform well if the underlying emissions of BVOCs and NO_x and the CS are well simulated.

Figure 7 shows the concentrations of the different HOMs from the box model version as a function of altitude above Hyttiala and over the Amazon rainforest near Manaus. In both locations, the 10-carbon HOM profiles roughly mirror ~~α -pinene~~ α -pinene with roughly equal abundance of the species from ozonolysis and OH oxidation. HOM from OH showed a significantly greater sensitivity to temperature, diverging from the HOM from O₃ at around 5 km in Hyttiala and 8 km in the Amazon due to the elevated temperature profile. This was attributed to the requirement for 1st generation OHRO₂ to undergo two autoxidation steps before HOMs can be formed (Section 2.2) while 1st generation O₃RO₂ only need to undergo one autoxidation step and thus have a weaker temperature dependence. This effect only becomes noticeable at temperatures below ~250 K when autoxidation ceases to compete effectively with bimolecular reactions. In spite of higher [BVOCs], the considerably higher CS in the Amazon region (Lee et al., 2016) resulted in lower [HOM] within the boundary layer than at Hyttiala, while the warmer temperatures also resulted in a negligible dependence on the activation energy in the lowest 4 km (i.e. the shaded areas are smaller in Fig. 7(b) than in Fig. 7(a)).

Hyytiälä and the Amazon represent very different chemical environments with the isoprene/ α -pinene ratio (I/AP) playing an important role in the accretion product distribution; 15-carbon accretion products are simulated as being more abundant than 20-carbon accretion products in the Amazon with the biggest difference predicted at low altitude where I/AP is greatest. By contrast, in Hyytiälä where I/AP is smaller, 20-carbon accretion products are more abundant.

Figure 7 highlights strong vertical profiles for the simulated [HOMs]. The simulations over the Amazon suggest a significant secondary peak in [HOMs] at around 4-5 km in altitude; in part linked to an increase in the [BVOCs] at this height. In our simulations each vertical level is represented by a different box model simulation so there is no simulation of the advection of HOMs. It will be interesting to see how future fully coupled model simulations simulate the vertical profile of [HOMs] and how this affects processes like aerosol formation and climate.

4.1 Nucleation Rates

Given the important role Gordon et al (2016) identified for HOMs in NPF we extend our 1-D calculations to investigate the implications of the predicted HOM profiles on nucleation rates using monthly mean climate model data from the PD and PI. Nucleation rates from two different nucleation mechanisms were studied: (i) neutral and ion-induced pure biogenic nucleation (PBN) (Kirkby et al., 2016); and (ii) activation of sulphuric acid (SA_{act}) (Kulmala et al., 2006; Sihto et al., 2006) suitable for the boundary layer. All HOMs were treated as being equally proficient at nucleating new particles, in agreement with approach and nucleation rates used by Kirkby et al (2016) and Gordon et al (2017). Recent work by Heinritzi et al (2020) suggests that 20-carbon accretion products may be better at nucleating new particles and therefore the results presented are likely to be an upper bound although nevertheless informative. Representing the different nucleation efficiencies of different HOM species will be investigated in future work. The results of the calculations of nucleation rates using these schemes are summarised in Figure 8. (The nucleation rate expressions are given in the SI.)

There exists little observational data on nucleation solely from PBN mechanisms, making model validation hard. Modelled surface sulphuric acid concentrations at Hyytiälä ($2-3 \times 10^6 \text{ cm}^{-3}$) fall within the range of observations ($3 \times 10^5 - 2 \times 10^7 \text{ cm}^{-3}$ (Boy et al., 2005, Petäjä et al., 2009)). Modelled concentrations in the Amazon ($3 \times 10^4 \text{ cm}^{-3}$) were slightly lower than observation ($10^5 - 10^6 \text{ cm}^{-3}$ (Wimmer et al., 2018)) although the observations were taken in a pasture site downwind of Manaus surrounded by the rainforest not in the rainforest itself and are therefore likely to be higher than in-situ rainforest values. Thus, the nucleation rates we have calculated for SA_{act} are likely to be a reasonable estimate in Hyytiälä and slightly low biased in the Amazon.

Figure 8 shows predicted nucleation rates in the PI and PD in the Amazon and Hyytiälä derived from our simulated [HOMs] vertical profile in the boundary layer and low free troposphere using June monthly mean data from a UKESM historical run taken from the PI (June average 1851-1856) and PD (June average 2009-2014). In all cases, the PBN nucleation rates decline rapidly with height above the boundary layer. In the Boreal forest, the nucleation rate from PBN at very low altitudes is calculated to be around 20-25% of that from SA_{act} in the PD. However, in the PI it is comparable to the SA_{act} rate, contributing 40-80 % of the total nucleation rate in the lowest 500 m (Fig. S234). The greater relative importance of PBN in the PI, despite lower predicted [HOM], was attributed to two factors. Firstly, predicted steady state ion concentrations were higher in the PI in Finland than the PD due to the PI's lower ion CS. This increased the rate of the ion-induced pathway PBN pathway. Secondly, the considerably lower modelled concentrations of sulphuric acid in PI (around 10x lower than in the PD) reduced the importance of SA_{act} . By contrast, the lower concentrations of predicted [HOM] in the Amazon led to PBN having a much

740 smaller contribution to the total nucleation rate (< 5% in the PD and a negligible impact in the PI). This is in agreement with multiple sources (Andreae et al., 2015, Wimmer et al., 2018, Rizzo et al., 2018). The importance of PBN in the PI atmosphere in certain locations, qualitatively in agreement with Gordon et al (2016), illustrates the potential importance including PBN in climate models could have on aerosol burden and the associated radiative effects.

5 Summary and Conclusions

745 We present a novel chemical mechanism, CRI-HOM, for simulating HOM formation based on the latest version of the Common Representative Intermediate scheme (CRI v2.2). Focusing on the most important natural source of HOMs, α -pinene, the CRI-HOM mechanism is one of the first HOM mechanisms ready for incorporation into existing chemistry-aerosol climate models. The scheme is much more complex than previous steady state approximations (Gordon et al., 2016) and so enables non-linear interactions and feedbacks with the chemical environment to be represented, but far more concise
750 than other mechanisms that have been developed which treat the complex structural characteristics of the formation of HOMs (Roldin et al., 2019). The addition of 12 new species and 66 reactions means that this scheme can be used for long term global chemistry-aerosol-climate studies.

755 Firstly, the mechanism was optimised against flow cell data and validated by comparison to observed HOM yields. A key result was the ability of the mechanism to reproduce observations of isoprene driving a decline in HOM peroxy radical precursors and 20-carbon accretion products (and total accretion product concentration) (McFiggans et al., 2019). The need for further research into the loss processes of the highly oxidised peroxy radicals was identified to reconcile the disparity between modelled and observed concentrations. The effect of other peroxy radicals, such as those from smaller more abundant organic species, on accretion product formation is also an area for future investigation.

760 After optimisation, the CRI-HOM was compared to the base mechanism (CRI v2.2) and very good agreement was observed for a wide range of atmospheric gases including O₃, OH and its precursors. This indicated that the important features of HO_x recycling and accurate O₃ representation, developed in the CRI v2.2, had been preserved in CRI-HOM.

765 In further tests of CRI-HOM, HOM yields and concentrations were predicted to decrease with increasing NO_x and increase with temperature, in agreement with previous theoretical and observational studies. The temperature dependence of autoxidation was investigated using activation energies spanning the range of values suggested in literature (Roldin et al., 2019, Schervish et al., 2019). Temperature dependence was predicted to have a significant effect on HOM yield at 270 K but a much smaller effect at 290 K and 310 K.

770 In a final experiment, vertical profiles of HOM were simulated using a pseudo 1D box model for Finland, Alabama and the Amazon using chemistry climate model data as inputs. The model performed well relative to observations in Finland and Alabama. The influence of the condensation sink (CS) value on [HOM] was shown to be significant with [HOM] predicted to be significantly lower in the Amazon, despite higher [BVOC], due to the higher CS. Improving the description of the CS within the mechanism has been identified as an important area of future work. The profiles also illustrated the dependence of HOM on the chemical environment, driven chiefly by the interaction of isoprene and monoterpenes. The higher concentrations of isoprene in the Amazon resulted in lower concentrations of the most involatile species, the 20-carbon accretion product. Simulated [HOM] were also used to probe the importance of various particle nucleation mechanisms. In Finland, pure biogenic nucleation mechanism (i.e. nucleation without sulphuric acid) at low altitude was predicted to be
780 responsible for around 60% of new particle formation in the lowest 500 m in the pre-industrial atmosphere and around 20%

in the present day, indicating the importance of HOMs, particularly in the pre-industrial, with implications for aerosol burden and climate. PBN was predicted to be less important in the Amazon given the lower simulated [HOM].

785 CRI-HOM can provide a framework for simulating HOMs in global chemistry-aerosol-climate studies and simulating the effects of isoprene-driven suppression of involatile biogenic-derived species and the consequences on SOA and NPF while also providing a state-of-the-art description of atmospheric chemistry. Such an effect, and the influence on the proposed “BVOC negative feedback”, is likely to be important in a warming climate with enhanced emissions of BVOCs and determining the size and sign of the feedback. Once incorporated into a global chemistry-aerosol-climate model, assessing the effect of HOMs on pre-industrial, present day and future climate will be key area of future work.

790

Supplement. The supplement related to the article is available online.

Financial Support. JW is funded by a Vice Chancellor’s Award from the Cambridge Trust. We would like to thank the Cambridge-LMU Strategic Partnership for supporting collaborations with the BOXMOX model. We would like to thank 795 NERC, through NCAS, and the Met Office for the support of the JWCRP UKCA project. SA and ATA would like to thank NERC PROMOTE (NE/P016383/1). HG is supported by the NASA ROSES Atmospheric Composition Modeling and Analysis Program under grant number 80NSSC19K0949.

800 *Data Availability.* All modelled data is available upon request from James Weber and all experimental data from Torsten Berndt. [The KPP files for the CRI-HOM mechanism have been deposited in the University of Cambridge data repository and can be viewed at doi.org/10.17863/CAM.54546.](https://doi.org/10.17863/CAM.54546)”

Author Contributions. Mechanism development was done by JW, ATA, ME, SA, modelling experiments were designed and executed by JW, ATA, PG, HG, CK and flow cell data was compiled and interpreted by TB. JW and ATA wrote the paper. 805 All co-authors discussed the results and commented on the paper.

Competing Interests. All authors declare that they have no competing interests.

References

810 Andreae, M. O., Acevedo, O. C., Araùjo, A., Artaxo, P., Barbosa, C. G. G., Barbosa, H. M. J., Brito, J., Carbone, S., Chi, X., Cintra, B. B. L., da Silva, N. F., Dias, N. L., Dias-Júnior, C. Q., Ditas, F., Ditz, R., Godoi, A. F. L., Godoi, R. H. M., Heimann, M., Hoffmann, T., Kesselmeier, J., Könemann, T., Krüger, M. L., Lavric, J. V., Manzi, A. O., Lopes, A. P., Martins, D. L., Mikhailov, E. F., Moran-Zuloaga, D., Nelson, B. W., Nölscher, A. C., Santos Nogueira, D., Piedade, M. T. F., Pöhlker, C., Pöschl, U., Quesada, C. A., Rizzo, L. V., Ro, C.-U., Ruckteschler, N., Sá, L. D. A., de Oliveira Sá, M., Sales, C. B., dos Santos, R. M. N., Saturno, J., Schöngart, J., Sörgel, M., de Souza, C. M., de Souza, R. A. F., Su, H., Targhetta, N., Tóta, J., Trebs, I., 815 Trumbore, S., van Eijck, A., Walter, D., Wang, Z., Weber, B., Williams, J., Winderlich, J., Wittmann, F., Wolff, S., and Yáñez-Serrano, A. M.: The Amazon Tall Tower Observatory (ATTO): overview of pilot measurements on ecosystem ecology, meteorology, trace gases, and aerosols,

820 Archibald, A.T., Abraham, N.L., Bellouin, N., Boucher, O., Braesicke, P., Bushell, A., Carslaw, K., Collins, B., Dalvi, M., Emmerson, K. and Folberth, G., 2019. Unified Model Documentation Paper No. 84: United Kingdom Chemistry and Aerosol (UKCA) Technical Description MetUM Version 11.3. UK Met Office, Exeter, UK.

Atkinson, R. and Arey, J.: Atmospheric degradation of volatile organic compounds. *Chemical reviews*, 12, 4605-4638, doi.org/10.1021/cr0206420, 2013.

825

Bates, K. H. and Jacob, D. J.: A new model mechanism for atmospheric oxidation of isoprene: global effects on oxidants, nitrogen oxides, organic products, and secondary organic aerosol, *Atmos. Chem. Phys.*, 19, 9613–9640, doi.org/10.5194/acp-19-9613-2019, 2019.

830

Berndt, T., Richters, S., Jokinen, T., Hyttinen, N., Kurtén, T., Otkjær, R.V., Kjaergaard, H.G., Stratmann, F., Herrmann, H., Sipilä, M. and Kulmala, M.: Hydroxyl radical-induced formation of highly oxidized organic compounds. *Nature communications*, 1, 1-8, 10.1038/ncomms13677, 2016.

Berndt, T., Scholz, W., Mentler, B., Fischer, L., Herrmann, H., Kulmala, M. and Hansel, A.: Accretion Product Formation from Self-and Cross-Reactions of RO₂ Radicals in the Atmosphere. *Angewandte Chemie International Edition*, 57, 3820-3824, doi.org/10.1002/anie.201710989, 2018a.

835

Berndt, T., Mentler, B., Scholz, W., Fischer, L., Herrmann, H., Kulmala, M. and Hansel, A.: Accretion product formation from ozonolysis and OH radical reaction of α -pinene: mechanistic insight and the influence of isoprene and ethylene. *Environmental science & technology*, 52, 11069-11077, doi.org/10.1021/acs.est.8b02210, 2018b.

840

Bianchi, F., Kurtén, T., Riva, M., Mohr, C., Rissanen, M.P., Roldin, P., Berndt, T., Crouse, J.D., Wennberg, P.O., Mentel, T.F. and Wildt, J.: Highly oxygenated organic molecules (HOM) from gas-phase autoxidation involving peroxy radicals: A key contributor to atmospheric aerosol. *Chemical reviews*, 119, 3472-3509, doi.org/10.1021/acs.chemrev.8b00395, 2019.

845

Boy, M., Kulmala, M., Ruuskanen, T. M., Pihlatie, M., Reissell, A., Aalto, P. P., Keronen, P., Dal Maso, M., Hellen, H., Hakola, H., Jansson, R., Hanke, M., and Arnold, F.: Sulphuric acid closure and contribution to nucleation mode particle growth, *Atmos. Chem. Phys.*, 5, 863–878, doi.org/10.5194/acp-5-863-2005, 2005.

Carslaw, K. S., Boucher, O., Spracklen, D. V., Mann, G. W., Rae, J. G. L., Woodward, S., and Kulmala, M.: A review of natural aerosol interactions and feedbacks within the Earth system, *Atmos. Chem. Phys.*, 10, 1701-1737, doi.org/10.5194/acp-10-1701-2010, 2010

850

Crouse, J.D., Nielsen, L.B., Jørgensen, S., Kjaergaard, H.G. and Wennberg, P.O.: Autoxidation of organic compounds in the atmosphere. *The Journal of Physical Chemistry Letters*, 4), 3513-3520, doi.org/10.1021/jz4019207, 2013.

855

Dal Maso, M., Kulmala, M., Lehtinen, K.E., Mäkelä, J.M., Aalto, P. and O'Dowd, C.D.: Condensation and coagulation sinks and formation of nucleation mode particles in coastal and boreal forest boundary layers. *Journal of Geophysical Research: Atmospheres*, D19, PAR-2, doi.org/10.1029/2001JD00053, 2002.

860

~~Ehn, M., Kleist, E., Junninen, H., Petäjä, T., Lönn, G., Schobesberger, S., Maso, M.D., Trimborn, A., Kulmala, M., Worsnop, D.R. and Wahner, A.: Gas phase formation of extremely oxidized pinene reaction products in chamber and ambient air. *Atmospheric chemistry and physics*, 12, 5113–5127, doi:10.5194/acpd-12-4589-2012, 2012.~~

865

~~Ehn, M., Kleist, E., Junninen, H., Petäjä, T., Lönn, G., Schobesberger, S., Dal Maso, M., Trimborn, A., Kulmala, M., Worsnop, D. R., Wahner, A., Wildt, J., and Mentel, Th. F.: Gas phase formation of extremely oxidized pinene reaction products in chamber and ambient air. *Atmos. Chem. Phys.*, 12, 5113–5127, <https://doi.org/10.5194/acp-12-5113-2012>, 2012.~~

870

~~Ehn, M., Thornton, J.A., Kleist, E., Sipilä, M., Junninen, H., Pullinen, I., Springer, M., Rubach, F., Tillmann, R., Lee, B. and Lopez-Hilfiker, F.: A large source of low-volatility secondary organic aerosol. *Nature*, 506, 476–479, 865 doi:10.1038/nature13032 2014.~~

875

~~Jokinen, T., Berndt, T., Makkonen, R., Kerminen, V.M., Junninen, H., Paasonen, P., Stratmann, F., Herrmann, H., Guenther, A.B., Worsnop, D.R. and Kulmala, M.: Production of extremely low volatile organic compounds from biogenic emissions: Measured yields and atmospheric implications. *Proceedings of the National Academy of Sciences*, 112, 7123–7128, doi.org/10.1073/pnas.1423977112, 2014.~~

Frege, C., Ortega, I. K., Rissanen, M. P., Praplan, A. P., Steiner, G., Heinritzi, M., Ahonen, L., Amorim, A., Bernhammer, A.-
880 K., Bianchi, F., Brilke, S., Breitenlechner, M., Dada, L., Dias, A., Duplissy, J., Ehrhart, S., El-Haddad, I., Fischer, L., Fuchs, C., Garmash, O., Gonin, M., Hansel, A., Hoyle, C. R., Jokinen, T., Junninen, H., Kirkby, J., Kürten, A., Lehtipalo, K., Leiminger, M., Mauldin, R. L., Molteni, U., Nichman, L., Petäjä, T., Sarnela, N., Schobesberger, S., Simon, M., Sipilä, M., Stolzenburg, D., Tomé, A., Vogel, A. L., Wagner, A. C., Wagner, R., Xiao, M., Yan, C., Ye, P., Curtius, J., Donahue, N. M., Flagan, R. C., Kulmala, M., Worsnop, D. R., Winkler, P. M., Dommen, J., and Baltensperger, U.: Influence of temperature on
885 the molecular composition of ions and charged clusters during pure biogenic nucleation, *Atmos. Chem. Phys.*, 18, 65–79, doi.org/10.5194/acp-18-65-2018, 2018.

Gordon, H., Kirkby, J., Baltensperger, U., Bianchi, F., Breitenlechner, M., Curtius, J., Dias, A., Dommen, J., Donahue, N.M., Dunne, E.M. and Duplissy, J.: Causes and importance of new particle formation in the present-day and preindustrial
890 atmospheres. *Journal of Geophysical Research: Atmospheres*, 122, 8739–8760, doi.org/10.1002/2017JD026844, 2017.

~~Heinritzi, M., Dada, L., Simon, M., Stolzenburg, D., Wagner, A. C., Fischer, L., Ahonen, L. R., Amanatidis, S., Baalbaki, R., Baccarini, A., Bauer, P. S., Baumgartner, B., Bianchi, F., Brilke, S., Chen, D., Chiu, R., Dias, A., Dommen, J., Duplissy, J., Finkenzeller, H., Frege, C., Fuchs, C., Garmash, O., Gordon, H., Granzin, M., Haddad, I. E., He, X., Helm, J., Hofbauer, V., Hoyle, C. R., Kangasluoma, J., Keber, T., Kim, C., Kürten, A., Lamkaddam, H., Lampilahti, J., Laurila, T. M., Lee, C. P., Lehtipalo, K., Leiminger, M., Mai, H., Makhmutov, V., Manninen, H. E., Marten, R., Mathot, S., Mauldin, R. L., Mentler, B., Molteni, U., Müller, T., Nie, W., Nieminen, T., Onnela, A., Partoll, E., Passananti, M., Petäjä, T., Pfeifer, J., Pospisilova, V., Quéléver, L., Rissanen, M. P., Rose, C., Schobesberger, S., Scholz, W., Scholze, K., Sipilä, M., Steiner, G., Stozhkov, Y., Tauber, C., Tham, Y. J., Vazquez-Puffleau, M., Virtanen, A., Vogel, A. L., Volkamer, R., Wagner, R., Wang, M., Weitz, L., Wimmer, D., Xiao, M., Yan, C., Ye, P., Zha, Q., Zhou, X., Amorim, A., Baltensperger, U., Hansel, A., Kulmala, M., Tomé, A., Winkler, P. M., Worsnop, D. R., Donahue, N. M., Kirkby, J., and Curtius, J.: Molecular understanding of the suppression of new-particle formation by isoprene, *Atmos. Chem. Phys. Discuss.*, doi.org/10.5194/acp-2020-51, in review, 2020.~~

900

905 Hirsikko, A., Nieminen, T., Gagné, S., Lehtipalo, K., Manninen, H. E., Ehn, M., Hörrak, U., Kerminen, V.-M., Laakso, L., McMurry, P. H., Mirme, A., Mirme, S., Petäjä, T., Tammet, H., Vakkari, V., Vana, M., and Kulmala, M.: Atmospheric ions and nucleation: a review of observations, *Atmos. Chem. Phys.*, 11, 767–798, doi.org/10.5194/acp-11-767-2011, 2011.

[IUPAC Task Group on Atmospheric Chemical Kinetic Data Evaluation, \(http://iupac.pole-ether.fr\)](http://iupac.pole-ether.fr), accessed 17th May 2020.

910

Jenkin, M.E., Saunders, S.M. and Pilling, M.J.: The tropospheric degradation of volatile organic compounds: a protocol for mechanism development. *Atmospheric Environment*, 31, 81-104, doi.org/10.1016/S1352-2310(96)00105-7, 1997.

Jenkin, M.E., Watson, L.A., Utembe, S.R. and Shallcross, D.E.: A Common Representative Intermediates (CRI) mechanism for VOC degradation. Part 1: Gas phase mechanism development. *Atmospheric Environment*, 42, 7185-7195, doi.org/10.1016/j.atmosenv.2008.07.028, 2008.

915

Jenkin, M. E., Young, J. C., and Rickard, A. R.: The MCM v3.3.1 degradation scheme for isoprene, *Atmos. Chem. Phys.*, 15, 11433–11459, doi.org/10.5194/acp-15-11433-2015, 2015.

920

Jenkin, M. E., Valorso, R., Aumont, B., and Rickard, A. R.: Estimation of rate coefficients and branching ratios for reactions of organic peroxy radicals for use in automated mechanism construction, *Atmos. Chem. Phys.*, 19, 7691–7717, doi.org/10.5194/acp-19-7691-2019, 2019a.

925 Jenkin, M.E., Khan, M.A.H., Shallcross, D.E., Bergström, R., Simpson, D., Murphy, K.L.C. and Rickard, A.R.: The CRI v2.2 reduced degradation scheme for isoprene. *Atmospheric Environment*, 212, 172-182, doi.org/10.1016/j.atmosenv.2019.05.055, 2019b.

[Johnson, D. and Marston, G.: The gas-phase ozonolysis of unsaturated volatile organic compounds in the troposphere. *Chemical Society Reviews*, 4, 699-716, doi.org/10.1039/B704260B, 2018.](https://doi.org/10.1039/B704260B)

930

Jokinen, T., Sipilä, M., Richters, S., Kerminen, V.M., Paasonen, P., Stratmann, F., Worsnop, D., Kulmala, M., Ehn, M., Herrmann, H. and Berndt, T.: Rapid autoxidation forms highly oxidized RO₂ radicals in the atmosphere. *Angewandte Chemie International Edition*, 53, 14596-14600, doi.org/10.1002/anie.201408566

935 2014.

[Jokinen, T., Berndt, T., Makkonen, R., Kerminen, V.M., Junninen, H., Paasonen, P., Stratmann, F., Herrmann, H., Guenther, A.B., Worsnop, D.R. and Kulmala, M.: Production of extremely low volatile organic compounds from biogenic emissions: Measured yields and atmospheric implications. *Proceedings of the National Academy of Sciences*, 112, 7123-7128, doi.org/10.1073/pnas.1423977112, 2015.](https://doi.org/10.1073/pnas.1423977112)

940

Kiendler-Scharr, A., Wildt, J., Dal Maso, M., Hohaus, T., Kleist, E., Mentel, T.F., Tillmann, R., Uerlings, R., Schurr, U. and Wahner, A.: New particle formation in forests inhibited by isoprene emissions. *Nature*, 461, 381-384, doi.org/10.1038/nature08292 2009.

945

- Kirkby, J., Duplissy, J., Sengupta, K., Frege, C., Gordon, H., Williamson, C., Heinritzi, M., Simon, M., Yan, C., Almeida, J. and Tröstl, J.: Ion-induced nucleation of pure biogenic particles. *Nature*, 533, 521–526, doi.org/10.1038/nature17953, 2016..
- 950 Knote, C., Tuccella, P., Curci, G., Emmons, L., Orlando, J.J., Madronich, S., Baró, R., Jiménez-Guerrero, P., Luecken, D., Hogrefe, C. and Forkel, R.: Influence of the choice of gas-phase mechanism on predictions of key gaseous pollutants during the AQMEII phase-2 intercomparison. *Atmospheric Environment*, 115, 553-568, /doi.org/10.1016/j.atmosenv.2014.11.066, 2015.
- 955 Kuhn, U., Andreae, M. O., Ammann, C., Araújo, A. C., Brancaleoni, E., Ciccioli, P., Dindorf, T., Frattoni, M., Gatti, L. V., Ganzeveld, L., Kruijt, B., Lelieveld, J., Lloyd, J., Meixner, F. X., Nobre, A. D., Pöschl, U., Spirig, C., Stefani, P., Thielmann, A., Valentini, R., and Kesselmeier, J.: Isoprene and monoterpene fluxes from Central Amazonian rainforest inferred from tower-based and airborne measurements, and implications on the atmospheric chemistry and the local carbon budget, *Atmos. Chem. Phys.*, 7, 2855–2879, doi.org/10.5194/acp-7-2855-2007, 2007.
- 960 Kulmala, M., Laaksonen, A. and Pirjola, L.: Parameterizations for sulfuric acid/water nucleation rates. *Journal of Geophysical Research: Atmospheres*, 103, 8301-8307, doi.org/10.1029/97JD03718, 1998.
- Kulmala, M., Lehtinen, K. E. J., and Laaksonen, A.: Cluster activation theory as an explanation of the linear dependence between formation rate of 3nm particles and sulphuric acid concentration, *Atmos. Chem. Phys.*, 6, 787–793, 965 doi.org/10.5194/acp-6-787-2006, 2006.
- Kulmala M., Nieminen T., Chellapermal R., Makkonen R., Bäck J., Kerminen VM.: Climate Feedbacks Linking the Increasing Atmospheric CO₂ Concentration, BVOC Emissions, Aerosols and Clouds in Forest Ecosystems. In: Niinemets Ü., Monson R. (eds) *Biology, Controls and Models of Tree Volatile Organic Compound Emissions*. *Tree Physiology*, vol 5. Springer, 970 Dordrecht, doi.org/10.1007/978-94-007-6606-8_17, 2013.
- Kurtén, T., Rissanen, M.P., Mackeprang, K., Thornton, J.A., Hyttinen, N., Jørgensen, S., Ehn, M. and Kjaergaard, H.G.: Computational study of hydrogen shifts and ring-opening mechanisms in α -pinene ozonolysis products. *The Journal of Physical Chemistry A*, 119, 11366-11375, doi.org/10.1021/acs.jpca.5b08948, 2015. 975
- [Kurtén, T., Tiusanen, K., Roldin, P., Rissanen, M., Luy, J.N., Boy, M., Ehn, M. and Donahue, N., 2016.: \$\alpha\$ -Pinene autoxidation products may not have extremely low saturation vapor pressures despite high O: C ratios. *The Journal of Physical Chemistry A*, 120, 2569-2582, oi.org/10.1021/acs.jpca.6b02196, 2016.](https://doi.org/10.1021/acs.jpca.6b02196)
- 980 Lee, S.H., Uin, J., Guenther, A.B., de Gouw, J.A., Yu, F., Nadykto, A.B., Herb, J., Ng, N.L., Koss, A., Brune, W.H. and Baumann, K.: Isoprene suppression of new particle formation: Potential mechanisms and implications. *Journal of Geophysical Research: Atmospheres*, 121,14-621, doi.org/10.1002/2016JD024844, 2016.
- 985 Lehtipalo, K., Yan, C., Dada, L., Bianchi, F., Xiao, M., Wagner, R., Stolzenburg, D., Ahonen, L.R., Amorim, A., Baccarini, A. and Bauer, P.S.: Multicomponent new particle formation from sulphuric acid, ammonia, and biogenic vapors. *Science advances*, 4, p.eaau5363, 10.1126/sciadv.aau5363, 2018.

McFiggans, G., Mentel, T.F., Wildt, J., Pullinen, I., Kang, S., Kleist, E., Schmitt, S., Springer, M., Tillmann, R., Wu, C. and
990 Zhao, D.: Secondary organic aerosol reduced by mixture of atmospheric vapours. *Nature*, 565, 587-593,
doi.org/10.1038/s41586-018-0871-y, 2019.

Mentel, T. F., Springer, M., Ehn, M., Kleist, E., Pullinen, I., Kurtén, T., Rissanen, M., Wahner, A., and Wildt, J.: Formation
of highly oxidized multifunctional compounds: autoxidation of peroxy radicals formed in the ozonolysis of alkenes – deduced
995 from structure-product relationships. *Atmos. Chem. Phys.*, 15, 6745–6765, doi.org/10.5194/acp-15-6745-2015, 2015.

Molteni, U., Simon, M., Heinritzi, M., Hoyle, C.R., Bernhammer, A.K., Bianchi, F., Breitenlechner, M., Brilke, S., Dias, A.,
Duplissy, J. and Frege, C.: Formation of Highly Oxygenated Organic Molecules from α -Pinene Ozonolysis: Chemical
Characteristics, Mechanism, and Kinetic Model Development. *ACS Earth and Space Chemistry*, 3, 873-
1000 883, doi.org/10.1021/acsearthspacechem.9b00035, 2019.

Otkjær, R.V., Jakobsen, H.H., Tram, C.M. and Kjaergaard, H.G.: Calculated hydrogen shift rate constants in substituted alkyl
peroxy radicals. *The Journal of Physical Chemistry A*, 122, 8665-8673, doi.org/10.1021/acs.jpca.8b06223, 2018.

1005 Petäjä, T., Mauldin, III, R. L., Kosciuch, E., McGrath, J., Nieminen, T., Paasonen, P., Boy, M., Adamov, A., Kotiaho, T., and
Kulmala, M.: Sulphuric acid and OH concentrations in a boreal forest site, *Atmos. Chem. Phys.*, 9, 7435–7448,
doi.org/10.5194/acp-9-7435-2009, 2009.

Praske, E., Otkjær, R.V., Crouse, J.D., Hethcox, J.C., Stoltz, B.M., Kjaergaard, H.G. and Wennberg, P.O.: Atmospheric
1010 autoxidation is increasingly important in urban and suburban North America. *Proceedings of the National Academy of
Sciences*, 115, 64-69, doi.org/10.1073/pnas.1715540115, 2018.

Pye, H.O., D'Ambro, E.L., Lee, B.H., Schobesberger, S., Takeuchi, M., Zhao, Y., Lopez-Hilfiker, F., Liu, J., Shilling, J.E.,
Xing, J. and Mathur, R.: Anthropogenic enhancements to production of highly oxygenated molecules from autoxidation.
1015 *Proceedings of the National Academy of Sciences*, 14, 6641-6646, doi.org/10.1073/pnas.1810774166, 2018.

Quéléver, L. L. J., Kristensen, K., Normann Jensen, L., Rosati, B., Teiwes, R., Daellenbach, K. R., Peräkylä, O., Roldin, P.,
Bossi, R., Pedersen, H. B., Glasius, M., Bilde, M., and Ehn, M.: Effect of temperature on the formation of highly oxygenated
organic molecules (HOMs) from alpha-pinene ozonolysis, *Atmos. Chem. Phys.*, 19, 7609–7625, doi.org/10.5194/acp-19-
1020 7609-2019, 2019.

Riccobono, F., Schobesberger, S., Scott, C.E., Dommen, J., Ortega, I.K., Rondo, L., Almeida, J., Amorim, A., Bianchi, F.,
Breitenlechner, M. and David, A.: Oxidation products of biogenic emissions contribute to nucleation of atmospheric particles.
Science, 344, 717-721, doi:10.1126/science.1243527 , 2014.

1025 Varanda Rizzo, L., Roldin, P., Brito, J., Backman, J., Swietlicki, E., Krejci, R., Tunved, P., Petäjä, T., Kulmala, M. and Artaxo,
P.: Multi-year statistical and modeling analysis of submicrometer aerosol number size distributions at a rain forest site in
Amazonia. *Atmospheric Chemistry and Physics*, 18, 10255-10274, /doi.org/10.5194/acp-18-10255-2018, 2018.

- 1030 Roldin, P., Ehn, M., Kurtén, T., Olenius, T., Rissanen, M.P., Sarnela, N., Elm, J., Rantala, P., Hao, L., Hyttinen, N. and Heikkinen, L.: The role of highly oxygenated organic molecules in the Boreal aerosol-cloud-climate system. *Nature communications*, 10, 1-15, doi.org/10.1038/s41467-019-12338-8, 2019.
- Sarnela, N., Jokinen, T., Duplissy, J., Yan, C., Nieminen, T., Ehn, M., Schobesberger, S., Heinritzi, M., Ehrhart, S., Lehtipalo, K., Tröstl, J., Simon, M., Kürten, A., Leiminger, M., Lawler, M. J., Rissanen, M. P., Bianchi, F., Praplan, A. P., Hakala, J., Amorim, A., Gonin, M., Hansel, A., Kirkby, J., Dommen, J., Curtius, J., Smith, J. N., Petäjä, T., Worsnop, D. R., Kulmala, M., Donahue, N. M., and Sipilä, M.: Measurement–model comparison of stabilized Criegee intermediate and highly oxygenated molecule production in the CLOUD chamber, *Atmos. Chem. Phys.*, 18, 2363–2380, doi.org/10.5194/acp-18-2363-2018, 2018.
- 1040 Saunders, S. M., Jenkin, M. E., Derwent, R. G., and Pilling, M. J.: Protocol for the development of the Master Chemical Mechanism, MCM v3 (Part A): tropospheric degradation of non-aromatic volatile organic compounds, *Atmos. Chem. Phys.*, 3, 161–180, doi.org/10.5194/acp-3-161-2003, 2003.
- 1045 Schervish, M. and Donahue, N. M.: Peroxy Radical Chemistry and the Volatility Basis Set, *Atmos. Chem. Phys. Discuss.*, doi.org/10.5194/acp-2019-509, *in review*, 2019.
- Shrivastava, M., Cappa, C.D., Fan, J., Goldstein, A.H., Guenther, A.B., Jimenez, J.L., Kuang, C., Laskin, A., Martin, S.T., Ng, N.L. and Petaja, T., 2017. Recent advances in understanding secondary organic aerosol: Implications for global climate forcing. *Reviews of Geophysics*, 55, 509-559, doi.org/10.1002/2016RG000540, 2017.
- 1050 Sihto, S.-L., Kulmala, M., Kerminen, V.-M., Dal Maso, M., Petäjä, T., Riipinen, I., Korhonen, H., Arnold, F., Janson, R., Boy, M., Laaksonen, A., and Lehtinen, K. E. J.: Atmospheric sulphuric acid and aerosol formation: implications from atmospheric measurements for nucleation and early growth mechanisms, *Atmos. Chem. Phys.*, 6, 4079–4091, doi:10.5194/acp-6-4079-2006, 2006
- 1055 [Simon, M., Dada, L., Heinritzi, M., Scholz, W., Stolzenburg, D., Fischer, L., Wagner, A. C., Kürten, A., Rörup, B., He, X.-C., Almeida, J., Baalbaki, R., Baccarini, A., Bauer, P. S., Beck, L., Bergen, A., Bianchi, F., Bräkling, S., Brilke, S., Caudillo, L., Chen, D., Chu, B., Dias, A., Draper, D. C., Duplissy, J., El Haddad, I., Finkenzeller, H., Frege, C., Gonzalez-Carracedo, L., Gordon, H., Granzin, M., Hakala, J., Hofbauer, V., Hoyle, C. R., Kim, C., Kong, W., Lamkaddam, H., Lee, C. P., Lehtipalo, K., Leiminger, M., Mai, H., Manninen, H. E., Marie, G., Marten, R., Mentler, B., Molteni, U., Nichman, L., Nie, W., Ojdanic, A., Onnela, A., Partoll, E., Petäjä, T., Pfeifer, J., Philippov, M., Quéléver, L. L. J., Ranjithkumar, A., Rissanen, M., Schallhart, S., Schobesberger, S., Schuchmann, S., Shen, J., Sipilä, M., Steiner, G., Stozhkov, Y., Tauber, C., Tham, Y. J., Tomé, A. R., Vazquez-Pufleau, M., Vogel, A., Wagner, R., Wang, M., Wang, D. S., Wang, Y., Weber, S. K., Wu, Y., Xiao, M., Yan, C., Ye, P., Ye, Q., Zauner-Wieczorek, M., Zhou, X., Baltensperger, U., Dommen, J., Flagan, R. C., Hansel, A., Kulmala, M., Volkamer, R., Winkler, P. M., Worsnop, D. R., Donahue, N. M., Kirkby, J., and Curtius, J. Molecular understanding of new-particle formation from alpha-pinene between –50 °C and 25 °C, *Atmos. Chem. Phys. Discuss.*, doi.org/10.5194/acp-2019-1058, *in review*, 2020.](#)
- 1060 [Simon, M., Dada, L., Heinritzi, M., Scholz, W., Stolzenburg, D., Fischer, L., Wagner, A. C., Kürten, A., Rörup, B., He, X.-C., Almeida, J., Baalbaki, R., Baccarini, A., Bauer, P. S., Beck, L., Bergen, A., Bianchi, F., Bräkling, S., Brilke, S., Caudillo, L., Chen, D., Chu, B., Dias, A., Draper, D. C., Duplissy, J., El Haddad, I., Finkenzeller, H., Frege, C., Gonzalez-Carracedo, L., Gordon, H., Granzin, M., Hakala, J., Hofbauer, V., Hoyle, C. R., Kim, C., Kong, W., Lamkaddam, H., Lee, C. P., Lehtipalo, K., Leiminger, M., Mai, H., Manninen, H. E., Marie, G., Marten, R., Mentler, B., Molteni, U., Nichman, L., Nie, W., Ojdanic, A., Onnela, A., Partoll, E., Petäjä, T., Pfeifer, J., Philippov, M., Quéléver, L. L. J., Ranjithkumar, A., Rissanen, M., Schallhart, S., Schobesberger, S., Schuchmann, S., Shen, J., Sipilä, M., Steiner, G., Stozhkov, Y., Tauber, C., Tham, Y. J., Tomé, A. R., Vazquez-Pufleau, M., Vogel, A., Wagner, R., Wang, M., Wang, D. S., Wang, Y., Weber, S. K., Wu, Y., Xiao, M., Yan, C., Ye, P., Ye, Q., Zauner-Wieczorek, M., Zhou, X., Baltensperger, U., Dommen, J., Flagan, R. C., Hansel, A., Kulmala, M., Volkamer, R., Winkler, P. M., Worsnop, D. R., Donahue, N. M., Kirkby, J., and Curtius, J. Molecular understanding of new-particle formation from alpha-pinene between –50 °C and 25 °C, *Atmos. Chem. Phys. Discuss.*, doi.org/10.5194/acp-2019-1058, *in review*, 2020.](#)
- 1065 [Simon, M., Dada, L., Heinritzi, M., Scholz, W., Stolzenburg, D., Fischer, L., Wagner, A. C., Kürten, A., Rörup, B., He, X.-C., Almeida, J., Baalbaki, R., Baccarini, A., Bauer, P. S., Beck, L., Bergen, A., Bianchi, F., Bräkling, S., Brilke, S., Caudillo, L., Chen, D., Chu, B., Dias, A., Draper, D. C., Duplissy, J., El Haddad, I., Finkenzeller, H., Frege, C., Gonzalez-Carracedo, L., Gordon, H., Granzin, M., Hakala, J., Hofbauer, V., Hoyle, C. R., Kim, C., Kong, W., Lamkaddam, H., Lee, C. P., Lehtipalo, K., Leiminger, M., Mai, H., Manninen, H. E., Marie, G., Marten, R., Mentler, B., Molteni, U., Nichman, L., Nie, W., Ojdanic, A., Onnela, A., Partoll, E., Petäjä, T., Pfeifer, J., Philippov, M., Quéléver, L. L. J., Ranjithkumar, A., Rissanen, M., Schallhart, S., Schobesberger, S., Schuchmann, S., Shen, J., Sipilä, M., Steiner, G., Stozhkov, Y., Tauber, C., Tham, Y. J., Tomé, A. R., Vazquez-Pufleau, M., Vogel, A., Wagner, R., Wang, M., Wang, D. S., Wang, Y., Weber, S. K., Wu, Y., Xiao, M., Yan, C., Ye, P., Ye, Q., Zauner-Wieczorek, M., Zhou, X., Baltensperger, U., Dommen, J., Flagan, R. C., Hansel, A., Kulmala, M., Volkamer, R., Winkler, P. M., Worsnop, D. R., Donahue, N. M., Kirkby, J., and Curtius, J. Molecular understanding of new-particle formation from alpha-pinene between –50 °C and 25 °C, *Atmos. Chem. Phys. Discuss.*, doi.org/10.5194/acp-2019-1058, *in review*, 2020.](#)
- 1070 [Sindelarova, K., Granier, C., Bouarar, I., Guenther, A., Tilmes, S., Stavrou, T., Müller, J.-F., Kuhn, U., Stefani, P., and Knorr, W.: Global data set of biogenic VOC emissions calculated by the MEGAN model over the last 30 years, *Atmos. Chem. Phys.*, 14, 9317–9341, doi.org/10.5194/acp-14-9317-2014, 2014.](#)

- 1075 Sporre, M.K., Blichner, S.M., Karset, I.H., Makkonen, R. and Berntsen, T.K.. BVOC–aerosol–climate feedbacks investigated using NorESM. *Atmospheric Chemistry and Physics*, 19, 4763-4782, doi.org/10.5194/acp-19-4763-2019, 2019.
- 1080 Stocker, T. F., Qin, D., Plattner, G.-K., Alexander, L. V., Allen, S. K., Bindoff, N. L., Brönn, F.-M., Church, J. A., Cubasch, U., Emori, S., Forster, P., Friedlingstein, P., Gillett, N., Gregory, J. M., Hartmann, D. L., Jansen, E., Kirtman, B., Knutti, R., Kumar, K. K., Lemke, P. et al (2013) Technical summary. In: *Climate Change 2013: The Physical Science Basis*. Cambridge University Press. ISBN 9781107661820
- 1085 Stolzenburg, D., Fischer, L., Vogel, A.L., Heinritzi, M., Schervish, M., Simon, M., Wagner, A.C., Dada, L., Ahonen, L.R., Amorim, A. and Baccarini, A.: Rapid growth of organic aerosol nanoparticles over a wide tropospheric temperature range. *Proceedings of the National Academy of Sciences*, 115, 9122-9127, doi.org/10.1073/pnas.1807604115, 2018.
- [Tan, Z., Rohrer, F., Lu, K., Ma, X., Bohn, B., Broch, S., Dong, H., Fuchs, H., Gkatzelis, G. I., Hofzumahaus, A., Holland, F., Li, X., Liu, Y., Liu, Y., Novelli, A., Shao, M., Wang, H., Wu, Y., Zeng, L., Hu, M., Kiendler-Scharr, A., Wahner, A., and Zhang, Y.: Wintertime photochemistry in Beijing: observations of ROx radical concentrations in the North China Plain during the BEST-ONE campaign, *Atmos. Chem. Phys.*, 18, 12391–12411, doi.org/10.5194/acp-18-12391-2018, 2018.](#)
- 1090 Twomey, S.: Pollution and the planetary albedo. *Atmospheric Environment*, 8, 1251-1256, doi.org/10.1016/j.atmosenv.2007.10.062, 1967.
- 1095 Watson, L.A., Shallcross, D.E., Utembe, S.R. and Jenkin, M.E.: A Common Representative Intermediates (CRI) mechanism for VOC degradation. Part 2: Gas phase mechanism reduction. *Atmospheric Environment*, 42, 7196-7204, doi.org/10.1016/j.atmosenv.2008.07.034, 2008.
- 1100 Wennberg, P.O., Bates, K.H., Crounse, J.D., Dodson, L.G., McVay, R.C., Mertens, L.A., Nguyen, T.B., Praske, E., Schwantes, R.H., Smarte, M.D. and St Clair, J.M.: Gas-phase reactions of isoprene and its major oxidation products. *Chemical reviews*, 118, 3337-3390, doi.org/10.1021/acs.chemrev.7b00439, 2018.
- 1105 Williamson, C.J., Kupc, A., Axisa, D., Bilsback, K.R., Bui, T., Campuzano-Jost, P., Dollner, M., Froyd, K.D., Hodshire, A.L., Jimenez, J.L. and Kodros, J.K.: A large source of cloud condensation nuclei from new particle formation in the tropics. *Nature*, 574, 399-403, doi.org/10.1038/s41586-019-1638-9, 2019.
- 1110 [Wimmer, D., Buenrostro Mazon, S., Manninen, H.E., Kangasluoma, J., Franchin, A., Nieminen, T., Backman, J., Wang, J., Kuang, C., Krejci, R. and Brito, J., 2018. Ground-based observation of clusters and nucleation-mode particles in the Amazon. *Atmospheric Chemistry and Physics*, 18, 13245-13264, 10.5194/acp-18-13245-2018, 2018.](#)
- [Wu, Z., Hu, M., Liu, S., Wehner, B., Bauer, S., Maßling, A., Wiedensohler, A., Petaja, T., Dal Maso, M. and Kulmala, M.: New particle formation in Beijing, China: Statistical analysis of a 1-year data set. *Journal of Geophysical Research: Atmospheres*, D9, doi.org/10.1029/2006JD007406, 2007.](#)

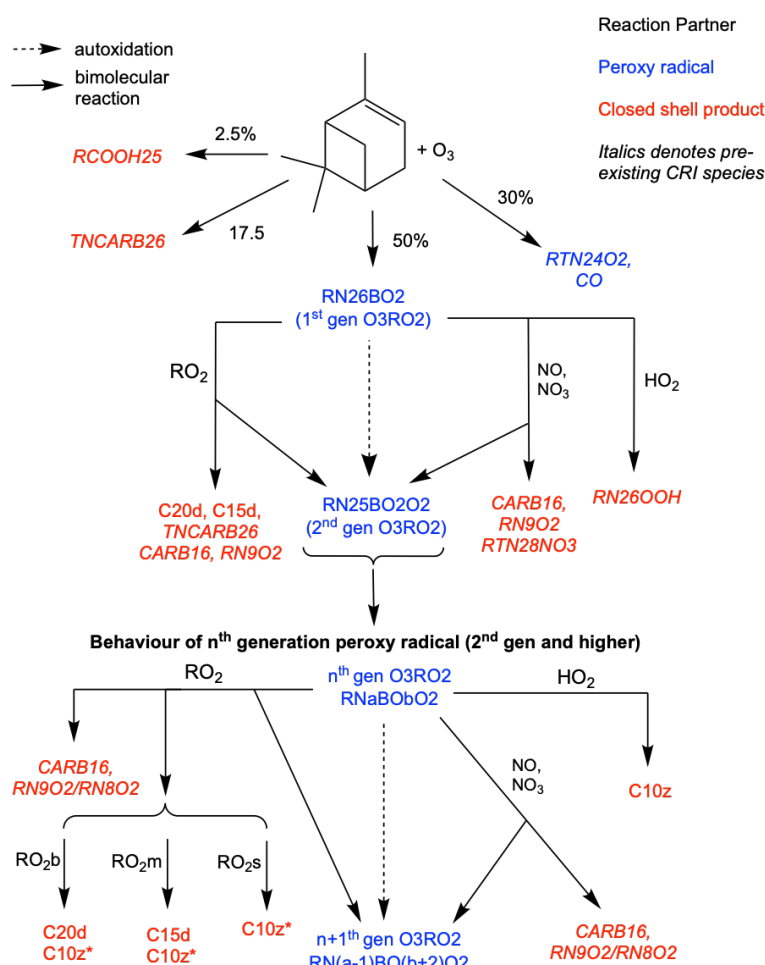
Utembe, S.R., Cooke, M.C., Archibald, A.T., Jenkin, M.E., Derwent, R.G. and Shallcross, D.E.: Using a reduced Common Representative Intermediates (CRIv2-R5) mechanism to simulate tropospheric ozone in a 3-D Lagrangian chemistry transport model. *Atmospheric Environment*, 44, 1609-1622, doi.org/10.1016/j.atmosenv.2010.01.044, 2010.

Xu, L., Møller, K.H., Crouse, J.D., Otkjær, R.V., Kjaergaard, H.G. and Wennberg, P.O.: Unimolecular reactions of peroxy radicals formed in the oxidation of α -pinene and β -pinene by hydroxyl radicals. *The Journal of Physical Chemistry A*, 123, 1661-1674, doi.org/10.1021/acs.jpca.8b11726, 2019.

Yáñez-Serrano, A. M., Nölscher, A. C., Williams, J., Wolff, S., Alves, E., Martins, G. A., Bourtsoukidis, E., Brito, J., Jardine, K., Artaxo, P., and Kesselmeier, J. Diel and seasonal changes of biogenic volatile organic compounds within and above an Amazonian rainforest, *Atmos. Chem. Phys.*, 15, 3359–3378, doi.org/10.5194/acp-15-3359-2015, 2015.

Zhu, J., Penner, J.E., Yu, F., Sillman, S., Andreae, M.O. and Coe, H.: Decrease in radiative forcing by organic aerosol nucleation, climate, and land use change. *Nature communications*, 10, 423, doi.org/10.1038/s41467-019-08407-7, 2019.

Zhao, Y., Thornton, J.A. and Pye, H.O.: Quantitative constraints on autoxidation and dimer formation from direct probing of monoterpene-derived peroxy radical chemistry. *Proceedings of the National Academy of Sciences*, 48, 12142-12147, doi.org/10.1073/pnas.1812147115, 2018.



1135

Figure 1: Schematic of additions to CRI v2.2 to represent autoxidation and HOM formation via ozonolysis of α -pinene. HOMs (C10z, C15d, C20d) can be produced via reaction of the O3RO2 with HO2 and RO2 while reaction with NO, NO3 and RO2 can produce alkoxy radicals which can fragment or isomerise. **New species introduced in this scheme are denoted by normal font, existing species by italics.** The RO2 pool is split into subsections covering big (RO2b), medium (RO2m) and small (RO2s) peroxy radicals to facilitate addition of accretion product formation.

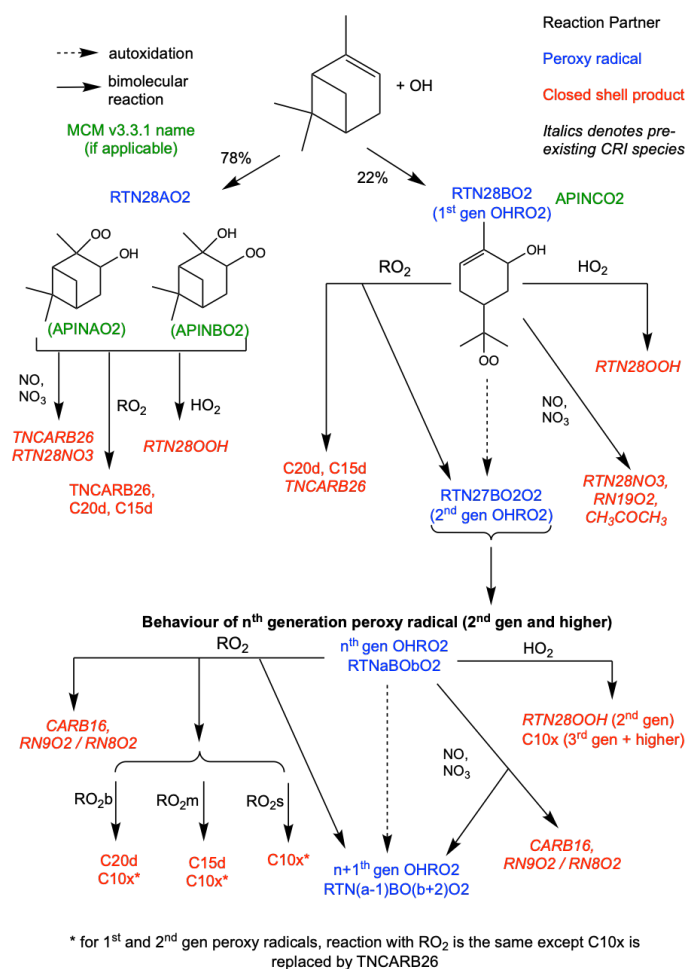


Figure 2 - Schematic of additions to CRI v2.2 to represent autoxidation and HOM formation via OH oxidation. HOMs can be produced via reaction with HO2 and RO2 while reaction with NO, NO3 and RO2 can produce alkoxy radicals which can fragment or isomerise. The RO2 pool is split into subsections covering big (RO2b), medium (RO2m) and small (RO2s) peroxy radicals to facilitate addition of accretion product formation.

Table 1 - Summary of new species added in HOM mechanism. The removal of species RN18AO2 and RTN28O2 results in a net increase of 12 species.

Species	Classification	Origin	MCM v3.3.1 equivalent
RN26BO2	1 st generation peroxy radical	Ozonolysis	C107O2, C109O2
RN25BO2O2	2 nd generation peroxy radical	Ozonolysis	Not in MCM
RN24BO4O2	3 rd generation peroxy radical	Ozonolysis	Not in MCM
RN23BO6O2	4 th generation peroxy radical	Ozonolysis	Not in MCM
RNxBOyO2	Lumped 5 th and higher generation peroxy radical	Ozonolysis	Not in MCM
RTN28AO2	1 st generation peroxy radical (no autoxidation)	Ozonolysis	APINAO2 and APINBO2

RTN28BO2	1 st <u>generation</u> peroxy radical (autoxidation possible)	OH oxidation	APINCO2
RTN27BO2O2	2 nd <u>generation</u> peroxy radical	OH oxidation	Not in MCM
RTN26BO4O2	3 rd <u>generation</u> peroxy radical	OH oxidation	Not in MCM
RTNxBOyO2	Lumped 4 th and higher <u>generation</u> peroxy radical	OH oxidation	Not in MCM
C10z	10-carbon HOM	Ozonolysis	Not in MCM
C10x	10-carbon HOM	OH oxidation	Not in MCM
C15d	15-carbon HOM	Ozonolysis and OH oxidation	Not in MCM
C20d	20-carbon HOM	Ozonolysis and OH oxidation	Not in MCM

1150

Table 2 - Summary of possible products formed for a particular peroxy radical reacting with the big, medium and small peroxy radical pools.

Size of reacting peroxy radical	Product of reaction with big pool	Product of reaction with medium pool	Product of reaction with small pool
Big (>7 C, e.g. RN26BO2)	C20 HOM accretion product C10 HOM / Existing CRI species* Peroxy radical	C15 HOM accretion product C10 HOM / Existing CRI species* Peroxy radical	C10 HOM / Existing CRI species* Peroxy radical
Medium (4-7 C, e.g. RU14O2)	Closed shell, alkoxy radical		
Small (<4 C, e.g. CH3O2)	Closed shell species, alkoxy radical (no change from CRI v2.2 treatment)		

* The result depends on the extent to which the reacting peroxy radical has been oxidised prior to the RO₂-RO₂ reaction. A HOM is classified as a species which has undergone at least one autoxidation step at atmospherically relevant temperatures and contains at least 6 oxygen atoms (Bianchi et al., 2019). Thus, some of the less oxidised peroxy radicals may not qualify as HOMs and are assigned to the most relevant non-HOM species already in the CRI.

1160

1165

Table 3 - Simulations used for developing and testing new mechanism

Simulation	Purpose	Mechanism Version(s) Used	Conditions
A: Flow cell experiment	Optimise mechanism by fitting autoxidation coefficients and rate coefficients for accretion product formation	Temperature independent mechanism	297 K, $\text{NO}_x < 10^8 \text{ cm}^{-3}$, dark 26 ppb O_3 , initial α -pinene concentration varied
B: Flow cell experiment	Along with Simulation A, optimise mechanism by fitting autoxidation coefficients and rate coefficients for accretion product formation	Temperature independent mechanism	297 K, $\text{NO}_x < 10^8 \text{ cm}^{-3}$, dark 80 ppb O_3 , 15.6 ppb α -pinene concentration, initial isoprene concentration varied
C: Chamber Experiment	HOM yield calculation	Temperature dependent mechanisms with autoxidation activation energies of 6000K, 9000K and 12077K	270 K, 290 K or 310 K α -pinene 15 ppb, O_3 40 ppb NO, NO_2 varied from 0.01-10 ppb
D: Tropical Boundary Layer Experiment	Compare new mechanism with concentrations predicted by CRI v2.2	Temperature independent and all temperature dependent mechanisms	8 day run with diurnally varying photolysis, temperature ($298 \pm 4 \text{ K}$), α -pinene and isoprene emissions Multiple runs performed with scaled NO and α -pinene emissions (Full details in SI)

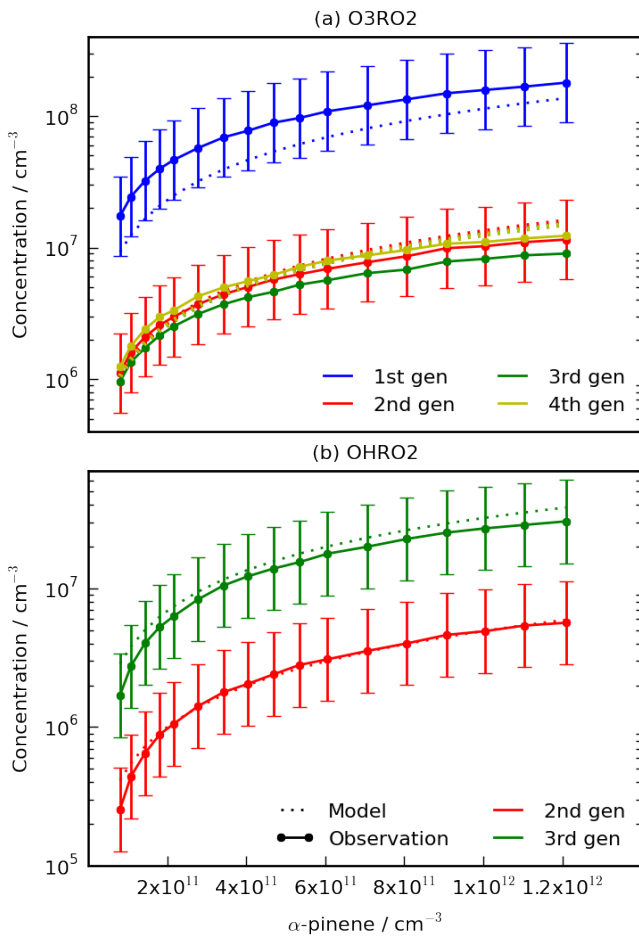
Table 4 – Autoxidation coefficients for the peroxy radicals after fitting to experimental data.

Generation	$\text{O}_3\text{RO}_2 / \text{s}^{-1}$	$\text{OHRO}_2 / \text{s}^{-1}$
1 st	0.206	2.1
2 nd	1.7	2.1
3 rd	1.7	0.25
4 th	1.6	N/A

170 **Table 4 - Autoxidation coefficients for peroxy radicals after fitting to experimental data (at 297 K) with estimated uncertainty.**

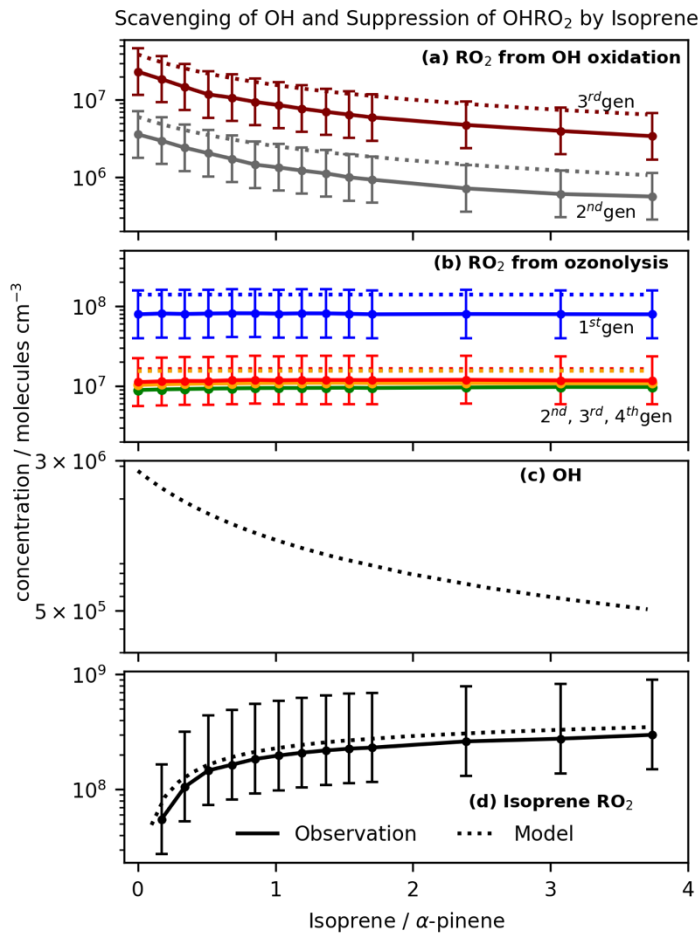
Generation	$\text{O}_3\text{RO}_2 / \text{s}^{-1}$	$\text{OHRO}_2 / \text{s}^{-1}$
1 st	0.206 (+0.025/ -0.04)	2.1 ^a
2 nd	1.7 (+1.1/-0.4)	2.1 (+1.6 / -0.2)
3 rd	1.7 (+1.1/-0.4)	0.25 (+0.3 /-0.1)
4 th	1.6 (+0.8/ -0.5)	N/A

^aTaken directly from Xu et al (2018)



1175

Figure 3 - Comparison of the HOM-precursors (a) O3RO2 and (b) OHRO2 produced by the model and from Berndt et al (2018b) for experiments performed with different initial concentrations of α -pinene (Simulation A). The model reproduces the increase in O3RO2 and 2nd and 3rd generation OHRO2 with initial α -pinene well. The model struggled to reproduce concentrations of the 1st generation OHRO2 (not shown). Note that the error shown is the experimental error from Berndt et al (2018b) and the error bars for the 3rd and 4th generation O3RO2 species are of very similar size to the error bars of the 2nd generation species but have been omitted for clarity.



1180

Figure 4 – Observed and modelled variation for Simulation B of OHRO₂ (a), O₃RO₂ (b), OH (c) and the peroxy radical formed from isoprene oxidation (d) with increasing isoprene (observed data from Berndt et al (2018b)). The model is able to reproduce the decrease in OHRO₂ as well as their concentrations. The fractional decline of OHRO₂ mirrors that observed in the OH concentration, suggesting the major driver is OH scavenging. The error shown is the experimental error from Berndt et al (2018b).

1185

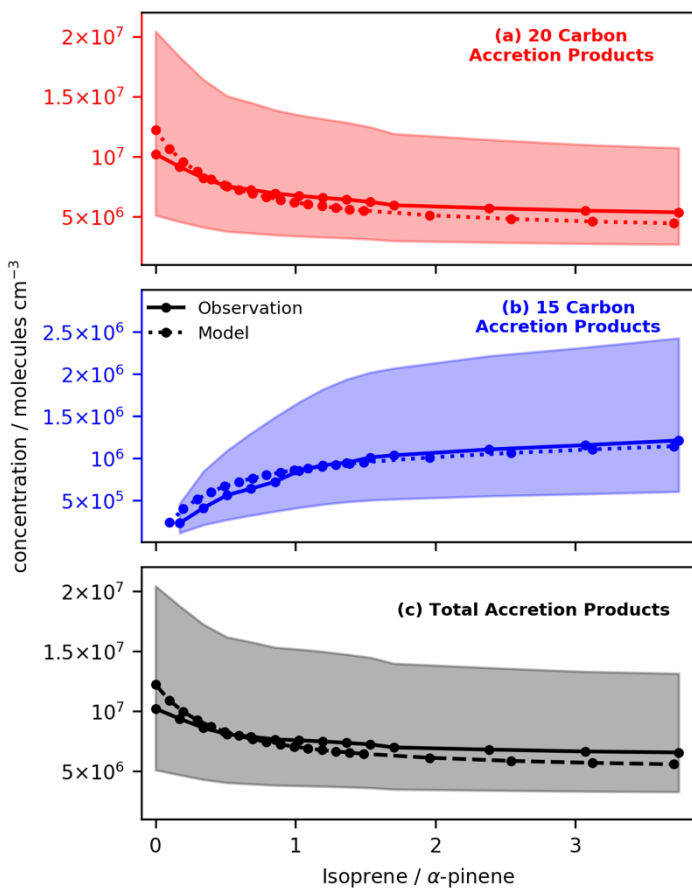
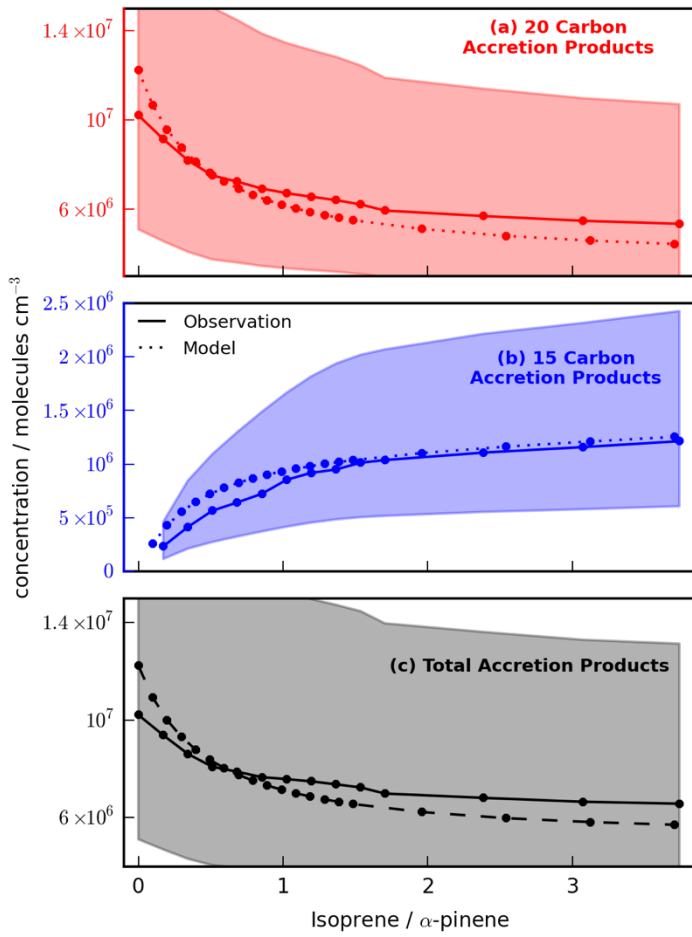
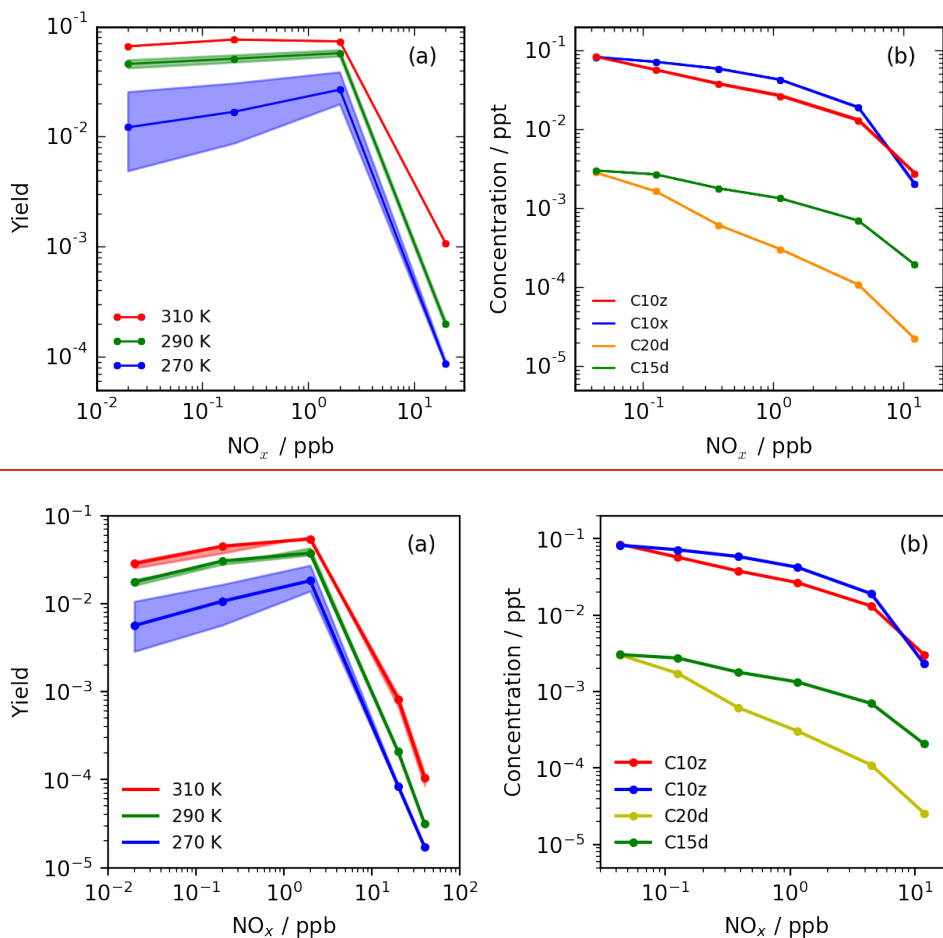


Figure 5 – Variation in Simulation B of observed and modelled concentrations of C20d (a), C15d (b) and total accretion products (c) with isoprene at fixed initial concentrations of α -pinene (observed data from Berndt et al (2018b)). The modelled data falls within

1190 the experimental uncertainty shown by the pale red, blue and grey regions. The model reproduces the observed decrease in C20 accretion products and increase in C15 accretion products well. Furthermore, the model reproduces qualitatively the result observed by McFiggans et al (2019) that addition of isoprene reduces the total accretion products concentration with potentially important implications for total aerosol burden and particle size distribution.

195



1200

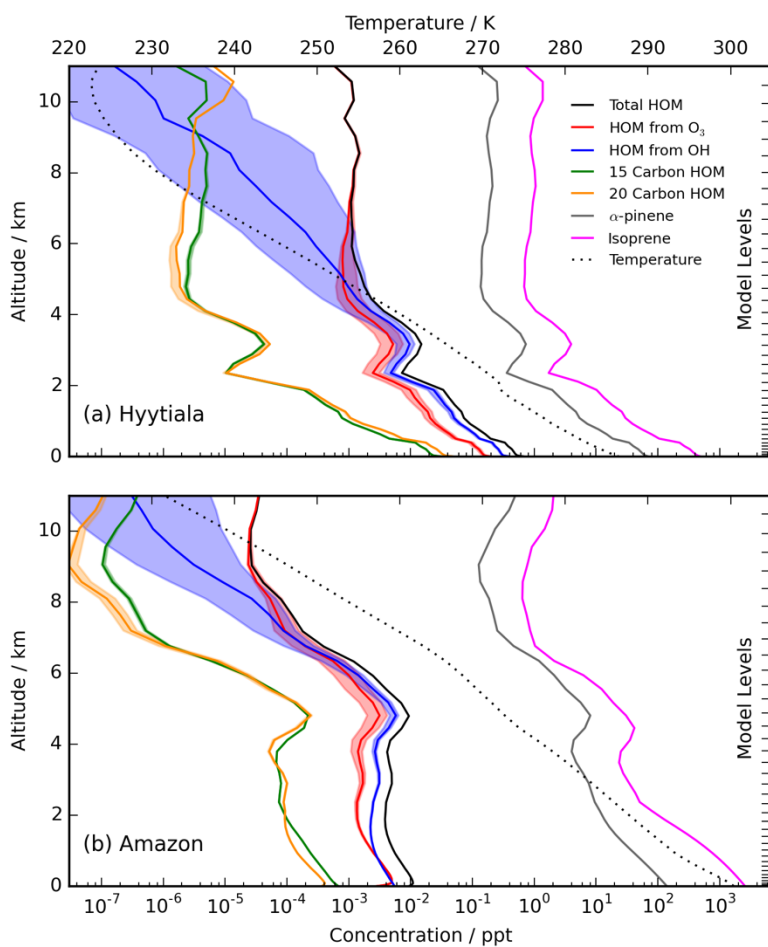
Figure 6 – (a) Maximum modelled HOM yields (C10x and C10z) exhibiting significant decline under high NO_x conditions (Simulation C). The spread in the modelled yield between HOM mechanisms (HOM₆₀₀₀, HOM₉₀₀₀ and HOM₁₂₀₇₇), shown by the shaded regions, indicates the lower sensitivity to autoxidation activation energy at temperatures above ~290 K. (b) Observed HOM concentrations from 8 day tropical PBL run (Simulation D) showing decrease in concentration for all HOM species with NO_x. Under tropical PBL conditions, negligible difference was observed between HOM mechanisms due to daytime temperatures exceeding 300 K.

1205

Table 5 - Observed and modelled concentrations after adjustment of model input. The model performs well in comparison to observed [HOM] at Hyytiala.

Location	Species Adjusted to Observations	Mean observed concentrations at relevant time of day / ppt ^e	Model concentrations with input adjusted to observations / ppt ^e
Hyytiala ^a	Monoterpene	10-carbon HOM: 0.2-0.8 ppt (mean 0.4 ppt) 20-carbon accretion product: 0.04-0.16 ppt (mean 0.08 ppt)	10-carbon HOM: 0.33-0.37 0.75-0.85 ppt 20-carbon accretion product: 0.18-0.19 0.28-0.30 ppt
Alabama ^b	Monoterpene, Isoprene, OH, O ₃	C9 & C10 ^d : 30 ppt	C10 ^f : 8.0-12.1 4.5-13.3

^aRoldin et al., 2019, ^bLee et al., 2016, ^cRanges given accounts for factor of 2 uncertainty in observed concentrations, ^dIncludes concentrations from C9 species (C₉H₁₄-20O₄-10) and C10 species (C₁₀H₁₆₋₂₂O₄₋₁₀), ^eModel was run with surface conditions in May for comparison to data from Roldin et al (2019). ^fRange arises from model runs using range of CS values suggested in Lee et al (2016)



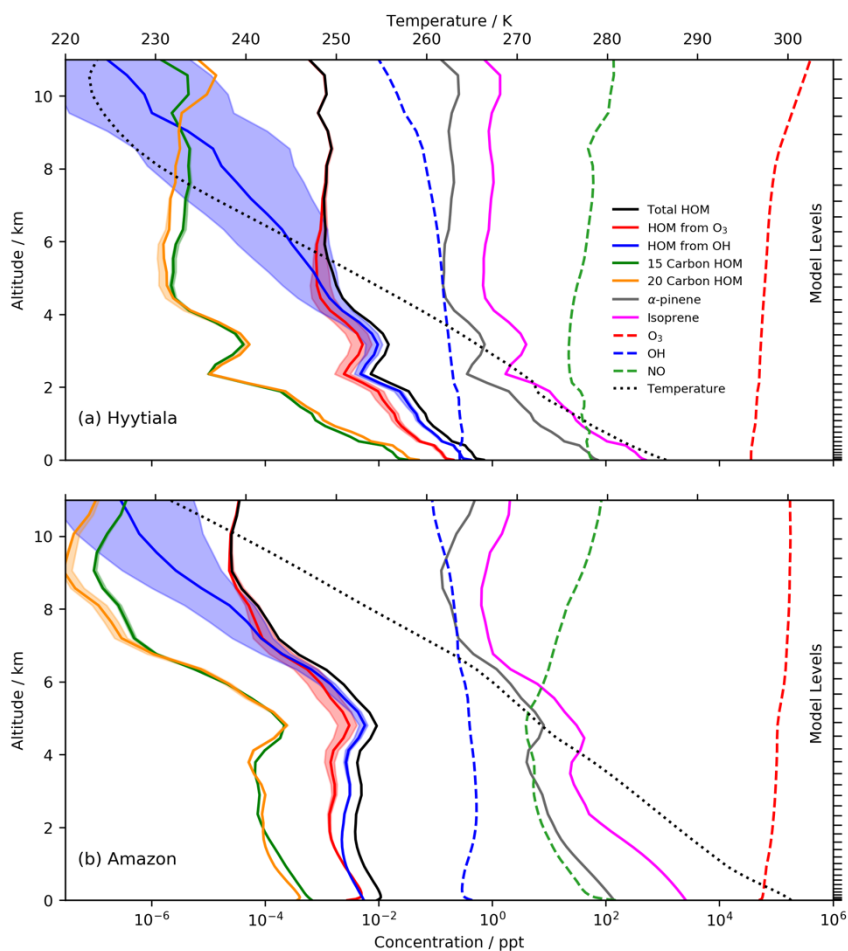
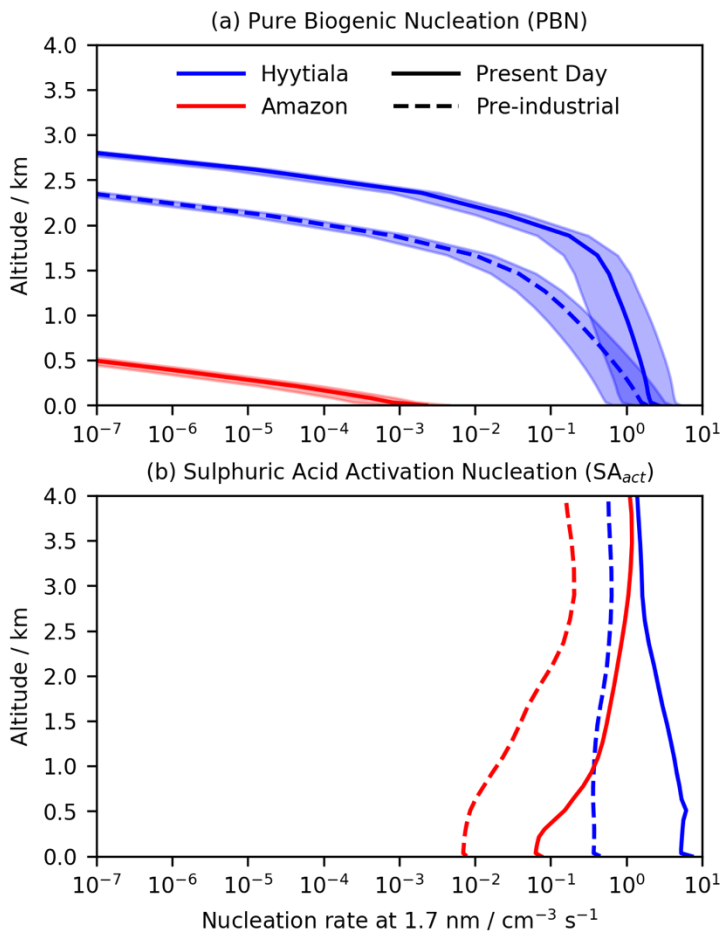
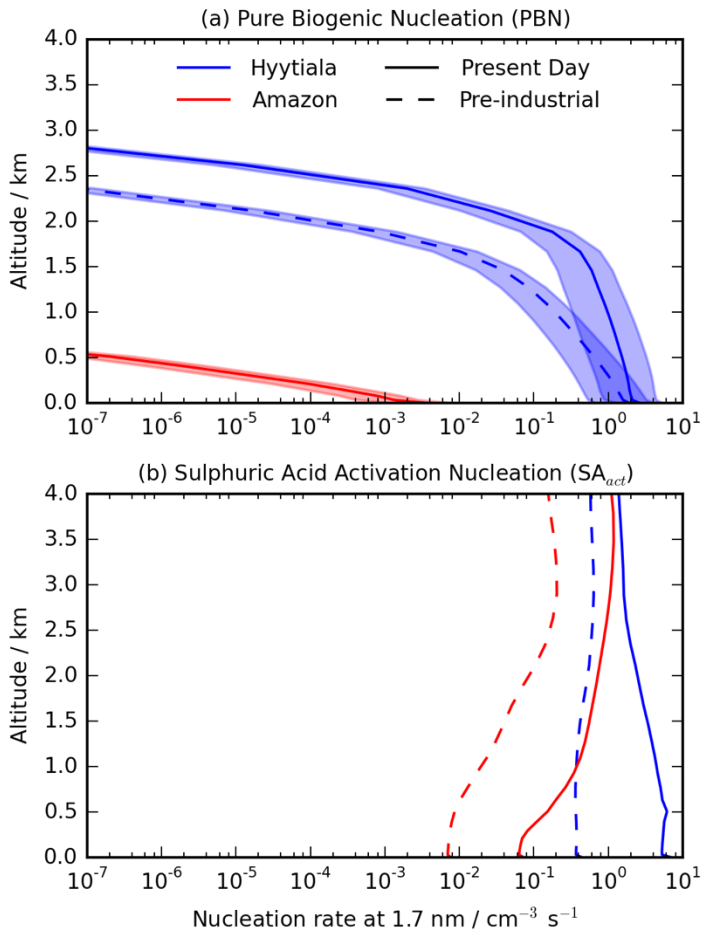


Figure 7 - HOM profiles in June (2pm LT) above (a) Hyytiälä and (b) the Amazon near Manaus. Despite higher [α -pinene], the significantly higher CS in the Amazon results in lower [HOM]. The temperature dependence (shown by the shading) is more significant at low altitude with Hyytiälä's cooler temperatures. ~~In (a) the reasonable performance of the model is shown by the overlap of the upper inward-facing arrows (total modelled surface concentrations for 10-carbon HOMs (red) and 20-carbon accretion products (black)) and the lower outward-facing arrows (mean observed surface concentrations).~~ The Amazon's higher isoprene/ α -pinene ratio (~ 20) resulted in greater suppression of the 20-carbon accretion product than at Hyytiälä.

1215



1225

Figure 8 - PD and PI modelled nucleation rates averaged over June for (a) summed (neutral + ion-induced) pure biogenic nucleation (assumes altitude-independent ion production rate (IPR) of $2 \text{ cm}^{-3} \text{ s}^{-1}$ (Hirsiko et al., 2011), shading shows IPR variation $0.5\text{-}5 \text{ cm}^{-3} \text{ s}^{-1}$) and (b) nucleation from sulphuric acid only (SA_{act}). Both mechanisms are predicted to produce greater nucleation rates in the PD due to greater concentrations of precursor species. Importantly however, PBN at low altitude at Hyytiala is predicted to be comparable to SA nucleation in the PI due to the greater modelled ion concentration arising from a lower condensation sink and reduction in rates from SA_{act} due to lower sulphuric acid concentrations. This leads to a larger increase in the total nucleation rate in the PI than the PD with potential implications for PI aerosol burden and climate.

Supplementary Information: CRI-HOM: A novel chemical mechanism for simulating Highly Oxygenated Organic Molecules (HOMs) in global chemistry-aerosol-climate models.

James Weber¹, ~~Scott Archer-Nicholls¹, Alexander T. Archibald^{1,2}~~, Paul Griffiths^{1,2}, ~~Scott Archer-Nicholls¹~~, Torsten Berndt³, Michael Jenkin⁴, Hamish Gordon⁵, Christoph Knöbe⁶, ~~Alexander T. Archibald^{1,2}~~

- 5 ¹Centre for Atmospheric Science, Department of Chemistry, University of Cambridge, Cambridge, CB2 1EW, UK
²National Centre for Atmospheric Science, Department of Chemistry, University of Cambridge, CB2 1EW, UK
³Atmospheric Chemistry Department (ACD), Leibniz Institute for Tropospheric Research (TROPOS), Leipzig, 04318, Germany
⁴Atmospheric Chemistry Services, Okehampton, Devon, UK
10 ~~⁵College of Engineering, Carnegie Mellon University, Pittsburgh, PA 15213, USA~~ ⁵Engineering Research Accelerator and Center for Atmospheric Particle Studies, Carnegie Mellon University, Pittsburgh, PA 15213, USA

⁶Meteorologisches Institut, Ludwig-Maximilians-Universität München, Munich, 80333, Germany

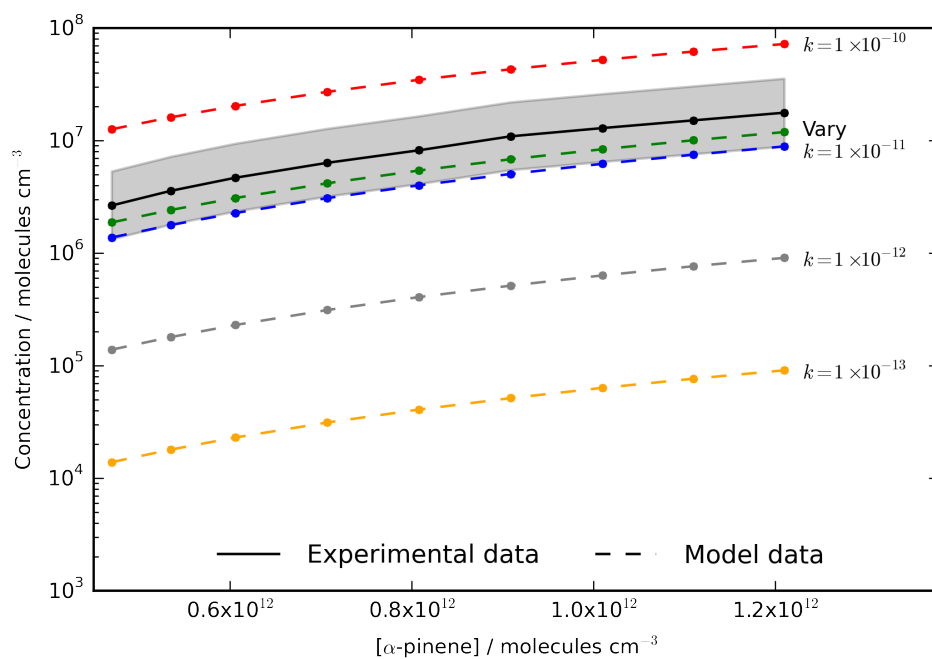
Correspondence to: James Weber (jmw240@cam.ac.uk)

15 **Table S1 - Summary of RO₂-RO₂ rate coefficients**

Reaction	Rate Coefficient / cm ³ molecules ⁻¹ s ⁻¹	Reference	Comments
All O ₃ RO ₂ + RO _{2b} = 0.5 C20d	0.97 - 3.6 × 10 ⁻¹¹ (See full reaction list)	Berndt et al., 2018b	Based on Berndt et al., then fitted to data <u>Derived from data from Berndt et al., 2018b</u>
All OHRO ₂ + RO _{2b} = 0.5 C20d	0.4 - 3.5 × 10 ⁻¹¹ (See full reaction list)	Berndt et al., 2018b	Based on Berndt et al., then fitted to data <u>Derived from data from Berndt et al., 2018b</u>
All O ₃ RO ₂ + RO _{2b} = C10x/CARB16	1.68 × 10 ⁻¹²	Molteni et al., 2019	
All O ₃ RO ₂ + RO _{2b} = Closed shell + peroxy radical	1.68 × 10 ⁻¹²	Molteni et al., 2019 Jenkin et al., 2019a	
RN26BO ₂ + RO _{2m} , RO _{2s} = C10x/TNCARB26	8.3 × 10 ⁻¹³	Jenkin et al., 2019a*	Weighted average of rate coefficients
RTN28AO ₂ + RO _{2b} , RO _{2m} , RO _{2s} = Closed shell	5.9 × 10 ⁻¹³	MCM	Weighted average of RO ₂ rate coefficients for species APINAO ₂ and APINBO ₂

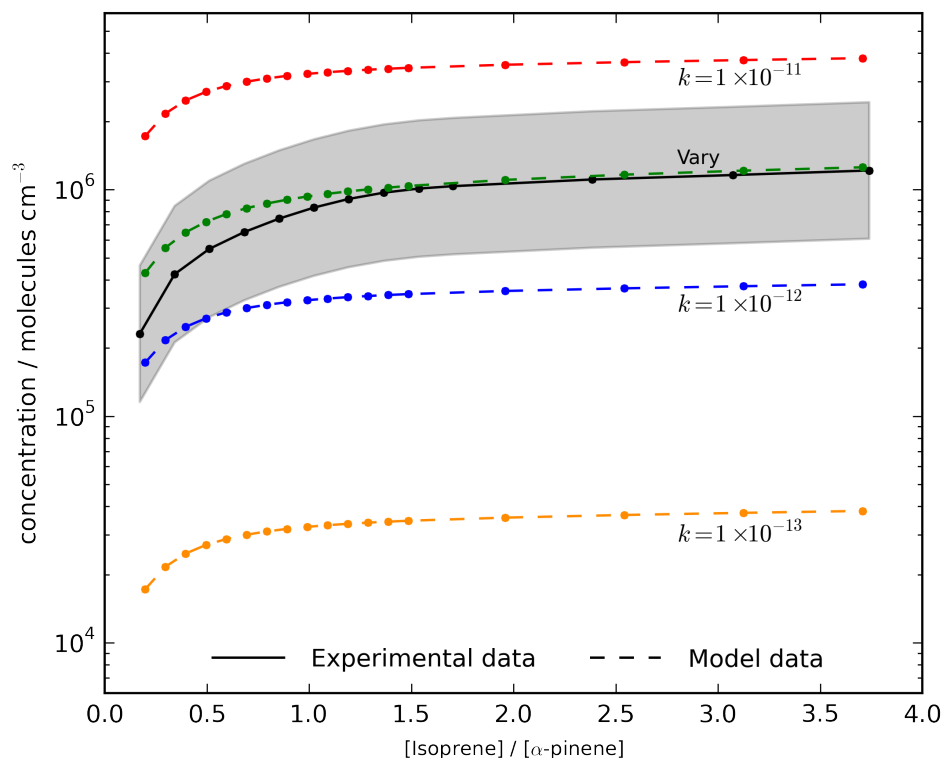
RTN28BO2 + RO2 _m , RO2 _s = Closed shell + peroxy radical	6.70×10^{-15}	MCM	MCM value for species APINCO2
2nd – 5th gen O3RO2 + RO2 _m , RO2 _s = Closed shell + peroxy radical	$5 \times 10^{-12} - 1 \times 10^{-11}$ (See full reaction list)	Roldin et al., 2019	Increases with increasing O3RO2 functionality
2nd – 5th gen OHRO2 + RO2 _b , RO2 _m , RO2 _s = Closed shell + peroxy radical	$5 \times 10^{-12} - 1 \times 10^{-11}$ (See full reaction list)	Roldin et al., 2019	Increases with increasing OHRO2 functionality
All O3RO2 + RO2 _m = C15d	$3.9 - 7.5 \times 10^{-12}$ (See full reaction list)	Berndt et al., 2018b	Based on Berndt et al, then fitted to data
All OHRO2 + RO2 _m = C15d	$1.28 - 2.53.75 \times 10^{-12}$ (See full reaction list)	Berndt et al., 2018b	Based on Berndt et al, then fitted to data

* The rate coefficient for the production of the closed shell and alkoxy radical from reaction of the first generation O3RO2 species, RN26BO2, with RO2_m and RO2_s was taken to be the average of the rate coefficients of the three actual species (C107O2, C109O2 and C10BO2 using the notation of Molteni et al (2019)), weighted by the branching ratio of their production. The rate coefficients for C107O2, C109O2 and C10BO2 were calculated using the methodology of Jenkin et al (2019a).

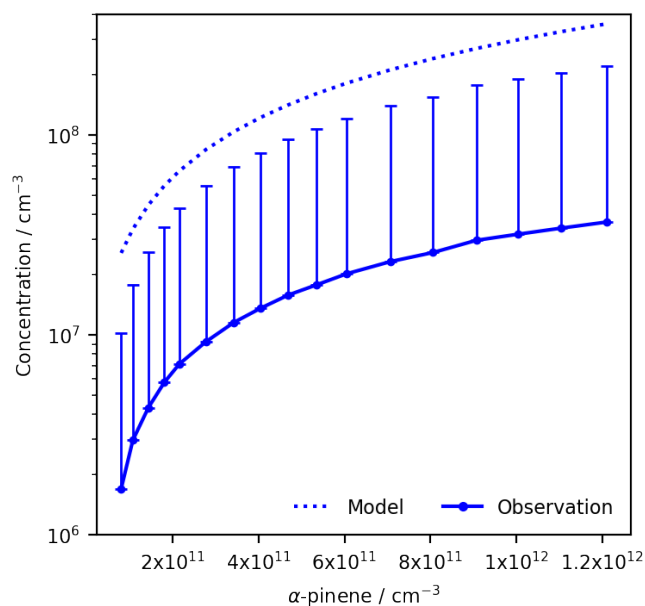


25 Figure S1 – Effect of C20d formation rate coefficient on model performance compared to observations from Berndt et al (2018b) under varying initial conditions of α -pinene (Simulation A, Table 3). The model was able to reproduce observed concentrations within experimental error (shaded region) here and in Fig 5 when the rate coefficients were increased with increasing peroxy radical functionalisation (line marked “Vary”). The lines with $k=1\times 10^{-10}$, 1×10^{-11} , 1×10^{-12} and 1×10^{-13} show model performance when the specified rate coefficient (in units of $\text{cm}^3 \text{molecules}^{-1} \text{s}^{-1}$) was used for all O3RO2 and OHRO2. The simulations with accretion formation rate coefficients suggested by Roldin et al (2019) ($\sim 10^{-13}$ - $10^{-12} \text{cm}^3 \text{molecules}^{-1} \text{s}^{-1}$) produced significantly lower C20d concentrations while using rate coefficients suggested by Molteni et al (2019) ($\geq 10^{-10} \text{cm}^3 \text{molecules}^{-1} \text{s}^{-1}$) overpredicted C20d concentrations.

30



35 Figure S2 – Effect of C15d formation rate coefficient on model performance compared to observations from Berndt et al (2018b) under conditions of fixed initial α -pinene concentration and varying initial isoprene concentration (Simulation B, Table 3). The model was able to replicate the general trend of increasing C15d with isoprene when the rate coefficients were increased with increasing peroxy radical functionalisation (line marked “Vary”), reproducing observation within experimental error (shaded region). The lines with $k=1\times 10^{-11}$, 1×10^{-12} and 1×10^{-13} show model performance when the specified rate coefficient (in units of $\text{cm}^3 \text{molecules}^{-1} \text{s}^{-1}$) was used for all O3RO2 and OHRO2.



40 **Figure S3 – 1st generation OHRO2 observation (Berndt et al., 2018b) and modelled with estimated experimental underprediction of factor of 5. Reasons for observation-model discrepancy are discussed in the main text.**

Table S2 - Summary of HOM mechanisms and autoxidation activation energies

Mechanism	Autoxidation Activation Energy / K	Comments
HOM _{Tl}	N/A - temperature independent	Autoxidation coefficients based on fitting from data from Berndt et al (2018b) at 297K
HOM ₆₀₀₀	6000	Representing possible lower bound of activation energy
HOM ₉₀₀₀	9000	Representing possible middle value of activation energy
HOM ₁₂₀₇₇	12077	Value suggested by Roldin et al (2019)

45 **HOM Yield Equations**

The yields for 10-carbon HOMs from ozonolysis (γ_{C10z}), OH oxidation (γ_{C10x}) and the total HOM yield (γ_{total}) are given by Eq. 1, Eq. 2 and Eq. 3 respectively.

$$\gamma_{C10x} = \frac{[C10x](k_{OH+HOM}+CS+J)}{k_{OH}[OH][AP]} \quad (1)$$

50

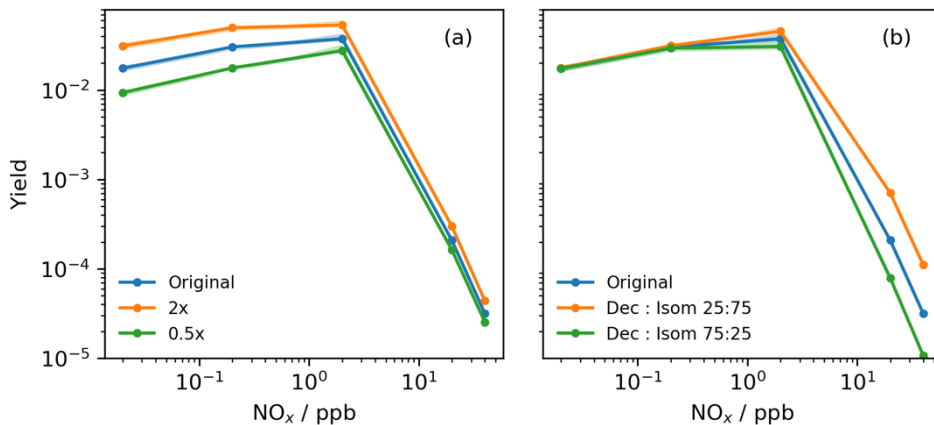
$$\gamma_{C10z} = \frac{[C10z](k_{OH+HOM}+CS+J)}{k_{O_3}[O_3][AP]} \quad (2)$$

$$\gamma_{total} = \frac{([C10z]+[C10x])(k_{OH+HOM}+CS+J)}{(k_{O_3}[O_3]+k_{OH}[OH])[AP]} \quad (3)$$

55

where $[O_3]$, $[OH]$, $[C10z]$ and $[C10x]$ are the concentrations of O_3 , OH and the 10-carbon HOMs formed from ozonolysis and OH oxidation respectively, k_{OH+HOM} is the rate coefficient for the reactions of HOMs with OH, CS is the HOM condensation sink, J is the HOM photolysis frequency and k_{O_3} and k_{OH} are the reaction rate coefficients of α -pinene with O_3 and OH respectively.

60



65 **Comparison to CRI v2.2**

The new mechanism and the CRI v2.2 were run in a box model (Simulation D, Table 3) for 8 days with varying temperature (298 K average, amplitude of 4 K) and emissions of isoprene and α -pinene varying sinusoidally (Fig S3). Time-independent base NO emissions of 4.7×10^9 molecules $m^{-2} s^{-1}$ were used with scaling factors of 1, 3, 10, 30, 100 and 200 employed in a manner consistent with Jenkin et al (2015). Time dependent isoprene emissions reached a maximum of 1.1×10^{12} molecules $m^{-2} s^{-1}$ at 13:00 local time and had an average of 7.1×10^{11} molecules $m^{-2} s^{-1}$ over the period 06:00 to 18:00, similar to emissions used in Jenkin et al (2015) and Bates et al (2019). Time dependent base α -pinene emissions with a mean of 3.23×10^9 molecules $m^{-2} s^{-1}$ and maximum of 5.30×10^9 molecules $m^{-2} s^{-1}$ at 1500 hours were applied. Further runs were performed with α -pinene emissions scaled by factors of 10^{-3} , 10^{-2} , 0.1, 0.2, 0.5, 1, 2, 3 and 5 to investigate the model's performance. Initial conditions of CH_4 (1.8 ppm), CO (100 ppb), O_3 (20 ppb) and HCHO (300 ppt) were applied.

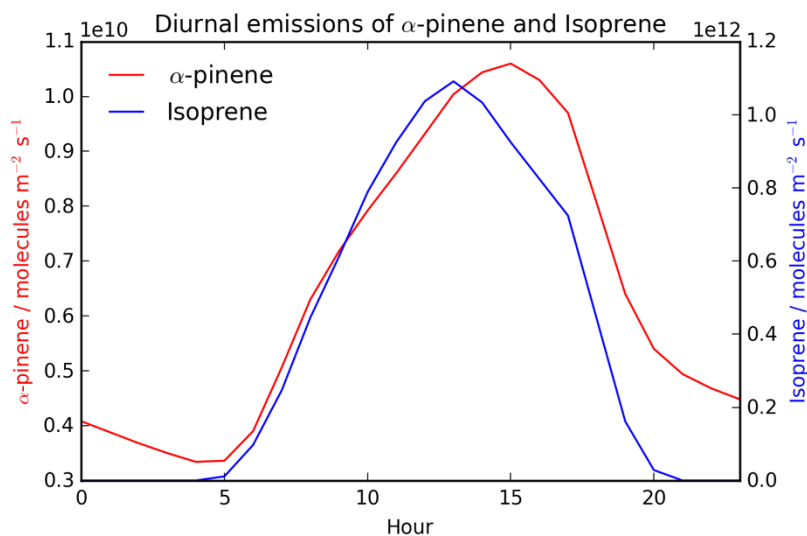
75

Photolysis frequencies simulating conditions at the equator also varied in the diurnal cycle. The box model simulated an instantaneously well-mixed planetary boundary with mixing with the free troposphere (with same composition of initial conditions) represented by the box height increasing from 250 m at night to 1500 m at midday before collapsing back to 250 m at 2100 hours.

80

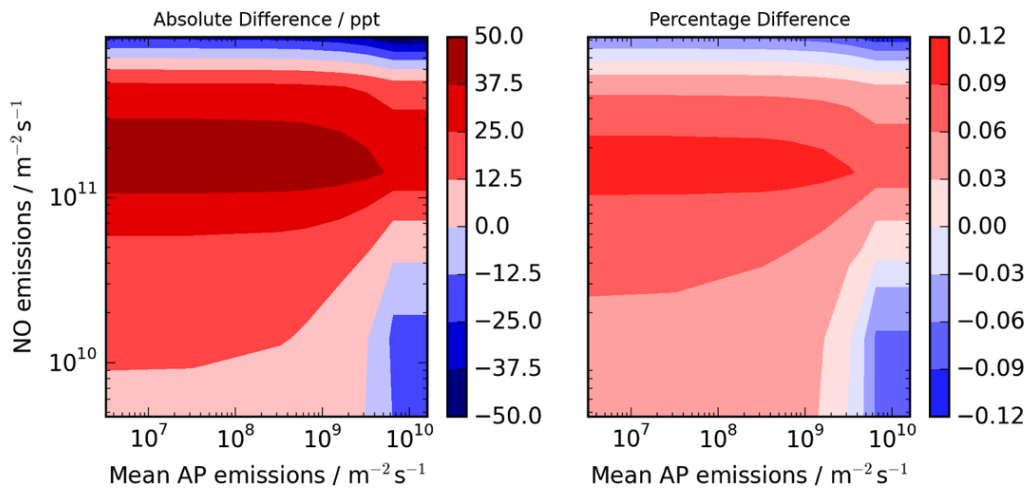
The “concentration” of a species was taken to be the mean daytime concentration on the 8th day, the metric used by Jenkin et al (2015) and Bates et al (2019). The performance of all the HOM mechanisms (HOM_{T1}, HOM₆₀₀₀, HOM₉₀₀₀ and HOM₁₂₀₇₇) was compared to the CRI v2.2.

85 The HOM mechanisms matched the CRI extremely well for OH, O_3 , NO, NO_2 , HO_2 , α -pinene and isoprene as well as the hydroperoxides and nitrates derived from isoprene, methyl vinyl ketone and methacrolein, and the important SOA precursor isoprene epoxy diol (IEPOX)).

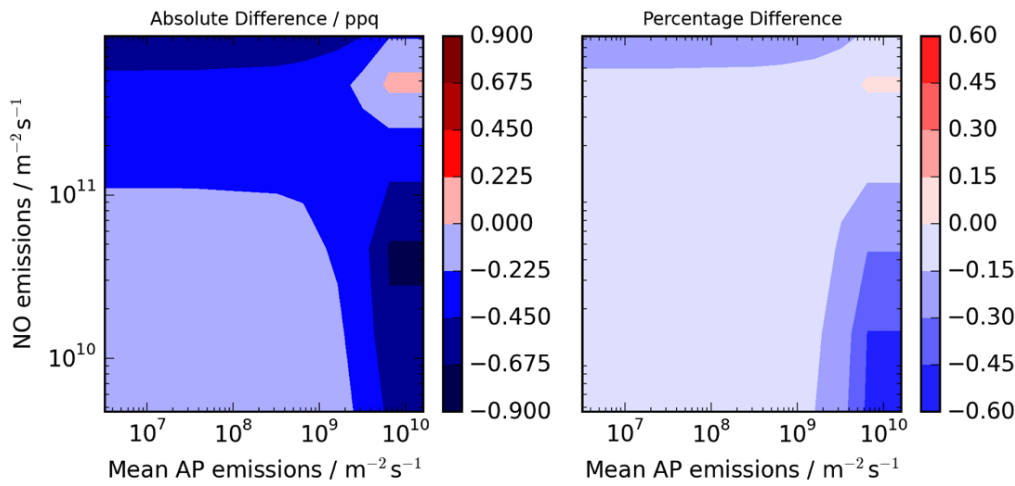


90

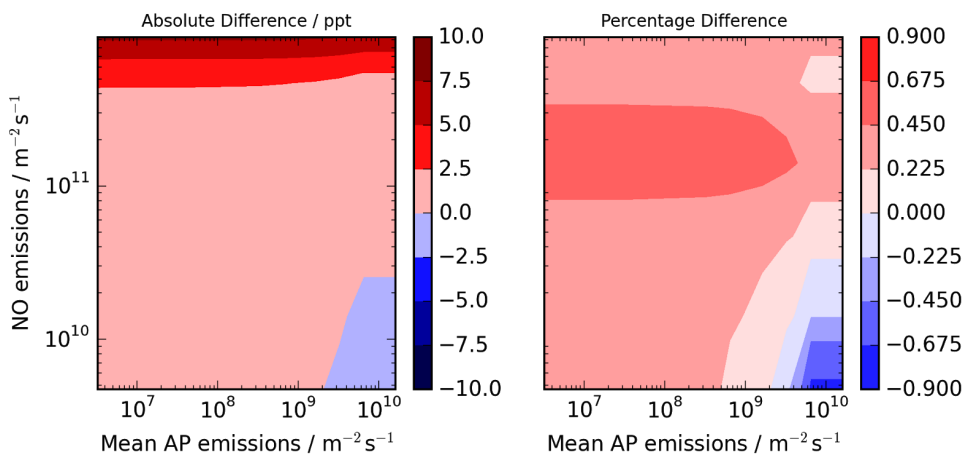
Figure S53 - Diurnal cycle of emissions of α -pinene and isoprene for 8-day comparison of CRI v2.2 R5 with HOM mechanism versions.



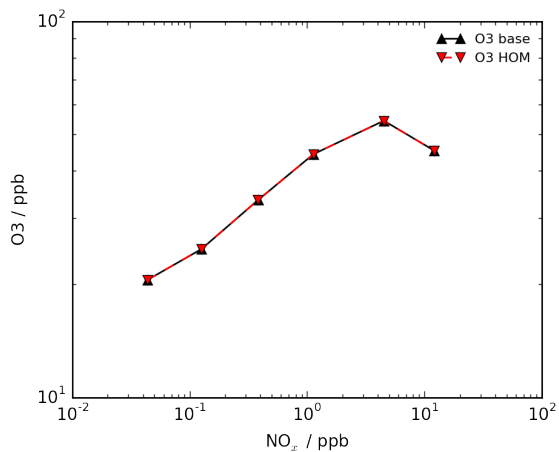
95 **Figure S64** - Absolute and percentage difference in 8th day daylight mean O₃ between the CRI v2.2 R5 and the HOM₉₀₀₀ mechanism. The difference between mechanisms is less than ±0.05 ppb.



100 **Figure S75** - Absolute and percentage difference in 8th day daylight mean OH between the CRI v2.2 R5 and the HOM₉₀₀₀ mechanism. The difference between mechanisms is less than ±0.3% for the vast majority of the emissions space with the difference exceeding this only under very high emissions of α -pinene.



105 **Figure S86** - Absolute difference in 8th day daylight mean NO between the CRI v2.2 R5 and the HOM₉₀₀₀ mechanism. The difference between mechanisms is less than ±2.5 ppt for the vast majority of the emissions space with the difference exceeding this only under very high emissions of NO and α -pinene.



110 **Figure S97** - 8th day daylight mean O₃ in CRI v2.2 R5 and HOM₉₀₀₀ model

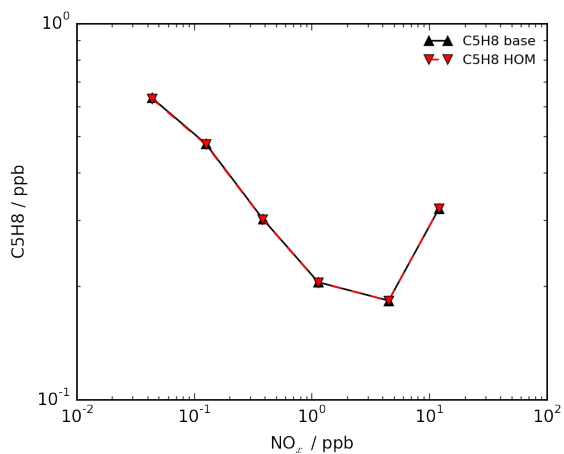


Figure S108 - 8th day daylight mean isoprene in CRI v2.2 R5 and HOM₉₀₀₀ model

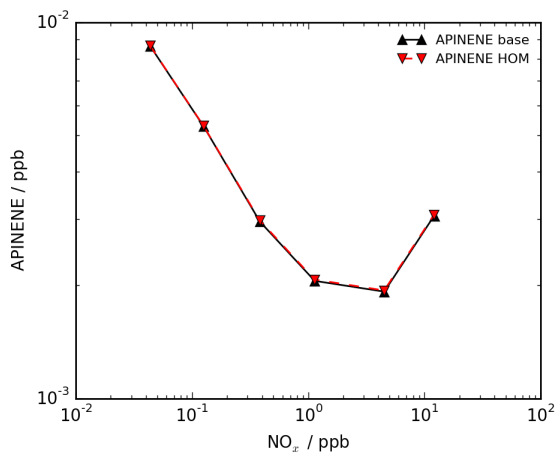
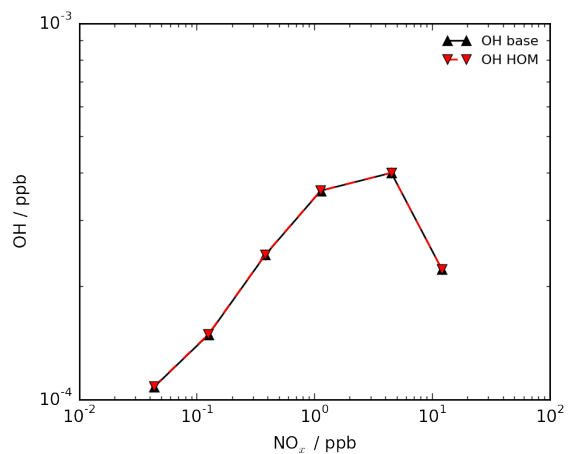


Figure S119 - 8th day daylight mean α -pinene in CRI v2.2 R5 and HOM₉₀₀₀ model



115

Figure S120 - 8th day daylight mean OH in CRI v2.2 R5 and HOM₉₀₀₀ model

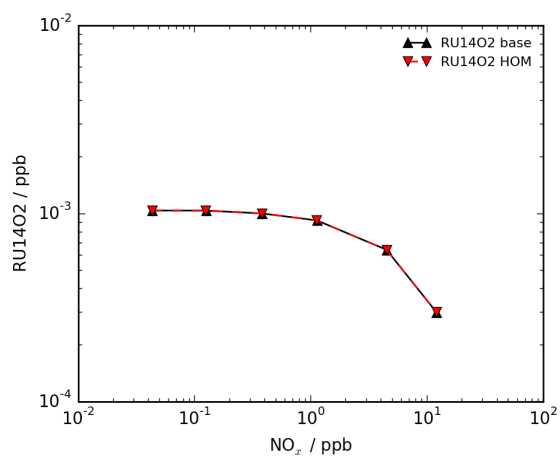
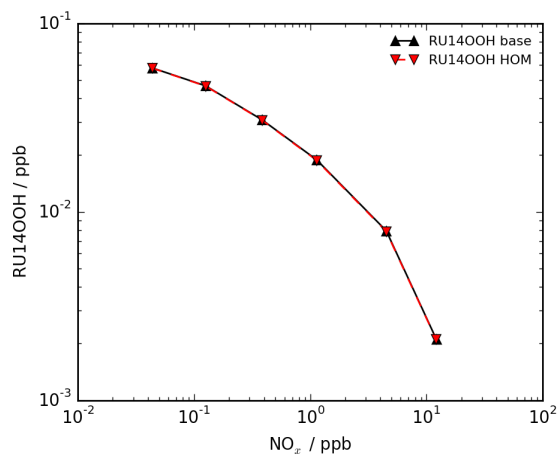


Figure S131 - 8th day daylight mean 1st generation isoprene peroxy radical in CRI v2.2 R5 and HOM₉₀₀₀ model



120

Figure S142 - 8th day daylight mean 1st generation isoprene hydroperoxide in CRI v2.2 R5 and HOM₉₀₀₀ model

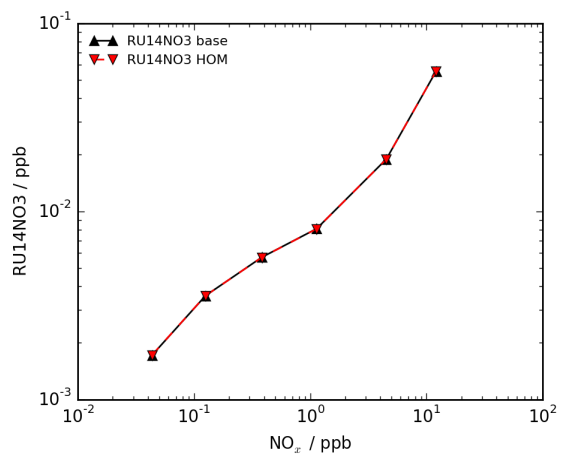


Figure S153 - 8th day daylight mean 1st generation isoprene nitrate in CRI v2.2 R5 and HOM₉₀₀₀ model

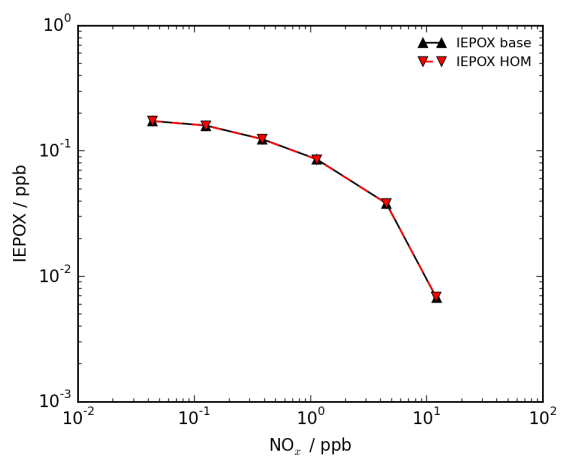


Figure S164 - 8th day daylight mean isoprene epoxydiol in CRI v2.2 R5 and HOM₉₀₀₀ model

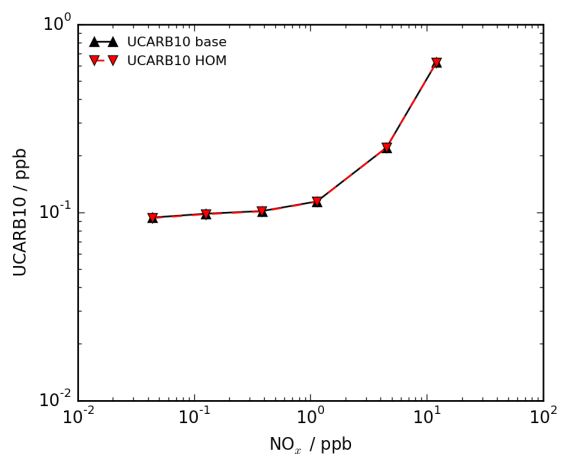
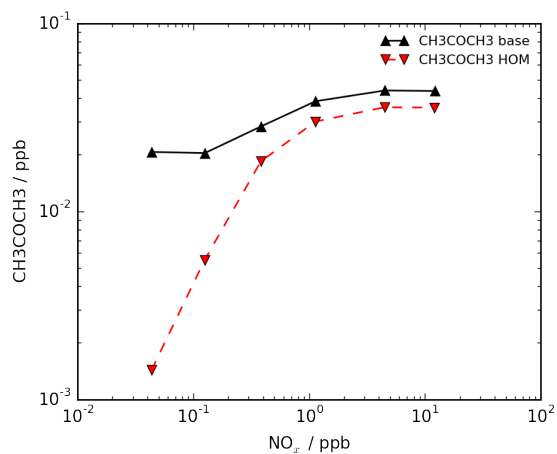
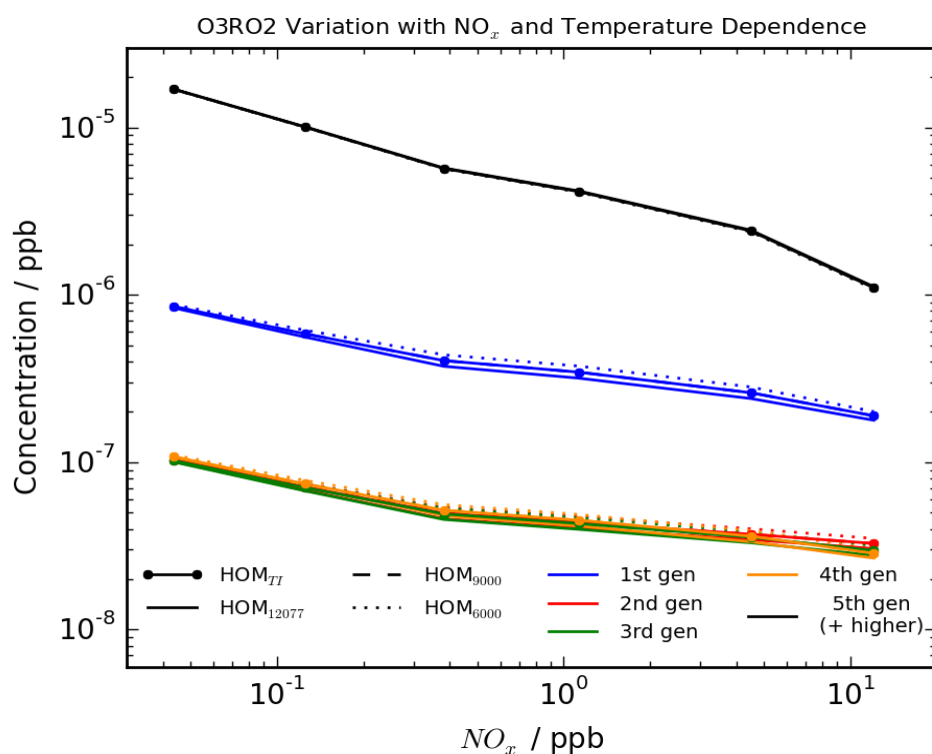


Figure S175 - 8th day daylight mean combined methyl vinyl ketone and methacrolein in CRI v2.2 R5 and HOM₉₀₀₀ model



130 | Figure S186 - 8th day daylight mean combined acetone in CRI v2.2 R5 and HOM₉₀₀₀ model. The difference was attributed to the added competition supplied by the autoxidation pathways, diverting the degradation of α -pinene away from the traditional pathways which form acetone. However, this discrepancy between mechanisms did not lead to significant disagreement between the HOM mechanism and CRI v2.2 R5 for O₃ and OH concentrations.



135 | Figure S197 - Peroxy radicals from ozonolysis (O3RO2) exhibiting a decrease with NO_x and the clear dominance of the highest generation peroxy radical. Negligible difference is observed between the 4 HOM mechanisms for each peroxy radical.

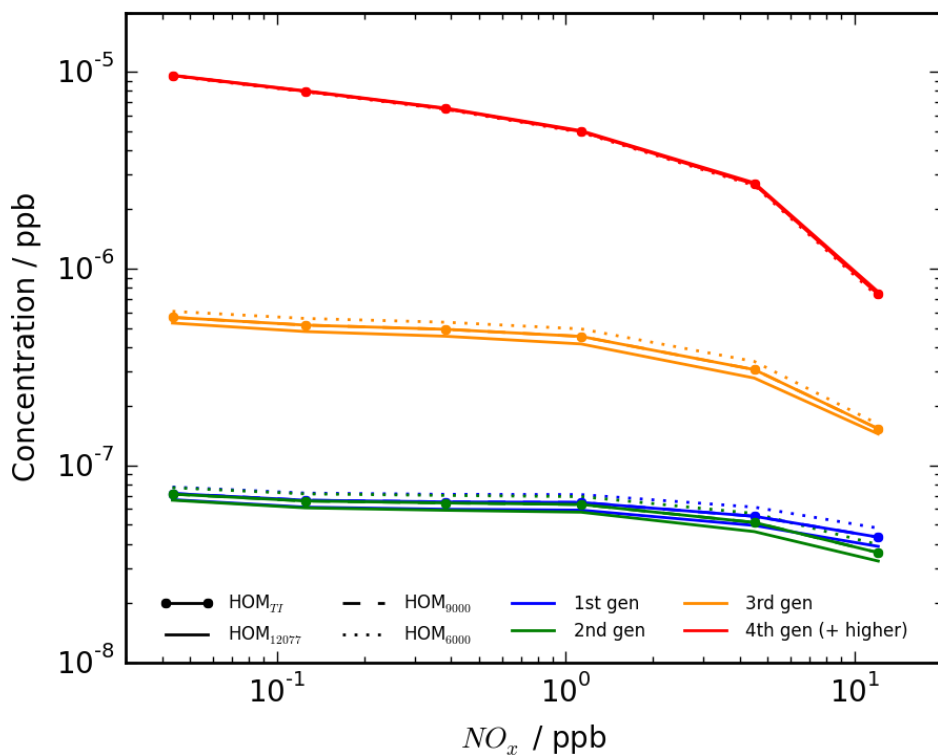


Figure S2018 – Peroxy radicals from OH oxidation (OHRO2) exhibiting a decrease with NO_x and the clear dominance of the highest generation peroxy radical. Negligible difference is observed between the 4 HOM mechanisms for each peroxy radical.

140

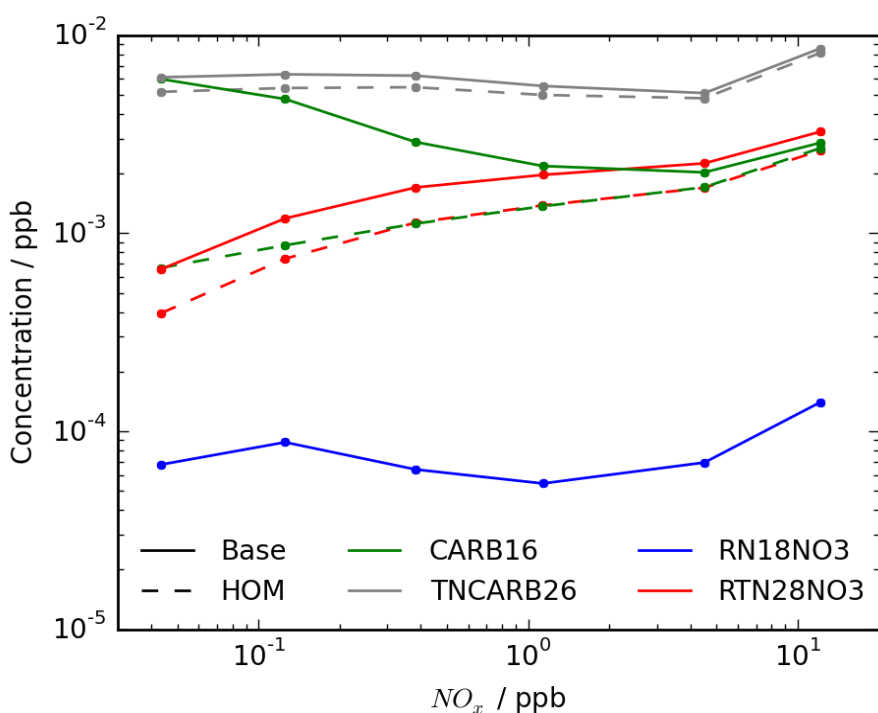
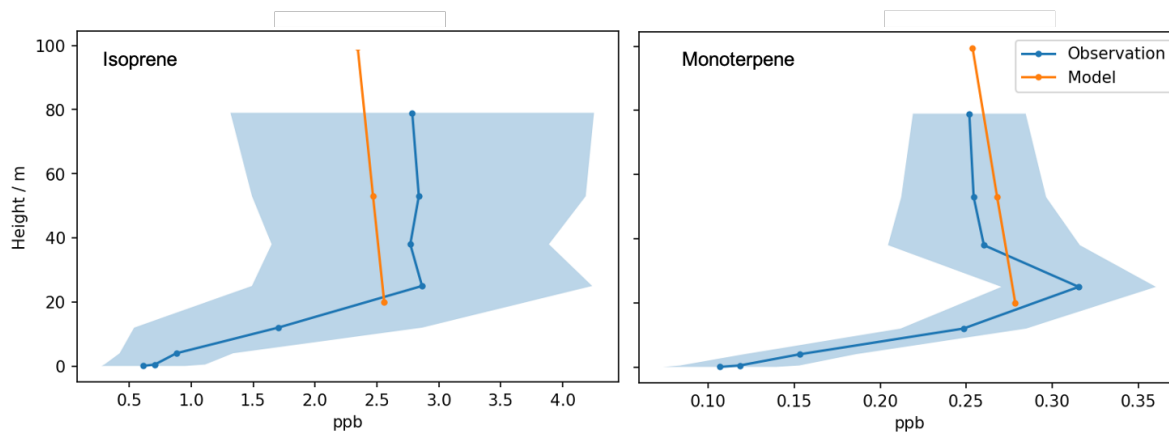


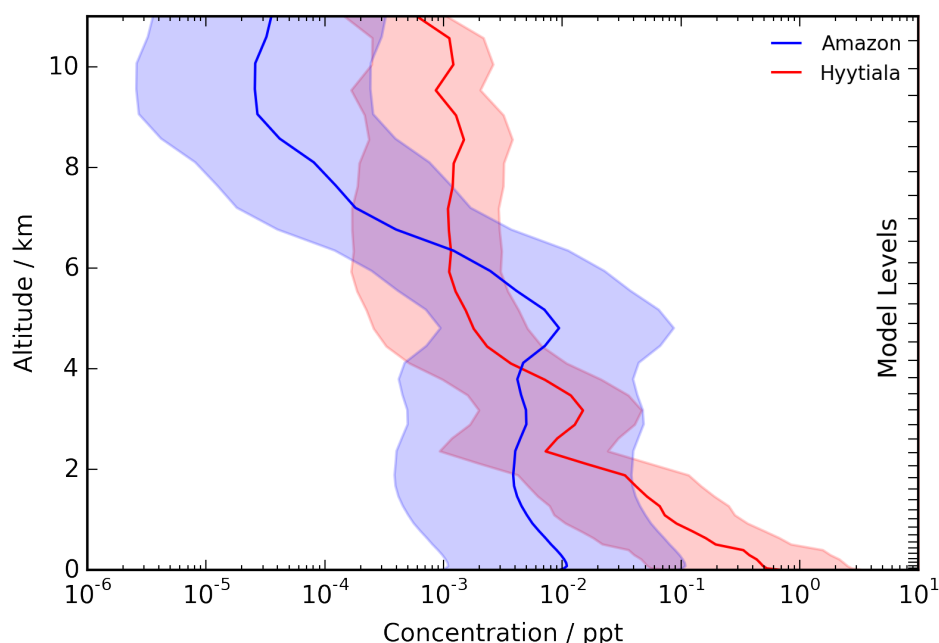
Figure S2149 – Closed shell species in base mechanism compared to HOM_{T1} mechanism. The lower concentrations of TNCARB26, CARB16 and RTN28NO3 were attributed to the increased competition from the autoxidation pathways in the HOM mechanism. RN18NO3 was significantly lower in the HOM mechanisms (not shown) as discussed in the main text.

145

150



155 **Figure S22 – Observed concentrations of isoprene (left) and monoterpene (right) at the ATTO tower at 1:30-2:30 pm in June 2013 (Yáñez-Serrano et al., 2015) (shading shows standard deviation of observational data) and modelled concentrations of species.**



160 **Figure S230 – Total HOM concentrations in Amazon and Hyytiälä with shaded region showing the effect of increasing/decreasing CS by a factor of 10. The value of the CS has a significant influence on HOM concentrations.**

165 **Table S3 – Species and physical parameters used in the HOM altitude profile modelling. Note that for nucleation calculations, the same input species and parameters were used but all data were monthly means.**

Data from UKCA run (2pm 16th June, averaged over 2010-2104)	Data from UKESM Historical
Temperature, pressure, O ₃ , OH, isoprene, monoterpene*, NO, NO ₂ , NO ₃ , N ₂ O ₅ , CO, HO ₂ , H ₂ O	CH ₄ , CO, HCHO, CH ₃ O ₂ , C ₂ H ₅ O ₂ , isoprene nitrate and hydroperoxides, H ₂ O ₂ , CH ₃ OOH, HONO, C ₂ H ₆ , C ₂ H ₅ OOH, CH ₃ CHO, PAN, C ₃ H ₈ , C ₃ H ₇ OOH, C ₂ H ₅ CHO, CH ₃ NO ₃ , Methacrolein, Methylglyoxal, HCOOH, CH ₃ CO ₃ , C ₃ H ₇ O ₂ , C ₂ H ₅ CO ₃ , CH ₃ OH

* The modelled monoterpene concentration was halved to approximate the α -pinene concentration (Rinne et al., 2002)

Table S4 - Values of surface level CS and local time of run used for HOM altitude profiles (Lee et al., 2016)

	Location		
	Hyytiala	Manaus	Brent, Alabama
CS / s ⁻¹	0.004	0.9	0.012 ± 0.006
Local time	14:00	14:00	12:00

170

Nucleation Parameterisations

The rates of neutral and ion-induced pure biogenic nucleation (J_n and J_{iin} respectively) are described by the parameterisations (Kirkby et al (2016)) in Eq. 4 and Eq. 5:

$$J_n = a_1[HOM]^{a_2 + \frac{a_5}{[HOM]}} \quad (4)$$

175 $J_{iin} = a_3[HOM]^{a_4 + \frac{a_5}{[HOM]}}[n_{\pm}] \quad (5)$

Where a_i are fitted parameters and $[n_{\pm}]$ the concentration of ions calculated by method described Kirkby et al (2016). In this work, no distinction was made between the different HOM species; the [HOM] term was taken as the sum of all HOM species. In reality, the larger accretion products are likely to be better at nucleating due to their lower volatility and even among 10-carbon HOMs, more oxidised species will also be more proficient at new particle formation. The condensation

180 sink for ions was calculated by summing over aerosol modes and (Eq. 6).

$$CS = \frac{2kT\mu}{\varepsilon} \sum (wd \times c) \times 10^6 \quad (6)$$

Where k is the Boltzmann constant, T temperature (in Kelvin), $\mu = 1.2 \times 10^{-4} \text{ m}^2 \text{ V}^{-1} \text{ s}^{-1}$, $\varepsilon = 1.6022 \times 10^{-19} \text{ C}$, wd is the wet diameter (in m) of the aerosol mode and c the mode's particle concentration (per cm³) (wd and c were taken from UKCA run).

185 The ion loss rate, X , was then calculated as the sum of the condensation and nucleation sinks (Eq. 7).

$$X = CS + a_3[HOM]^{a_4 + \frac{a_5}{[HOM]}} \quad (7)$$

The recombination coefficient, α , is given by Eq. 8:

$$\alpha = 6 \times 10^{-8} \sqrt{\frac{300}{T}} + 6 \times 10^{-26} c_{air} \left(\frac{300}{T}\right)^4 \quad (8)$$

Where c_{air} is the concentration of air in molecules per cm³.

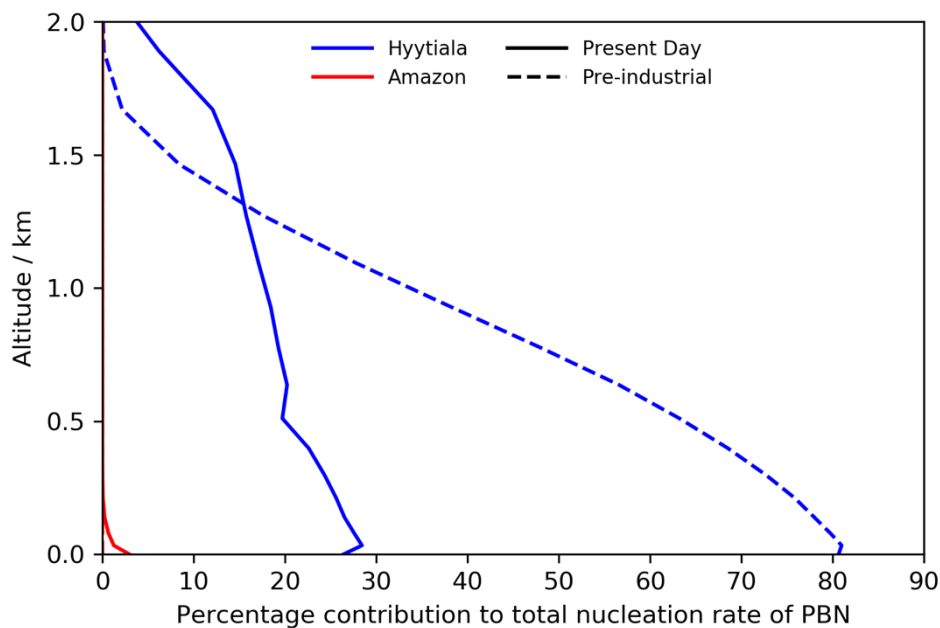
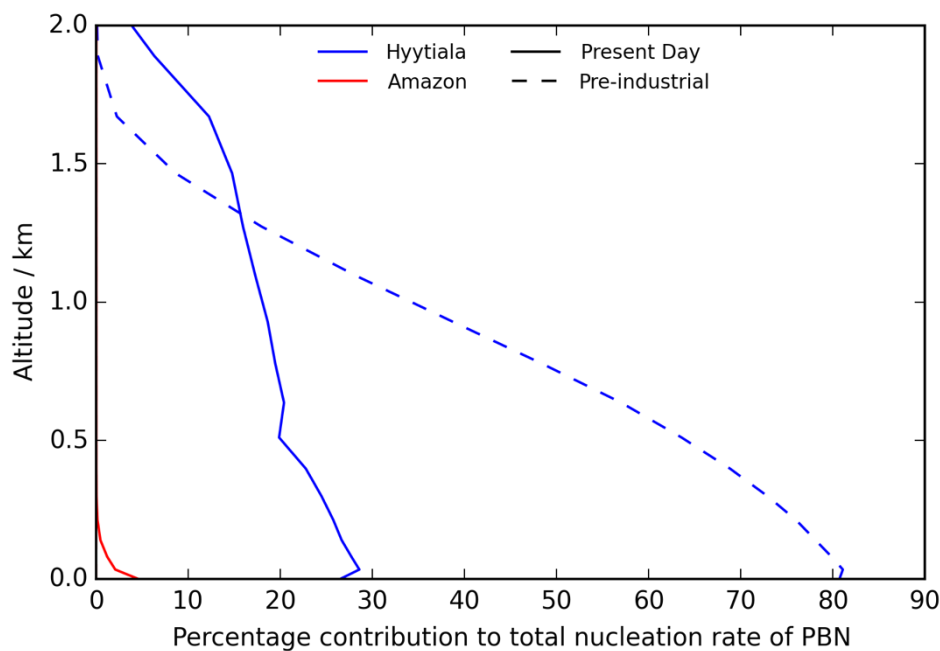
190 $[n_{\pm}] = \frac{\sqrt{(X^2 - 4\alpha q)} - X}{2\alpha} \quad (9)$

Where q is the rate of ion-pair production in cm⁻³ s⁻¹.

The sulphuric acid activation parameterisation used was that developed by Kulmala et al (2006) with coefficient from Sihto et al (2006) as used by Scott et al (2014) (Eq. 10).

$$J_{act} = A[H_2SO_4]$$

Where $A=2 \times 10^{-6} \text{ s}^{-1}$

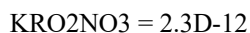
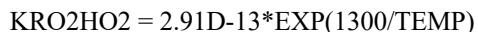
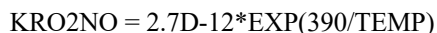


200 **Figure S241** – Percentage contribution to total nucleation rate (PBN + SA_{act}) of PBN. Significant increase is predicted for the PI Hyytiala case in particular, indicating the important implications of including PBN in climate models.

Changes to CRI v2.2 R5 mechanism

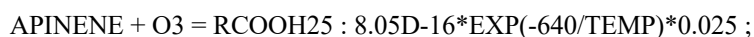
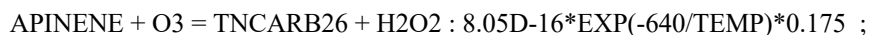
Simple rate coefficients (e.g. k_{RO_2NO}) and photolysis frequencies (e.g. J_{41}) were taken from CRI (Jenkin et al., 2008, Jenkin et al., 2019b). Unless otherwise stated, unimolecular rate coefficients have units of s^{-1} . The peroxy radical pools (RO_{2b}, RO_{2m}, RO_{2s} and RO₂) represent the total concentration of peroxy radicals falling within the respective pool. In the
 205 mechanism used in modelling, certain reactions were lumped together with product fractions weighted by relative rate coefficients to reduce the total number of reactions. For clarity, reactions have been decomposed below. The autoxidation coefficients provided are those fitted at 297 K. Table S5 shows the expressions for the autoxidation coefficients in the 3 temperature dependent mechanisms.

210 The standard reactions rate coefficients used by the CRI are as follows:

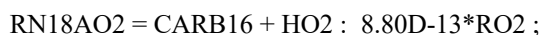
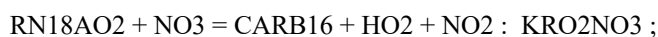


Reactions removed from CRI v2.2 R5 mechanism

215 **Ozonolysis of alpha pinene and treatment of resulting peroxy radical RN18AO2**

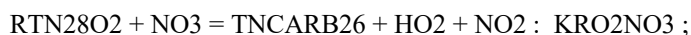
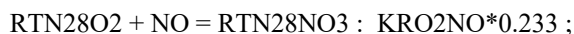
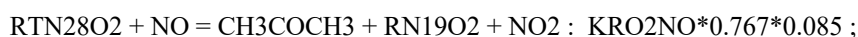


220 $RN18AO2 + NO = RN18NO3 : KRO2NO*0.054 ;$

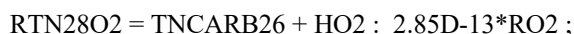


OH oxidation of alpha pinene and treatment of resulting peroxy radical RTN28O2

225 $APINENE + OH = RTN28O2 : 1.20D-11*EXP(444/TEMP) ;$



230 $RTN28O2 + HO2 = RTN28OOH : KRO2HO2*0.914 ;$



Reactions added

Ozonolysis of α -pinene producing 1st generation O3RO2, RN26BO2 - branching ratio set to 50% based on experimental observations of Berndt et al (2018b)

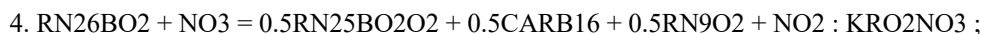
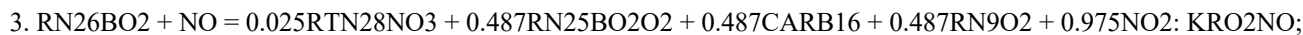
235 1. $APINENE + O3 = 0.14375TNCARB26 + 0.0625RCOOH25 + 0.85OH + 0.5RN26BO2 + 0.3RTN2402 : 8.05E-16*EXP(-640/TEMP);$

Reactions of RN26BO2

Reaction with HO2 forms hydroperoxide species already in CRI, not a HOM due to insufficient oxygens.



240 Reaction with NO, NO₃ forms next generation O3RO2 via alkoxy radical isomerisation and fragmentation products (smaller RO2, RN9O2, and closed shell species, CARB16) at 50:50 branching ratio). NO also forms small yield of RN18NO3, estimated from original CRI v2.2 R5.

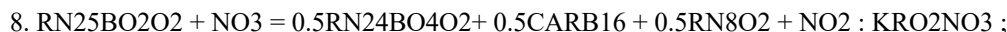
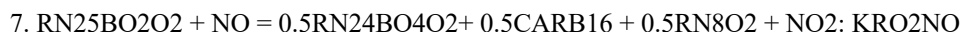
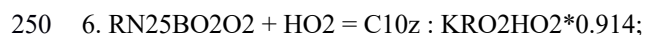


245 **Autoxidation of RN26BO2 to 2nd generation O3RO2, RN25BO2O2**

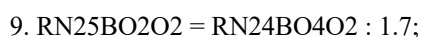


Reactions of RN25BO2O2

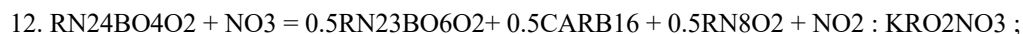
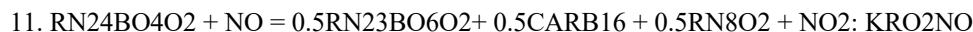
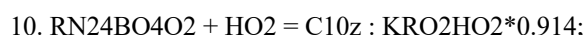
Reaction with HO2 forms HOM monomer C10z as product has sufficient oxygens. Reaction with NO, NO₃ follows the same principle as RN26BO2.



Autoxidation of RN25BO2O2 to 3rd generation O3RO2, RN24BO4O2



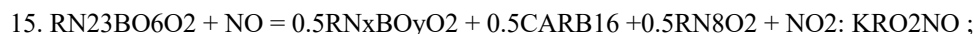
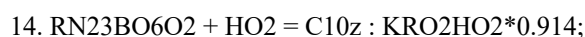
255 **Reactions of RN24BO4O2**

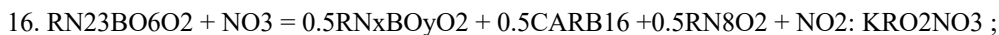


Autoxidation of RN24BO4O2 to 4th generation O3RO2, RN23BO6O2

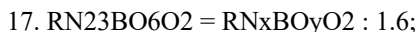


Reactions of RN23BO6O2

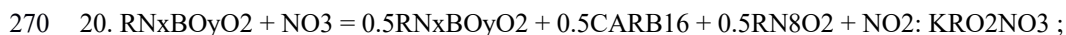
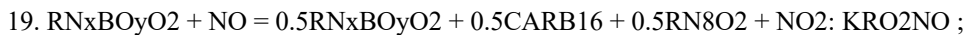
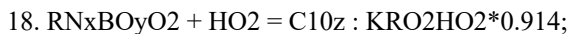




265 **Autoxidation of $RN_{23}BO_6O_2$ to lumped “5th generation and higher” O_3RO_2 , $RN_xBO_yO_2$**

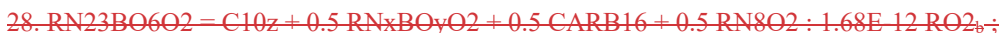
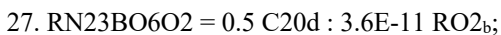
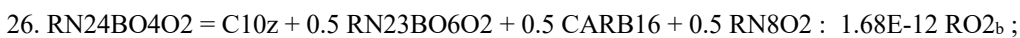
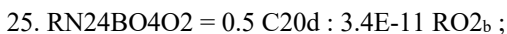
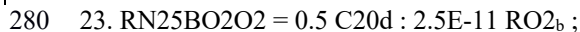
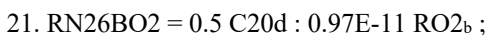


Reactions of $RN_xBO_yO_2$ - no further autoxidation

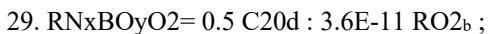


Reactions of O_3RO_2 with big peroxy radical pool (RO_2_b)

275 All reactions with RO_2_b produce a 20-carbon accretion product at a rate coefficient from fitting to experimental data (Berndt et al., 2018b). Reactions also produce, with equal rate coefficients (from Molteni et al., 2019), closed shell species which are classified as HOMs for all cases (except for the reaction of $RN_{26}BO_2$ which is not sufficiently oxidised) and alkoxy radicals which go on to react as previously described in this work.



290



$$30. \text{RNxBOyO}_2 = 0.5\text{C10z} + 0.25\text{RNxBOyO}_2 + 0.25\text{CARB16} + 0.255\text{RN8O}_2 : 3.36\text{E-12}*\text{RO}_2 \text{ b};$$

295 **Reactions of O3RO2 with medium and small peroxy radical pools (RO2_m and RO2_s)**

Reaction of RN26BO2 is based on corresponding species in MCM.

$$31. \text{RN26BO}_2 = 0.5\text{RN25BO}_2\text{O}_2 + 0.5\text{CARB16} + 0.5\text{RN9O}_2 + \text{NO}_2 : 8.13\text{E-13} (\text{RO}_{2s} + \text{RO}_{2m});$$

Rate coefficient and branching ratios of later generation O3RO2 with medium and small peroxy radical pools taken from Roldin et al (2019). The alkoxy radical produced goes on to react as described earlier in this work.

300 32. $\text{RN25BO}_2\text{O}_2 = 0.3\text{RN24BO}_4\text{O}_2 + 0.3\text{CARB16} + 0.3\text{RN8O}_2 + 0.4\text{C10z} : 5\text{E-12} (\text{RO}_{2s} + \text{RO}_{2m});$

$$33. \text{RN24BO}_4\text{O}_2 = 0.2\text{RN23BO}_6\text{O}_2 + 0.2\text{CARB16} + 0.2\text{RN8O}_2 + 0.6\text{C10z} : 7\text{E-12} (\text{RO}_{2s} + \text{RO}_{2m});$$

$$34. \text{RN23BO}_6\text{O}_2 = 0.1\text{RNxBOyO}_2 + 0.1\text{CARB16} + 0.1\text{RN8O}_2 + 0.8\text{C10z} : 9\text{E-12} (\text{RO}_{2s} + \text{RO}_{2m});$$

$$35. \text{RNxBOyO}_2 = 0.1\text{RNxBOyO}_2 + 0.1\text{CARB16} + 0.1\text{RN8O}_2 + 0.8\text{C10z} : 1\text{E-11} (\text{RO}_{2s} + \text{RO}_{2m});$$

305 Rate coefficient of O3RO2 with isoprene-derived peroxy radical from fitting of model to experimental data (Berndt et al, 2018b).

$$36. \text{RN26BO}_2 = 0.667\text{C15d} : 3.9\text{E-12} \text{RO}_{2m};$$

$$37. \text{RN25BO}_2\text{O}_2 = 0.667\text{C15d} : 5.24\text{E-12} \text{RO}_{2m};$$

$$38. \text{RN24BO}_4\text{O}_2 = 0.667\text{C15d} : 6.5\text{E-12} \text{RO}_{2m};$$

$$39. \text{RN23BO}_6\text{O}_2 = 0.667\text{C15d} : 6.5\text{E-12} \text{RO}_{2m};$$

310 40. $\text{RNxBOyO}_2 = 0.667\text{C15d} : 7.55\text{E-12} \text{RO}_{2m};$

OH oxidation of alpha pinene producing two OHRO2 - RTN28AO2 + RTN28BO2

$$41. \text{APINENE} + \text{OH} = 0.78 \text{RTN28AO}_2 + 0.22 \text{RTN28BO}_2 : 1.20\text{E-11}*\text{EXP}(440/\text{TEMP});$$

Reactions of RTN28AO2 are the same as for RTN28O2 in original CRI v2.2 R5 except for accretion product formation. RTN28AO2 does not undergo autoxidation.

315 42. $\text{RTN28AO}_2 + \text{NO} = 0.23\text{RTN28NO}_3 + 0.77\text{TNCARB26} + 0.77\text{NO}_2 : 2.7\text{D-12}*\text{EXP}(360/\text{TEMP})*0.767;$

$$43. \text{RTN28AO}_2 + \text{HO}_2 = \text{RTN28OOH} : 2.91\text{D-13}*\text{EXP}(1300/\text{TEMP})*0.914;$$

$$44. \text{RTN28AO}_2 + \text{NO}_3 = \text{TNCARB26} + \text{HO}_2 + \text{NO}_2 : 2.3\text{D-12};$$

$$45. \text{RTN28AO}_2 = \text{TNCARB26} : 6.65\text{E-13}*\text{RO}_2;$$

$$46. \text{RTN28AO}_2 = 0.5 \text{C20d} : 0.4\text{E-11}*\text{RO}_2 \text{ b};$$

320 47. $\text{RTN28AO}_2 = 0.667\text{C15d} : 1.82\text{E-12}*\text{RO}_2 \text{ m};$

Reactions of RTN28BO2

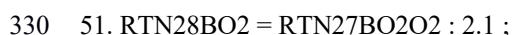
Reaction with HO2 forms hydroperoxide species already in CRI, not a HOM due to insufficient oxygens.



325 Reaction with NO, NO₃ forms next generation OHRO2 via alkoxy radical isomerisation and fragmentation products (smaller RO2, RN9O2, and closed shell species, CARB16) at 50:50 branching ratio). NO also forms small yield of RN18NO3, estimated from original CRI v2.2 R5.

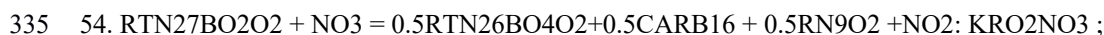
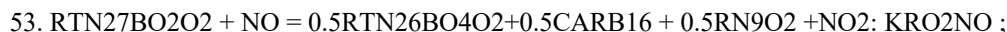


Autoxidation of RTN28BO2 to produce 2nd generation OHRO2, RTN27BO2O2

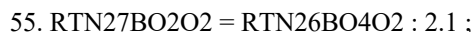


Reactions of RTN27BO2O2

Reaction with HO2 forms hydroperoxide species already in CRI, not a HOM due to insufficient oxygens.

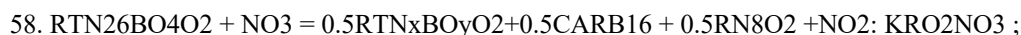
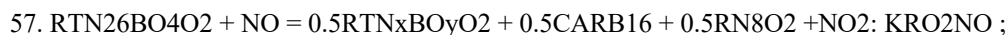


Autoxidation of RTN27BO2O2 to produce 3rd generation OHRO2, RTN26BO4O2

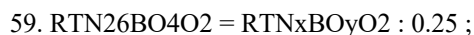


Reactions of RTN26BO4O2

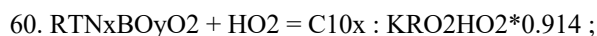
Hydroperoxide from RTN26BO4O2 has sufficient oxygens to be classified as a HOM.



Autoxidation of RTN26BO4O2 to produce "4th generation and higher" OHRO2, RTNxBOyO2



345 Reactions of RTNxBOyO2 - no further autoxidation occurs



61. $\text{RTN}_x\text{BO}_y\text{O}_2 + \text{NO} = 0.5\text{RTN}_x\text{BO}_y\text{O}_2 + 0.5\text{CARB16} + 0.5\text{RN8O}_2 + \text{NO}_2$: KRO2NO ;

62. $\text{RTN}_x\text{BO}_y\text{O}_2 + \text{NO}_3 = 0.5\text{RTN}_x\text{BO}_y\text{O}_2 + 0.5\text{CARB16} + 0.5\text{RN8O}_2 + \text{NO}_2$: KRO2NO3 ;

Reactions of OHRO2 with big peroxy radical pool (RO2_b)

350 Rate coefficient from fitting of model to experimental data (Berndt et al, 2018b).

63. $\text{RTN}_{28}\text{BO}_2 = 0.5 \text{C}_{20d} : 0.4\text{E-}11 \text{RO}_{2b}$;

64. $\text{RTN}_{27}\text{BO}_2\text{O}_2 = 0.5 \text{C}_{20d} : 2.5\text{E-}11 \text{RO}_{2b}$;

65. $\text{RTN}_{26}\text{BO}_4\text{O}_2 = 0.5 \text{C}_{20d} : 5.5\text{E-}11 \text{RO}_{2b}$;

66. $\text{RTN}_x\text{BO}_y\text{O}_2 = 0.5 \text{C}_{20d} : 3.5\text{E-}11 \text{RO}_{2b}$;

355 **Reactions of OHRO2 with medium, small and total peroxy radical pools (RO2_m, RO2_s and RO2)**

67. $\text{RTN}_{28}\text{BO}_2 = 0.7\text{TNCARB26} + 0.3\text{CH}_3\text{COCH}_3 + 0.3\text{RN17O}_2 : 6.7\text{E-}15*\text{RO}_2$

68. $\text{RTN}_{27}\text{BO}_2\text{O}_2 = 0.4\text{TNCARB26} + 0.3\text{RTN}_{26}\text{BO}_4\text{O}_2 + 0.3\text{CARB16} + 0.3\text{RN10O}_2 : 5\text{E-}12*\text{RO}_2$;

69. $\text{RTN}_{26}\text{BO}_4\text{O}_2 = 0.4\text{C}_{10x} + 0.3\text{RTN}_x\text{BO}_y\text{O}_2 + 0.3\text{CARB16} + 0.3\text{RN9O}_2 : 8\text{E-}12*\text{RO}_2$;

70. $\text{RTN}_x\text{BO}_y\text{O}_2 = 0.8\text{C}_{10x} + 0.1\text{RTN}_x\text{BO}_y\text{O}_2 + 0.1\text{CARB16} + 0.1\text{RN8O}_2 : 1\text{E-}11*\text{RO}_2$;

360 Rate coefficient of OHRO2 with isoprene-derived peroxy radical from fitting of model to experimental data (Berndt et al, 2018b).

71. $\text{RTN}_{28}\text{BO}_2 = 0.667\text{C}_{15d} : 1.82\text{E-}12 \text{RO}_{2m}$;

72. $\text{RTN}_{27}\text{BO}_2\text{O}_2 = 0.667\text{C}_{15d} : 3.752.5\text{E-}12 \text{RO}_{2m}$;

73. $\text{RTN}_{26}\text{BO}_4\text{O}_2 = 0.667\text{C}_{15d} : 3.75:2.5\text{E-}12 \text{RO}_{2m}$;

365 74. $\text{RTN}_x\text{BO}_y\text{O}_2 = 0.667\text{C}_{15d} : 3.752.5\text{E-}12 \text{RO}_{2m}$;

Photolysis of HOMs

Photolysis of peroxide linkage and carbonyl linkages were considered using MCM frequencies J41 and J4522 respectively. The KPP parameter “SUN” was used ~~to-in~~ experiments where the photolysis frequency was varied.

370 Photolysis of peroxide linkage in HOM monomer produces one OH and one alkoxy radical which behaves as previously discussed (50% decomposition, 50% isomerisation). As the extent of oxidation of the HOM is unknown, isomerisation produces second generation peroxy radical by default.

75. $\text{C}_{10z} = 0.5\text{CARB16} + 0.5\text{RN9O}_2 + 0.5\text{RN}_{25}\text{BO}_2\text{O}_2 + \text{OH} : \text{SUN}*\text{J41}$;

76. $\text{C}_{10x} = 0.5\text{CARB16} + 0.5\text{RN9O}_2 + 0.5\text{RTN}_{27}\text{BO}_2\text{O}_2 + \text{OH} : \text{SUN}*\text{J41}$;

Photolysis of C20d produces two alkoxy radicals. The isomerisation products are 2nd gen OHRO2 and 2nd gen O3RO2.

375 77. $C20d = 0.5RN25BO2O2 + 0.5RTN27BO2O2 + RN9O2 + CARB16$: ~~SUN*~~J41;

Photolysis of C15d produces two alkoxy radicals. The isoprene-derived alkoxy radical produces UCARB12 (as inCRI v2.2 R5) while the alkoxy radical from alpha pinene forms next generation peroxy radicals via isomerisation (50 % OHRO2 and 50% O3RO2) and fragmentation products.

78. $C15d = UCARB12 + 0.25RN25BO2O2 + 0.25RTN27BO2O2 + 0.5RN9O2 + 0.5CARB16$: ~~SUN*~~J41;

380 Photolysis of carbonyl linkage produces an acyl radical and an alkyl radical which will form peroxy radicals. It is assumed that one of these peroxy radicals is big enough to be considered (2nd generation) O3RO2 or OHRO2-

79. $C10z = RN25BO2O2$: ~~J45~~J22;

80. $C10x = RTN27BO2O2$: ~~J45~~J22;

81. $C20d = 0.5RN25BO2O2 + 0.5RTN27BO2O2$: ~~J22~~J45;

385 For C15d, one of the two peroxy radicals formed is assumed to be of medium size and produce UCARB12 which isomerisation (as occurs for isoprene-derived peroxy radicals).

82. $C15d = 0.5RN25BO2O2 + 0.5RTN27BO2O2 + UCARB12$: ~~J22~~J45;

HOM loss to OH

390 All HOM species are lost to OH with same rate coefficient as that for large hydroperoxide RTN28OOH in CRI v2.2 R5. The products, closed shell CRI species CARB10 and CARB15, were chosen under the assumption that the HOM fragments and the sum of CRI indices of the product is close to the CRI index of the peroxy radical which formed the HOM (23-27). The reaction of C15d also produces a product featured in the oxidation pathway of isoprene, UCARB10.

83. $C10z + OH = CARB10 + CARB15 + OH$: 2.38E-11 ;

84. $C10x + OH = CARB10 + CARB15 + OH$: 2.38E-11 ;

395 85. $C15d + OH = CARB10 + CARB15 + UCARB10 + OH$: 2.38E-11 ;

86. $C20d + OH = 2CARB10 + 2CARB15 + OH$: 2.38E-11 ;

Table S5 - Temperature dependencies used for 3 temperature dependent mechanism versions.

Species	HOM ₆₀₀₀	HOM ₉₀₀₀	HOM ₁₂₀₇₇
RN26BO2	1.223E8*EXP(-6000/T)	2.981E12*EXP(-9000/T)	9.413E16*EXP(-12077/T)
RN25BO2O2	1.009E9*EXP(-6000/T)	2.460E13*EXP(-9000/T)	7.768E17*EXP(-12077/T)

RN24BO4O2	1.009E9*EXP(-6000/T)	2.460E13*EXP(-9000/T)	7.768 E17*EXP(-12077/T)
RN23BO6O2	9.500E8*EXP(-6000/T)	2.315E13*EXP(-9000/T)	7.311E17*EXP(-12077/T)
RTN28BO2	1.247E9*EXP(-6000/T)	3.038E13*EXP(-9000/T)	9.595E17*EXP(-12077/T)
RTN27BO2O2	1.247E9*EXP(-6000/T)	3.038E13*EXP(-9000/T)	9.595E17*EXP(-12077/T)
RTN26BO4O2	1.484E8*EXP(-6000/T)	3.617E12*EXP(-9000/T)	1.142E17*EXP(-12077/T)

400 The uncertainty in the autoxidation coefficients was estimated by further box models simulations where an autoxidation coefficient was adjusted so that the corresponding species was simulated at the upper and lower concentrations values given the experimental uncertainty.

Table S6—Estimated Uncertainty in Autoxidation Coefficients (at 297 K)

Species	Coefficient / s ⁻¹
RN26BO2	0.206 (+0.025 / - 0.04)
RN25BO2O2	1.7 (+1.1 / - 0.4)
RN24BO4O2	1.7(+1.1 / - 0.4)
RN23BO6O2	1.6 (+0.8 / - 0.5)
RTN28BO2	2.1 Taken directly from Xu et al., 2018
RTN27BO2O2	2.1 (+1.6 / - 0.2)
RTN26BO4O2	0.25 (+0.3 / - 0.1)

405 **Table S6 – References for model parameters and confidence**

Parameter	Value(s)	Source	Confidence
<u>Autoxidation Coefficients</u>	<u>Detailed in Table 4</u>	<u>Derived in this work*</u>	<u>Estimated uncertainty in Table 4</u>
<u>Rate coefficients for C20d formation (k13)</u>	<u>Section 2.3.1 and SI reaction list: 21, 23, 25, 27, 29, 46, 63, 64, 65, 66</u>	<u>Derived in this work</u>	<u>Sensitivity tests suggested uncertainty range of +100% / - 35% (scalings of 0.65-2)</u>
<u>Rate coefficients for C15d formation (k16)</u>	<u>Section 2.3.2 and SI reaction list: 36, 37, 38, 39, 40, 47, 71, 72, 73, 74</u>	<u>Derived in this work</u>	<u>Sensitivity tests suggested uncertainty range of ±50% (scalings of 0.5-1.5)</u>

<u>Closed Shell / Alkoxy radical from a specific big RO₂ reacting with RO₂b pool (k14, k15)</u>	<u>Section 2.3.1 and SI reaction list: 22, 24, 26, 28, 30, 32-35</u>	<u>Molteni et al (2019), Roldin et al (2019)</u>	<u>Scaling by factors of 10 and 0.1 did not affect rate coefficients fitted for autoxidation or accretion product formation. HOM yield greater sensitivity with universal scalings of +100% and -50% resulting in a doubling and halving of HOM yield respectively.</u>
<u>k14/k15 branching ratio</u>	<u>50:50</u>	<u>Ratio similar to Jenkin et al (2019a) values of 40:60 (1° RO₂), 20:80 (3° RO₂)</u>	<u>Sensitivity tests with ratios of 40:60 and 20:80 did not affect rate coefficients fitted for autoxidation or accretion product formation and had minor effects on HOM yield.</u>
<u>HOM + OH rate coefficient</u>	<u>2.38×10^{-11} molecules⁻¹ cm³ s⁻¹</u>	<u>Based on comparable species in CRI v2.2, RTN28OOH</u>	<u>Increasing rate coefficient to collision limit (as suggested by Bianchi et al., 2019) had negligible affect</u>
<u>Alkoxy radical decomposition-isomerisation branching ratio</u>	<u>50:50</u>	<u>Estimate</u>	<u>Sensitivity tests with ratios of 75:25 and 25:75 did not affect rate coefficients fitted for autoxidation or accretion product formation. HOM yield below 200 ppt NO_x was unaffected and at 2 ppb NO_x, uncertainty in autoxidation temperature dependence dwarfed this uncertainty. Ratio more important at higher NO_x but this coincided with drastically reduced HOM yield.</u>

*Note that the autoxidation rate coefficient for the 1st generation species RTN28BO₂ was taken from Xu et al (2018)

Breakdown of Peroxy Radical Pools In CRI-HOM

Large Peroxy Radical Pool (8 or more carbons)

410 RTN28AO₂, RTN28BO₂, RTN27BO₂O₂, RTN26BO₄O₂, RTN_xBO_yO₂, RN26BO₂, RTN24O₂, RN25BO₂O₂, RN24BO₄O₂, RN23BO₆O₂, RN_xBO_yO₂, NRTN28O₂, RA19CO₂, RTX28O₂, NRTX28O₂, RTN26O₂, RTN25O₂, RTX22O₂, RTN24O₂, RTN23O₂

Medium Peroxy Radical Pool (4-7 carbons)

415 RU12O₂, NRU12O₂, RN13O₂, RN12O₂, NRN12O₂, RA13O₂, DHPR12O₂, RN11O₂, RA16O₂, RU10O₂, RU10AO₂, MACO₃, RN13AO₂, RU12O₂, NRU12O₂, RTN14O₂, RN16AO₂, RN14O₂, RTN10O₂, RN17O₂, RN15AO₂, RN15O₂, RN18AO₂, RN16O₂, RN18O₂, RN19O₂

Small Peroxy Radical Pool (3 or fewer carbons)

CH3O2, C2H5O2, HOCH2CH2O2, CH3CO3, C2H5CO3, ICH3H7O2, RN10O2, HOCH2CO3, NRN6O2, RN9O2, NRN9O2, RN8O2

420

Sensitivity Tests

425

Initial concentrations of 4 ppt of NO, NO₂ and HO₂ ($1 \times 10^8 \text{ cm}^{-3}$) and $1 \times 10^6 \text{ cm}^{-3}$ OH were used in the modelling of flow cell data from Berndt et al (2018b). The uncertainty in the experimental concentrations of NO, HO₂ and OH has an effect on the modelled concentrations of O₃RO₂, OHRO₂ and accretion products and thus fitted the autoxidation coefficients and accretion production formation rates coefficients. To assess the effect of this uncertainty, multiple model runs were carried out with different initial conditions of NO, HO and HO₂.

430

NO

NO concentrations were believed to be below $1 \times 10^8 \text{ cm}^{-3}$ (~4 ppt) and initial conditions from $1 \times 10^7 \text{ cm}^{-3}$ (0.4 ppt) to $1 \times 10^{10} \text{ cm}^{-3}$ (0.4 ppb) were considered with particular attention paid to the range 5×10^7 – $5 \times 10^8 \text{ cm}^{-3}$. The O₃RO₂ exhibited negligible dependence on initial NO while OHRO₂ displayed a noticeable but small dependence. Relative to the assumed NO concentration of $1 \times 10^8 \text{ cm}^{-3}$, NO of $5 \times 10^8 \text{ cm}^{-3}$ increased OHRO₂ concentrations by <10% (slightly larger than experimental uncertainty) while NO of $5 \times 10^7 \text{ cm}^{-3}$ led to a decrease of <5%. C_{20d} also exhibited negligible dependence on NO (<2%). Given that NO was likely to be less than $1 \times 10^8 \text{ cm}^{-3}$ and the effect of lowering the concentration further was observed to be considerably smaller than experimental error, the uncertainty in NO was considered of minor importance.

435

HO₂

The initial concentration HO₂ was varied from $1 \times 10^7 \text{ cm}^{-3}$ (0.4 ppt) to $1 \times 10^{10} \text{ cm}^{-3}$ (0.4 ppb) (initial NO of $1 \times 10^8 \text{ cm}^{-3}$). O₃RO₂ species showed little dependence to initial HO₂ between 0.4 ppt and 80 ppt while OHRO₂ exhibited greater dependence with 40 ppt increasing OHRO₂ by up to 35% relative to 4 ppt and 0.4 ppt decreasing OHRO₂ by <10% and C_{20d} varied by <±10% from 0.4 ppt to 40 ppt initial HO₂ (all within experimental uncertainty).

440

OH

Initial OH concentration had negligible effect on O₃RO₂, C_{20d} and OHRO₂ even when it was varied over two orders of magnitude (10^5 – 10^7 cm^{-3}).

References

445 Bates, K. H. and Jacob, D. J.: A new model mechanism for atmospheric oxidation of isoprene: global effects on oxidants, nitrogen oxides, organic products, and secondary organic aerosol, Atmos. Chem. Phys., 19, 9613–9640, doi.org/10.5194/acp-19-9613-2019, 2019.

450 Berndt, T., Mentler, B., Scholz, W., Fischer, L., Herrmann, H., Kulmala, M. and Hansel, A.: Accretion product formation from ozonolysis and OH radical reaction of α -pinene: mechanistic insight and the influence of isoprene and ethylene. Environmental science & technology, 52,11069-11077, doi.org/10.1021/acs.est.8b02210, 2018b.

Jenkin, M. E., Valorso, R., Aumont, B., and Rickard, A. R.: Estimation of rate coefficients and branching ratios for reactions of organic peroxy radicals for use in automated mechanism construction, *Atmos. Chem. Phys.*, 19, 7691–7717, doi.org/10.5194/acp-19-7691-2019, 2019a.

455

Lee, S.H., Uin, J., Guenther, A.B., de Gouw, J.A., Yu, F., Nadykto, A.B., Herb, J., Ng, N.L., Koss, A., Brune, W.H. and Baumann, K.: Isoprene suppression of new particle formation: Potential mechanisms and implications. *Journal of Geophysical Research: Atmospheres*, 121,14-621, doi.org/10.1002/2016JD024844, 2016.

460 Molteni, U., Simon, M., Heinritzi, M., Hoyle, C.R., Bernhammer, A.K., Bianchi, F., Breitenlechner, M., Brilke, S., Dias, A., Duplissy, J. and Frege, C.: Formation of Highly Oxygenated Organic Molecules from α -Pinene Ozonolysis: Chemical Characteristics, Mechanism, and Kinetic Model Development. *ACS Earth and Space Chemistry*, 3, 873-883,doi.org/10.1021/acsearthspacechem.9b00035, 2019.

465 Rinne, H.J.I., Guenther, A.B., Greenberg, J.P. and Harley, P.C.: Isoprene and monoterpene fluxes measured above Amazonian rainforest and their dependence on light and temperature. *Atmos Env*, 36, 2421-2426. doi.org/10.1016/S1352-2310(01)00523-4, 2002

Roldin, P., Ehn, M., Kurtén, T., Olenius, T., Rissanen, M.P., Sarnela, N., Elm, J., Rantala, P., Hao, L., Hyttinen, N. and
470 Heikkinen, L.: The role of highly oxygenated organic molecules in the Boreal aerosol-cloud-climate system. *Nature communications*, 10, 1-15, doi.org/10.1038/s41467-019-12338-8, 2019.

Scott, C. E., Rap, A., Spracklen, D. V., Forster, P. M., Carslaw, K. S., Mann, G. W., Pringle, K. J., Kivekäs, N., Kulmala, M., Lihavainen, H., and Tunved, P.: The direct and indirect radiative effects of biogenic secondary organic aerosol, *Atmos.*
475 *Chem. Phys.*, 14, 447–470, doi.org/10.5194/acp-14-447-2014, 2014.

Sihto, S.-L., Kulmala, M., Kerminen, V.-M., Dal Maso, M., Petäjä, T., Riipinen, I., Korhonen, H., Arnold, F., Janson, R., Boy, M., Laaksonen, A., and Lehtinen, K. E. J.: Atmospheric sulphuric acid and aerosol formation: implications from atmospheric measurements for nucleation and early growth mechanisms, *Atmos. Chem. Phys.*, 6, 4079–4091,
480 doi:10.5194/acp-6-4079-2006, 2006

Xu, L., Møller, K.H., Crouse, J.D., Otkjær, R.V., Kjaergaard, H.G. and Wennberg, P.O.: Unimolecular reactions of peroxy radicals formed in the oxidation of α -pinene and β -pinene by hydroxyl radicals. *The Journal of Physical Chemistry A*, 123, 1661-1674, doi.org/10.1021/acs.jpca.8b11726, 2019.

485